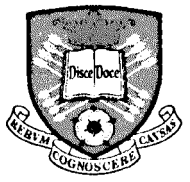

The
University
Of
Sheffield.

AN INVESTIGATION INTO CARBON DEPOSITION GROWTH IN JET ENGINE INJECTOR FEED ARM DUE TO FUEL THERMAL DEGRADATION

By

EHSAN ALBORZI

Supervisor

CHRISTOPHER W WILSON

Submitted in accordance with the requirements for the degree of

Doctor of Philosophy

The University of Sheffield

Mechanical Engineering Department

June 2009

ACKNOWLEDGEMENTS

Many thanks go to my supervisor, Prof. Christopher Wilson for his continuous advice, encouragement, guidance, and financial supports during the course of my research. I would also like to convey my gratitude to Dr.Simon Blakey for his invaluable helps and supports on providing both experimental and theoretical advices.

I would particularly like to express my gratitude to my friend Richard Collins because of his priceless and immeasurable helps throughout my thesis.

Many thanks go to my friends Dr.Mohammad Reza Mofakhami, Dr.Mohammad Zanganeh, Hasan.Ghadbeygi, Spiros Sioris, Lucas Rye, and Chris Leong for their assistance during my research.

I would like to express my heartfelt appreciation to my uncles Dr. Mahmoud Alborzi, Abbas Alborzi and Mohammad Reza Sotoudehnia and also Shariatzadeh family from back home in Iran who were always very encouraging.

It is very difficult to look for the conventional words to express my mother's kindness, love, and supports during my years of education, the sorrowful years of being without my father.

Last but by no means least, I would like to express my sincere gratefulness and feeling to wonderful, unbeatable and flawless love, Maryam, however, words are too limited to describe her patience, sacrifice, encouragement and etc. She is without a doubt the most stable fuel of my life!!

ABSTRACT

Investigation of tube fouling was carried out employing the heated nozzle module of Aviation Fuel Thermal Stability Test Unit (AFTSTU). This includes straight, thick-walled stainless steel tube, exposed to a constant heat flux provided by a Radio Frequency (RF) heating unit that is coiled around the tube. In this situation, deposits are allowed to form on the inner surface of the tube. Due to the considerably lower thermal conductivity of the deposit compared to the stainless steel, temperature at the tube external wall increases with time. This was recorded by the application of three pairs of thermocouple situated at different axial locations along the tube. Each pair of thermocouple monitored the data from two different radial positions. The fuel temperature at the tube exit was recorded by the use of another thermocouple. The recorded results for each thermocouple indicate that three distinct stages can be observed as function of time. The first stage represents a temperature invariant zone, known as induction period, followed by a remarkable temperature rise. The third stage represents a level off zone. Experiments were carried out for two different baselines fuels each experiment consists of four stages. In each baseline test, four different thermal powers were supplied by RF heater. Consequently, four initial tube wall temperatures were set. Then surface deposition was investigated during four different exposure time. The second baseline test is different from the first test in that the fuel inlet was kept at higher temperature. In order to imitate the temperature rise across the heated tube, a two dimensional, axis symmetric, time dependent Computational Fluid Dynamic (CFD) model was developed. In this model dynamic mesh technique was employed to predict the temperature rise in a changing boundary. This technique was also used to imitate the surface deposition in Near Isothermal Flowing Tube Reactor (NIFTR) where the tube is subject to the constant wall temperature. The experimental results of the NIFTR for code validation were taken from the literature.

A number of preliminary investigations were performed prior to the CFD modelling on the chemistry of autoxidation, the process which is responsible for the formation of species precursor. Pseudo-detailed mechanism of liquid phase autoxidation which is widely used in most of the investigations was used for in this thesis.

In order to develop an integrator code for the investigation of rate equations, two different approaches were applied. Firstly an integration based on the Taylor series was applied. In spite of the applicability of this method for the reduced chemical schemes (3-4 reaction steps), it proved to be computationally very expensive for the integration of pseudo-detailed mechanism. Hence, it was not included for the further applications. Secondly, an integrated program was developed in MATLAB to integrate the system of non linear ordinary differential equations. In order to overcome the stiffness caused by different time scales, Gear's method was used. Furthermore, a function was developed to calculate the sensitivity of dissolved oxygen profile as well as the hydroperoxide species to the rate constants of each reaction steps. It was proved that the reaction steps can be classified as high sensitive, low sensitive and no sensitive. As a result, the chemical scheme was reduced and applied in the CFD calculations.

It is very important to take in consideration the fact that fuel sample faces different temperature regimes through the various compartments of the AFTSTU. Unfortunately, due to the experimental constraints it was impractical to have an online measurement of jet fuel chemical compositions at tube inlet. Therefore, by the application of perfectly stirred reactor based on the residence time and temperature of each compartment, the species boundary condition for the tube inlet was calculated.

Table of Content

List of the Figures

CHAPTER 1

INTRODUCTION

1.1 Evolution of Jet Fuel Thermal Stability

In modern military aircraft, prior to the combustion chamber, jet fuel is the main source of cooling. Heat transfer from the hot components can result in degradation of the bulk fuel. This causes the emergence detrimental materials. These materials can adversely affect the performance and the durability of the aircraft engine. Insoluble deposits may cause the blockage in fine mesh screens or nozzles. Correspondingly, gums can form on fuel injectors resulting in degraded atomisation and reduced flow rate. The ability of jet fuel to absorb heat with less tendency of deposit formation is a key factor for the design of high performance aircraft. Given the amount of heat loads generated by the current aircraft systems, jet fuel can offer an adequate heat-sink without considerable fuel degradation. However, increased thermal loads for the next generation of propulsion system may create significant difficulties.

Figure 1-1 indicates that for the military propulsion systems, the quantity of jet fuel as heat sink changes markedly with the Mach number value. It is also pointed by Hazlett (1991) that commercial jet fuels and some of the military fuels exhibit good thermal stability at the speed range up to about Mach 2.0 while operation at higher range causes the thermal degradation to be noticeable.

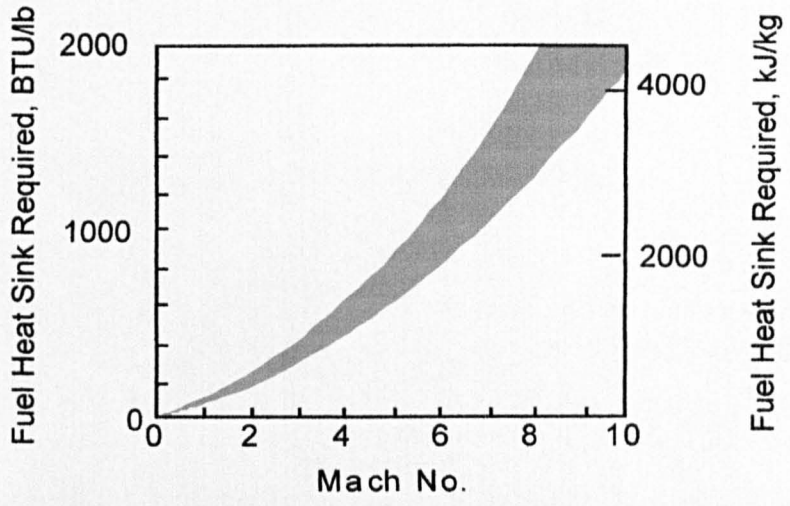

Figure 1-1: Variation of the quantity of jet fuel required as heat sink vs. Mach number (J.E. Sinor Consultants Inc., 2001).

The subject of jet fuel thermal stability became important in the early 1950s and a number of investigations were initiated over the next decade.

Following the early reports on the impact of jet fuel chemical composition on failure in the jet fuel system, a number of investigations attempted to relate the chemistry of fuel on thermal stability, see Schwartz (1962).Two decades later, another survey of multiple authors, highlighted the various topics related on thermal stability. This addressed the significance of thermal stability, experimental methods and relevant test devices, physico chemical aspects, and lastly the inhibitory role of additives in reduction of deposit formation, See CRC(1983) and CRC(1984).

In 1989, a research program was initiated by the US Air Force Wright Laboratory, known as "near term high temperature stability requirements." The main objective of this program, known as USAF JP8+100, was to enhance the thermal stability of JP8 by 50% from 325°F(163°C) to 425°F(218°C) by way of developing appropriate additive at a reasonably low cost, see Biddle (1993) and Morris *et al* (2002).

The main topics of JP8+100 program were relatively analogous to the CRC reports, however, an extra task was added to investigate for more thermally stable jet fuels in actual aircraft flight conditions.

While the impact of inhibitory additives is one of the key solutions, design of such additives has been overdue by the lack of reliable experimental methods. In addition, theoretical investigation of additives and their impact on thermal stability along with

the other influencing species necessitate a comprehensive framework being provided. Even though, variety of parameters and conditions has been the major reasons thereby this to be postponed by far.

1.1.1 Definition of Jet Fuel Thermal Stability

Exposure of jet fuel to the elevated temperature in jet fuel system may cause the fuel to approach to a temperature of approximately 200°C, see Hazlett (1991), Biddle (1993), Dagget *et al* (1995), Heneghan *et al* (1996), Pande *et al* (2001).

Subjecting the jet fuel to such a high temperature, results in the formation of both oxidised soluble and insoluble products through a multitude of complex chemical reactions. This in due course causes the emergence of surface deposit, see Jones and Balster (1993), and Pickard and Jones(1998).

The entire process of deposition is influenced by various parameters such as the catalytic effect of the wall surface, the amount of dissolved O_2 ,natural antioxidant, sulphur compounds, and metal deactivators in the bulk fuel, see Hazlett *et al* (1977), Mushrush *et al* (1985), Mushrush *et al* (1991), Jones and Balster(1993), Pickard and Jones(1997), Jones *et al*(1997), Pickard and Jones(1998). In addition, the bulk fuel exposure temperature, duration of exposure and flow characteristics are also dominant parameters, see Marteney and Spadaccini (1986), Chin and Lefebvre (1993) and Spadaccini *et al* (2001).

1.1.2 Significance of Modelling and Validation

A broad range of conditions can be encountered in terms of temperature, thermal stress time, chemical composition, and flow regime within the real jet fuel system. Moreover, the geometry of the entire fuel system is very complex. Therefore, the integrated simulation of deposition in jet fuel system is not practical. Alternatively, investigation of deposition in such a complicated system can be carried out assuming that it is consisted of a number of less intricate elements. Once the geometrical simplification is established, a physical model is required to accurately illustrate the most of fuel thermal degradation aspects. To date, however, the fundamental features of thermal stability are not clearly understood.

In contrast to the complexity associated with the surface deposit phenomena, a number of investigations have been focused on the preliminary stages of thermal

stability, i.e. liquid phase autoxidation. It is assumed that, creation of deposit precursor species is governed by the chemistry of autoxidation and once is generated; the fluid dynamics are responsible for its migration from the bulk fuel towards the wall. Therefore, prior to the application of Computational Fluid Dynamics (CFD) on thermal stability, a mathematical formulation capable of describing the rate of chemical transformations is essential. It is, however, important to understand that such chemical mechanism is an intrinsic property of a given system and is not a function of any physical process such as mixing or heat and mass transfer. Once this scheme is available, the production rate of the products can be related to the transport equations for the further modelling.

The physics of precursor adhesion at wall and surface deposition is in the early stage of the research. There are a number of hypothesis and assumptions related to this stage which are reviewed in Chapter 2. However, the manifestation of such complicated phenomena, in the existing CFD models, is disguised by a simplified reaction mechanism. This includes the Arrhenius type equations whose kinetic parameters (activation energy and pre exponential factor) are adjusted for the particular cases in less stringent conditions. Application of these simplified deposition model in CFD proved to be practical for the simulation of less realistic experimental conditions such as Near-Isothermal Flowing Tube Reactor (NIFTR). However, the reliability of these models in simulation of more severe situations where the thermo fluid conditions are far from the isothermal and laminar is under debate.

For more realistic experimental situations such as those provided by the Aviation Fuel Thermal Stability Test Unit (AFTSTU), whose data have been used in this thesis, the new adjustment of kinetic parameters for the surface deposition stage, with respect to the experimental data, seems to be practical. In addition, adding more steps for the surface deposition may represent a better description of the phenomena.

The primary purpose of this thesis is to investigate the growth of deposit on the inner surface of AFTSTU heated nozzle module which is assimilated to the feed arm injector in jet fuel system.

For the theoretical investigation, the global chemistry model of Katta and Roquemore (1993) as well as the pseudo detailed chemistry scheme of liquid phase autoxidation along with the subsequent surface reactions of Kuprowicz *et al* (2007) were used. Firstly, a reactor modelling technique in conjunction with the preliminary CFD calculations was employed. In this approach, the heated nozzle of AFTSTU was

considered as a multitude of axially and radially linked perfectly stirred reactor. Every reactor represents a tiny region of tube in which mixing is assumed to be perfect, hence, the distribution of temperature and species concentrations is uniform within the reactor volume. In this way, the system of ordinary differential equations representing the chemistry of thermal stability was required to be solved. Accordingly, a code was developed in Matlab 7.1 that integrates the multistep chemistry of jet fuel autoxidation. Solution of energy equation was not included in the integrator as the energetic of the jet fuel autoxidation is negligible. Another computer program was developed to read the local values of temperature and velocity given by CFD calculations that are required for the reactor calculations. The third program was written to link the multitude of reactors and to perform the summation of deposit over the tube. In spite of the simplicity, since this model does not consider the change of the tube geometry due to the deposition, it was not used for the further study.

In the second modelling approach, a time dependent model based on the dynamic mesh technique was developed to imitate the real time evolution of deposition across the AFTSTU heated tube. Moreover, the surface sticking probability based on the formulation of Katta and Roquemore(1993) and Ervin *et al*(2000) was also considered in this modelling approach for which two User Defined Functions (UDFs) were developed and implemented in Fluent 6.3.26.

For the experimental part of this research, after the recomissioning of the test unit, a series of experiments were carried out using the heated nozzle module of AFTSTU aiming to investigate deposit formation on the inner surface of the tube, under a turbulent flow regime within the cylindrical flow passage.

1.2 Outline of Thesis

Chapter 2 reviews the most of the published works by different investigators in various subjects related to the jet fuel thermal stability as followings:

i. Significance of fuel thermal stability study;
ii. Thermo chemical aspects of thermal stability;
iii. A review of experimental techniques ;
iv. The impacts of various influencing species on fuel stability;
v. Recent developments in zero dimensional models(chemical kinetic) as well as in multidimensional models(Computational Fluid Dynamics)

Chapter 3 presents a mathematical modelling for the solution of chemical kinetic scheme and the sensitivity analysis. Accordingly, an integrated code based on Gear's method was written in Matlab to solve the system of ordinary differential equations representing the liquid phase oxidation scheme for the jet fuel. A computer code was also developed to calculate the sensitivity of dissolved oxygen concentration as well as deposit precursor to the rate parameters in the mechanism. Consequently, a reduction in the total number of reaction steps was proposed.

Chapter 4 illustrates the various elements AFTSTU along with the description of the test procedures. The topics of this chapter are listed as following:

i. Fuel system thermal management in aircraft engines and its similarities with AFTSTU;
ii. Capabilities of AFTSTU;
iii. A fully description of test unit;
iv. Specifications of different parameters in AFTSTU;
v. Explanation of test methods;
vi. Experimental results;
vii. Discussion

Chapter 5 addresses the reactor modelling as well as time dependent CFD modelling aiming to simulate the real time growth of deposit in inner surface of AFSTSTU heated nozzle module.

Chapter 6 Recapitulates the presented work in each chapters of thesis and emphasises the level of achievements. In the second section of this chapter, the results have been discussed. Lastly, the further works which can be carried out in different areas of jet fuel thermal stability have been provided.

CHAPTER 2

A LITERATURE SURVEY ON AVIATION FUEL THERMAL STABILITY

2.1 Overview

Throughout the jet engine manufacturing section, the main debate has been on the quest of the most efficient methods for cooling process in different component of the fuel system. Application of air as heat sink necessitates the employment of relatively heavy heat exchangers which results in higher vehicle drag penalty. In supersonic and hypersonic aircrafts, the increase of flight speed may lead to the temperature rise in the ram air intake. Therefore, the air temperature will be relatively high for the cooling process.

The preference of jet fuel as coolant substitute, in spite of its wide applicability and benefits, has been one of the other controversial subject for many decades, see Schreifels *et al*(1991) and Hazlett *et al* (1991). Although cryogenic fuels such as liquid methane and liquid hydrogen can be used as coolant, their application is limited by a number of factors including low densities, cost, logistic and safety problems, see Huang *et al* (2002).

Concerning the amount of heat loads generated by the current aircraft, jet fuel can offer adequate heat-sink, even though, increased temperature requirements for the next generation of propulsion system may cause the fuel to approach a temperature of approximately 200°C, see Hazlett (1991), Jones *et al* (1993), Zabarnick (1993). Under this elevated temperature regime and also in the presence of other parameters, a multitude of chemical reactions may proceed within the bulk fuel which at last results in the surface deposition processes.

It has been known for many years that the traces of hetero atomic compound in jet fuel, particularly those containing oxygen, nitrogen and sulphur, contribute in jet fuel thermal degradation process, see Mushrush *et al*(1985), Hazzlet(1991), Pickard and Jones(1998), Zabarnick and Mick(1999), Kuprowicz *et al* (2004) and Kuprowicz *et al* (2007).

Hazlett (1991) referred the failures in the fuel system, reported by the U.S.Navy and some commercial air carriers, to the peroxide species in jet fuel. It was believed that hydroperoxides in jet fuel may attack elastomers in the aircraft fuel systems resulting in leakage. Similarly, in 1976, the US Navy faced with attack on fuel pump diaphragms in jets operating in Philippine, see Watkins (1989).

. Figure 2-1 presents the deposition in swirl vane. Surface deposition within the swirl vanes and injectors can have severe consequences on the spray pattern on which the efficiency of combustion depends. Fuel spray pattern, in turn, has a significant effect on the temperature profile at the gas turbine combustor exit.

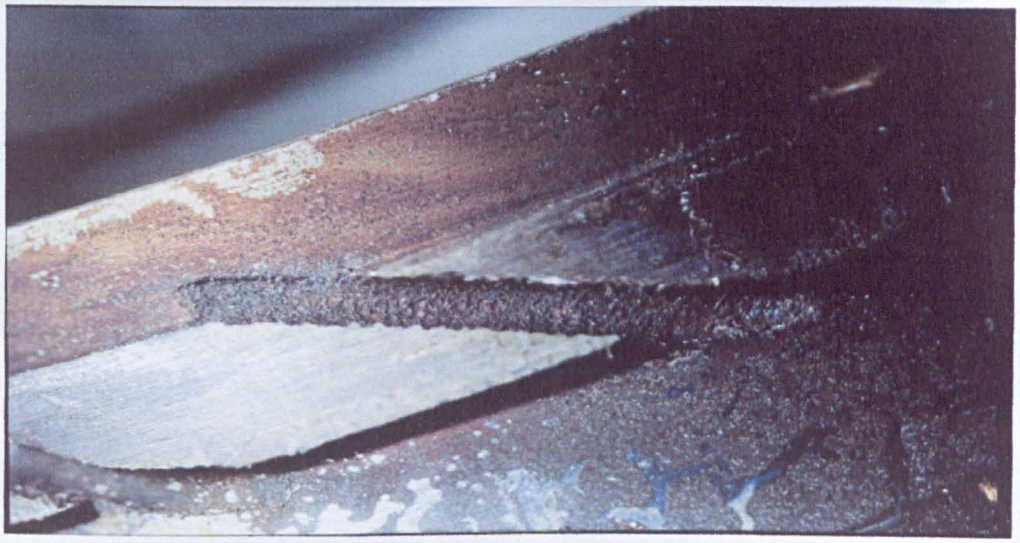

Figure 2-1: Accumulation of deposit in Injector, see Hobday and Lewis (1995)

Figure 2-2 indicates the deficiency of a spray nozzle due to the carbon deposition. Following on the fouling in the atomisers, spray cannot keep its typical conical shape in combustion chamber. The spray cone angle has a strong impact on ignition; stability limits, and exhaust smoke.

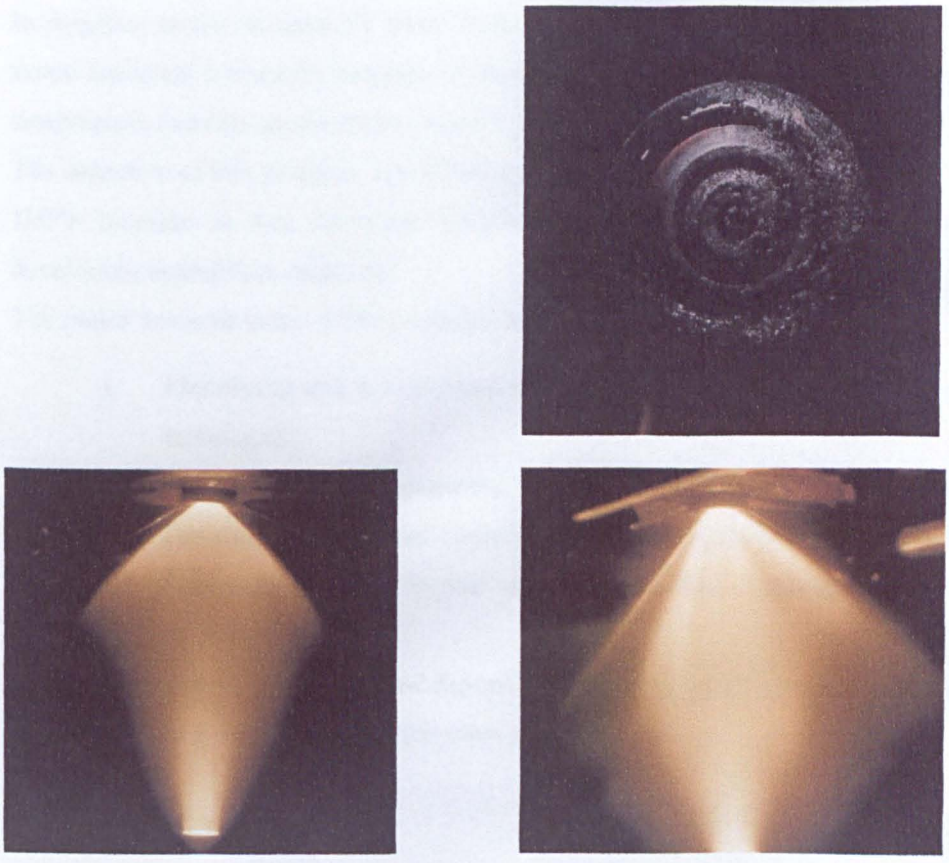

Figure 2-2: Poor combustion consequences due to the spray pattern disorder, see Taylor(2005)

In 1950's and 60's a great deal of efforts was devoted through different research programs to identify the feasibility of the solution methods. This resulted into a large body of scientific literature. A Russian literature review, published by Bolshakov(1974) lists around 122 references related to the fuel thermal degradation. A report by Taylor and Frankenfield (1988) surveys 55 references and Fathoni (1991) lists as many as 140 references. In 1980s a multiple authors survey was published by the Coordinating Research Council, CRC(1984). This work was based on the various topics mainly focused on the significance of jet fuel thermal degradation in jet engine, experimental methods, investigation of deposit formation form the view point of thermo-chemistry, and lastly the role of additives in deposit formation.

In response to the demand for more thermally stable jet fuels, in 1989, the US Air Force launched a research program at Wright Laboratory, known as near term high temperature stability requirements, known as the USAF JP8+100 program.

The objective of this program was to boost the thermal stability of JP8 by 50% that is 100°F increase in fuel operation temperature from 325°F to 425°F by way of developing appropriate additives

The major research tasks of this program are listed below:

i. Identifying and development of new fuel thermal stability experimental techniques;
ii. Advancement of fundamental understanding of the fuel thermal stability;
iii. Development of global chemistry models and a thermal stability scale;
iv. Formulation of effective thermal stability improvement additive packages

Figure 2-3 compares the severity of deposit formation for two cases, namely JP-8 and JP-8+100 in an F-16 engine after the same period of time.

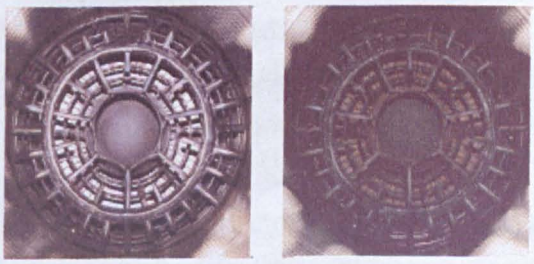

Figure 2-3 : A comparison between the deposit formation with the application of JP-8 fuel, and (b) JP-8+100 for the same period of operation in an F-16/F100-200 engine, see Maurice *et al*(2000)

The purpose of this chapter is to review the thermo chemical aspects of fundamental processes associated with the jet fuel thermal stability. The existing physical models of solid particle deposition are also partly addressed in this chapter.

The principal experimental techniques applicable for the investigation jet fuel thermal stability, has been also reviewed in this chapter. Lastly, the numerical works that has been applied in the field of jet fuel thermal stability are reviewed to some extent.

2.2 Physico-Chemical Aspects of Jet Fuel Thermal Stability

2.2.1 Definition of thermal Stability

Thermal stability is defined as the tendency of fuel to undergo the autoxidative chemical transformations leading to the formation of soluble and insoluble materials, beginning from the moment of production until the point of the application. see Hazlett(1991). In general, fuel thermal stability is classified in two forms, storage stability, and thermal oxidative stability. In addition, another form frequently used in the literature, is referred to as "thermal stability", see Zabarnick (1993).

Storage stability is more often associated with the low quality fuels such as marine gas turbine fuels, see Fathoni (1991).Thermal stability is different from the "oxidative stability" based on the fact the latter refers to the situation in which the dissolved oxygen in bulk fuel is completely consumed, while "thermal stability" refers to the formation of the solid deposit, see Zabarnick(1993).

Several investigators addressed that the rate of deposit formation is proportional to the fuel's autoxidation tendency. Naegli (1997) proved that an anomalous relationship exits between the autoxidation rate at moderate temperatures (<150°C) and the rate of surface deposition. Accordingly, fuels with higher propensity of autoxidation tend to form fewer amount of deposits, or require higher temperatures to form comparable deposits. Similarly, Hardy *et al* (1992) found that a non linear relationship exists between thermal deposition and peroxide formation. It was also stated by Heneghan *et al* (1996) that fuels that exhibit poor oxidative stability tend to have good thermal stability. On the other hand, those fuels showing good oxidative stability exhibit poor thermal stability. Although, Jones *et al*(1998) and Pickard and Jones(1998) reported that considerably lower deposition rates is observed for the deoxygenated hydrocarbons.

The mechanism of deposit formation in jet fuel is a complex process involving a number of chemical reactions, mass transport, and complex surface phenomena.

2.2.2 Kinetics of Autoxidation

It has been known that the formation of peroxides in fuels is due to the autoxidation process, see Thomas(1959), Fish(1970). The rate of process is relatively slow at ambient temperatures; however, at higher temperatures it is considerably increased.
In organic chemistry, the transformation of C-H bond of a molecule into C-O-O-H throughout a very slow process is called autoxidation. This can be generically presented according to the below expression:

$$RH + O_2 \rightarrow R-O-O-H$$

The hydroperoxides react further to yield alcohols, ketones, aldehydes, acids and etc. Aldehydes are easily transformed to the corresponding carboxylic acid (RCOOH) by a number of oxidant agent such as alkaline hydrogen peroxide, peracides and molecular oxygen, see Hazlett *et al* (1977) and Mushrush *et al*(1985).
If enough dissolved oxygen exists in the bulk hydrocarbon, the total concentration of hydroperoxide species will reach to a high level. In contrast, if the concentration of oxygen is low and the temperature is raised, the hydroperoxide concentration will be limited by the thermal decomposition process. The latter situation is similar to the aircraft fuel system.
The accurate kinetic path of hydroperoxide must be described through a simultaneous mechanism of formation and decomposition. However, the chemistry of thermal decomposition of alkyl hydroperoxides is complicated by high sensitivity of radicals to structural, solvent and streoelectronic effects which are far beyond the objective of this thesis. Moreover, the entire process of jet fuel autoxidation is influenced by various parameters including the catalytic effect of the wall surface, the amount of dissolved O_2, the percentage of natural antioxidant, sulphur compounds and the amount of metal deactivators in the bulk fuel, see Denison and Condit(1945), Denison and Condit(1949), Benson and Shaw(1970), Fathoni and Batts (1991),Heneghan and Zabarnick(1994).

From the view point of a crude oil refining processing, aviation fuel is known as the fraction among the middle distillates whose normal boiling point varies from 60°C to 288°C. In this way, jet fuel is considered a multi component mixture, composed of a large number of different hydrocarbons, possibly as many as a thousand or more. However, the major constituents of jet fuels are branched (25%) and straight-chain alkanes (20%), alkyl cycloparaffins (30%), aromatics and olefins (20%) along with the traces of hetero atomic species. Due to this composition variability, the response of various fuels to thermal stress is different. For example, the space of the time required to complete autoxidation at 185°C for 16 air-saturated aviation fuels vary from about 1.5 to 15 minutes, see Jones *et al* (1996).Accordingly, the construction of an appropriate chemical mechanism capable of imitating the oxidative behaviour for most of the jet fuels is complicated.

For the theoretical investigation of jet fuel thermal oxidative stability, a realistic kinetic model requires to include the most sensitive reaction steps of the entire process.

The Basic Autoxidation Scheme (BAS) of pure normal paraffins, presented in Table 2-1 describes the main features of liquid phase autoxidative tendency of hydrocarbons, see Benson and Shaw(1970), Walling(1957) and Emanuel *et al* (1967).

Reaction Type	Reaction	Index
Initiation	Formation of $R^{\bullet}$	1
Propagation	$R^{\bullet} + O_2 \rightarrow RO_2^{\bullet}$	2
	$RO_2^{\bullet} + RH \rightarrow RO_2H + R^{\bullet}$	3
Termination	$2RO_2^{\bullet} \rightarrow$ Alcohol+Ketone+O_2	4
	$RO_2^{\bullet} + R^{\bullet} \rightarrow ROOR$	5
	$R^{\bullet} + R^{\bullet} \rightarrow R_2$	6

Table 2-1: Basic Autoxidation Scheme (BAS) for pure normal paraffins

This scheme illustrates that the autoxidation reactions for liquid hydrocarbons proceed through a chain reaction mechanism. A chain reaction consists of at least two reaction steps, the initiation step and termination. The initiation step involves the formation of free radicals, usually through the homolytic cleavage of covalent bond in which each fragment forms an unpaired electron. This step proceeds either spontaneously or by

the intervention of an external source of excitation such as heat, light and etc. The termination step involves the destruction of free radicals by the combination two similar or dissimilar radicals. This occurs through a process opposite to the initiation. It is not typical for the termination step to happen directly after initiation. The reason is due to the higher probability of the combination of a radical with a neutral species (atoms and molecules) than other radicals. Via this reaction, the radical species pairs its shell and another radical is produced. This step which is known as the propagation step is repeated thousands times hence carrying on the process. Propagation step terminates by the combination of two unpaired species or by collision against the vessel's wall.

Similarly, the three main processes in jet fuel autoxidation are initiation, propagation, and termination. Propagation and termination are classified as homogeneous, but initiation at lower temperatures is frequently dominated by heterogeneous reactions via a catalytic process.

Formation of alkyl radical ($\dot{R}$) during the liquid phase autoxidation is not clearly understood. However, it is generally assumed that this step is affected by the catalytic nature of the surface, see Emanuel *et al* (1967) Benson and Shaw(1970), Hazlett (1991), Jones *et al* (1995).

It was suggested by Emanuel *et al*(1967) that alkyl radical ($\dot{R}$) in the low temperature regimes is mainly produced through a termolecular reaction as following:

$$2RH + O_2 \rightarrow 2\dot{R} + H_2O_2$$

Another suggestive path for the initiation of jet fuel thermal stability by the same authors is presented as follows:, see Zabarnick (1993).

$$RH + O_2 \rightarrow \dot{R} + H\dot{O}_2$$

Benson and Nangia (see Fathoni (1990)) reported that both these reactions are too slow to justify the initiation step at temperature lower than 450°C.

Pickard *et al* (1998) carried out a series of experiments to investigate the autoxidation of Exxsol D-80. This mixture of hydrocarbons is composed of 58% normal paraffins, 41% cycloparaffins and 0.8% aromatics, equivalent to a JP-7 fuel without a lubricity

additive. This is also a representative of severely hydrotreated fuel with low aromatics The results proved that initiation involves trace quantities of hydroperoxide. Hence, the BAS can be presented as in Table 2-2.

Reaction Type	Reaction	Index
Initiation	$RO_2H \rightarrow R\dot{O}+O\dot{H}$	1
Propagation	$O\dot{H}+RH \rightarrow \dot{R}+H_2O$	2
	$R\dot{O}+RH \rightarrow \dot{R}+ROH$	3
	$\dot{R}+O_2 \rightarrow R\dot{O}_2$	4
	$RH+R\dot{O}_2 \rightarrow RO_2H+\dot{R}$	5
Termination	$2R\dot{O}_2 \rightarrow P_1+P_2$	6
	$2\dot{R} \rightarrow R_2$	7
	$\dot{R}+R\dot{O}_2 \rightarrow RRO_2$	8

Table 2-2: Basic Autoxidation Scheme (BAS) for pure normal paraffins without the catalytic effect of the surface

Jones *et al* (1996) assumed that active sites on the stainless steel fuel line surface, can be a source of alkyl radicals. This step can be expressed as a heterogeneous catalytic reaction, for instance, a surface assisted thermal dissociation of hydroperoxide which proceeds in the surface catalysis porous as following:

$$ROOH \xrightarrow{\text{active-surface}} R\dot{O}+O\dot{H}$$

Alternatively, traces of fuel components having a weak covalent bond may contribute in the initiation step. Although, metal-catalysed autoxidation involving salts of heavy metals are potential agents for oxidations/reductions reactions between metal cations and hydroperoxides as homogenous source of free radical initiation. This behaviour was experimentally demonstrated by Jones *et al* (1996) for a jet fuel sample named as POSF-2693 doped with Cu.

Any process such as the aforementioned reactions which lower the need for the activation energy in the initiation step also lower the overall activation energy for entire process. It is important to consider that the same active surface sites may not be

available on heavily covered tubes as a consequence of deposition; therefore, the autoxidation would be expected to become slower as the surface coverage persists.

The alkyl radical reacts rapidly with molecular oxygen through reaction step 2 to yield alkyl peroxy radical ($R\dot{O}_2$). During reaction step 3, an alkyl peroxy radical abstracts a hydrogen atom from the fuel molecule. This results in the formation of a hydroperoxide (RO_2H) and a new alkyl radical, hence propagating the chain. Amongst the three termination steps, reaction step 4 is the dominant process since alcohol and ketones were detected in the temperature regime up to 300°C, see Mushrush *et al* (1985) and Reddy *et al* (1988).

It was shown by Reddy that reaction step 6 is not significant as R_2 were detected at the temperature regime lower than 300°C; however, at higher temperatures in a condition where all oxygen has been consumed, alkyl radicals recombine to produce dimmeric species. These dimmers were observed in the autoxidation of octane and n-dodecane at 480°C, see Edward and Zabarnick(1993). At the same time, the low concentration of secondary alkyl radical throughout the entire process indicates that reaction step 5 is improbable. At sufficiently high temperatures, the additional reaction steps related to the thermal decomposition of RO_2H ought to be included in to the BAS.

Various RO_2H decomposition paths can be included in the course of higher temperature regimes, however, the simplest way of description is to begin with unimolecular homolysis of O–O giving alkoxy radical($R\dot{O}$)in conjunction with hydroxyl radical($O\dot{H}$). Alkoxy radicals primarily abstract hydrogen to form group III alcohol. At temperature 300°C and higher some of the alkoxy radicals decompose through β-Scission forming n-alkane and an alkyl radical via intramolecular H-atom abstraction from an RH molecule.

The additional RO_2H thermal decomposition along with the chemistry of anti oxidant species (AH) were added to the BAS by Zabarnick. This scheme was limited to relatively short reaction times prior to the moment that substantial consumption of the antioxidant species occurs, see Kuprowicz *et al* (2004). In addition, due to the lack of appropriate experimental data, this new designed mechanism was not validated. Later on, the experimental results of Jones *et al*(1996) and Balster *et al* (1996) provided reasonable data for the validation of the mechanism.

In this mechanism, AH behaves mainly by competing with bulk fuel for alkyl peroxy radical, hence preventing the formation of alkyl radical. Through the reaction of alkyl

peroxy radical with antioxidant species, a hydroperoxide species (RO_2H) and antioxidant radical are generated.

This mechanism also addresses the strong synergism between the two groups of radical that are peroxy radical inhibiting anti oxidant and hydroperoxide decomposers SH in a slowing/delaying oxidation process, see Zabarnick and Mick (1999). It was shown by Kendall *et al* (1986) that the presence of Sulphur containing natural inhibitors protect the fuel from a fast autoxidation by removing hydroperoxides which in turn results in the slowing the self initiation step. Denison and Condit (1945) and Denison and Condit (1949)showed that alkyl sulfides and slenides exhibit significant oxidation delays through the autoxidation of desulfurised lubricating oils. Their conclusion was based on the fact that alkyl sulfides react with the alkyl hydroperoxides through a non radical pathway generating a sulfoxide and an alcohol through the following reaction:

$$RSR + ROOH \rightarrow R_2S = O + ROH$$

It is assumed that the elimination of hydroperoxides through this process results in a substantial retardation of autoxidation rate. In contrast, Zabarnick and Mick (1999) showed that hydroperoxide decomposing species, such as alkyl sulfides cannot retard the autoxidation rate of hydrocarbons at 140°C. However, in the presence of phenolic species (AH), in the natural and/or synthetic form, significant retardation in autoxidation process occurs. This experimental observation was added to the BAS. Such expanded mechanism is known as a pseudo-detailed mechanism of jet fuel autoxidation. Since, the early version of mechanism showed less capability of prediction for dissolved oxygen consumption at different initial concentration of oxygen, the inclusion of an alkyl-peroxy radical decomposition ($R\dot{O}_2 \rightarrow \dot{R} + O_2$) was suggested, see Kuprowicz *et al* (2004).

It was reported by Mayo and Lan(1986) that in most autoxidation process, chain termination is a bimolecular including two radicals presented as following:

$$2RO_2^{\bullet} \rightarrow \text{alcohol} + \text{Ketone} + O_2$$

$$2RO_2^{\bullet} \rightarrow R_2O_2 + O_2$$

$$RO_2^{\bullet} + R^{\bullet} \rightarrow R_2O_2$$

$$2R^{\bullet} \rightarrow R_2$$

Mayo and Lan(1987) elsewhere reported that if the chain termination involves only monomeric peroxy radicals, the gums will be only dimeric as presented in the following reaction step:

$$2RO_2^{\bullet} \rightarrow R_2O_2 + O_2$$

To obtain larger gum molecules, some of the dimmeric R_2O_2 must be involved in both propagation and termination step to yield RO_2RO_2R and larger molecules. Hence, the longer propagation prior to termination will result in the greater average size of a gum molecule. However, the termination step in the most of the suggested chemical schemes ignored this complexity.

In addition to the self termination reactions involving ($R\dot{O}_2$) and ($\dot{R}$) in BAS, a further termination step ($R\dot{O}_2 + \dot{R} \rightarrow$ termination) is also included in the mechanism, to enhance the prediction capability for the dissolved oxygen depletion at negligible initial concentration of oxygen.

Eventually, in the most recent version of pseudo-detailed mechanism, a refined set of reactions for peroxy radical inhibition is suggested.

The pseudo-detailed mechanism is presented in Table 2-3, see Kuprowicz *et al* (2007). This version of mechanism has been validated by the experimental results of carried out on the Near Isothermal Flow Thermal Reactor(NIFTR) by Jones *et al* (1995) for various fuel samples.

No	Reaction	A[mol,L,s]	Ea[kcal/mol]	No	Reaction	A[mol,L,s]	Ea[kcal/mol]
1	$I \rightarrow R^{\bullet}$	1×10^{-3}	0	10	$RO^{\bullet}+RH \rightarrow ROH+ R^{\bullet}$	3×10^{9}	10
2	$R^{\bullet}+ O_2 \rightarrow RO_2^{\bullet}$	3×10^{9}	0	11	$RO^{\bullet} \rightarrow$ Rprime +Carbonyl	1×10^{16}	15
3	$RO_2^{\bullet}+ RH \rightarrow RO_2H+ R^{\bullet}$	3×10^{9}	12	12	$OH^{\bullet}+RH \rightarrow H_2O+ R^{\bullet}$	3×10^{9}	10
4	$RO_2^{\bullet}+ RO_2^{\bullet} \rightarrow$ termination	3×10^{9}	0	13	$RO^{\bullet} + RO^{\bullet} \rightarrow RO_{term}$	3×10^{9}	0
5	$RO_2^{\bullet}+ AH \rightarrow RO_2H+A^{\bullet}$	3×10^{9}	5	14	Rprime+RH $\rightarrow$ alkane+ $R^{\bullet}$	3×10^{9}	10
6	$A^{\bullet}+RH \rightarrow AH+ R^{\bullet}$	1×10^{5}	12	15	$RO_2H+SH \rightarrow Product_{SH}$	3×10^{9}	18
7	$A^{\bullet}+ RO_2^{\bullet} \rightarrow Products_{AH}$	3×10^{9}	0	16	$RO_2^{\bullet} \rightarrow R^{\bullet}+ O_2$	1×10^{16}	19
8	$R^{\bullet}+ R^{\bullet} \rightarrow R_2$	3×10^{9}	0	17	$RO_2^{\bullet}+ R^{\bullet} \rightarrow$ termination	3×10^{9}	0
9	$RO_2H \rightarrow RO^{\bullet}+OH^{\bullet}$	1×10^{15}	39	18	$RO_2H+M \rightarrow RO^{\bullet}+OH^{\bullet}+M$	3×10^{10}	15

Table 2-3: pseudo detailed mechanism of normal paraffin liquid phase autoxidation

The "fake" presentation of initiation step in the mechanisms exists since the chain requires an initial source to start the cycle. Normally, when this step is used, its rate is adjusted to be as small as possible to begin the chain. Hence, the rate constant can be increased until oxidation starts and then it is reduced gradually until is just fast enough to start the chain. It supplies a very low level of radicals that are insufficient to interfere with the overall oxidation, see private communication (2005). For the simulation of autoxidation process, another option is to start with an initial low level of alkyl radical ($\dot{R}$) as this would also start the chain.

2.2.3 Surface Deposition

Formation of precursor species is governed by the liquid phase autoxidation. Once generated in bulk fuel, it is transferred from the main stream of bulk fuel, sticking on the wall surface to form deposit layer. Figure 2-4 schematically explains the possible hypothetical paths for surface deposition process.

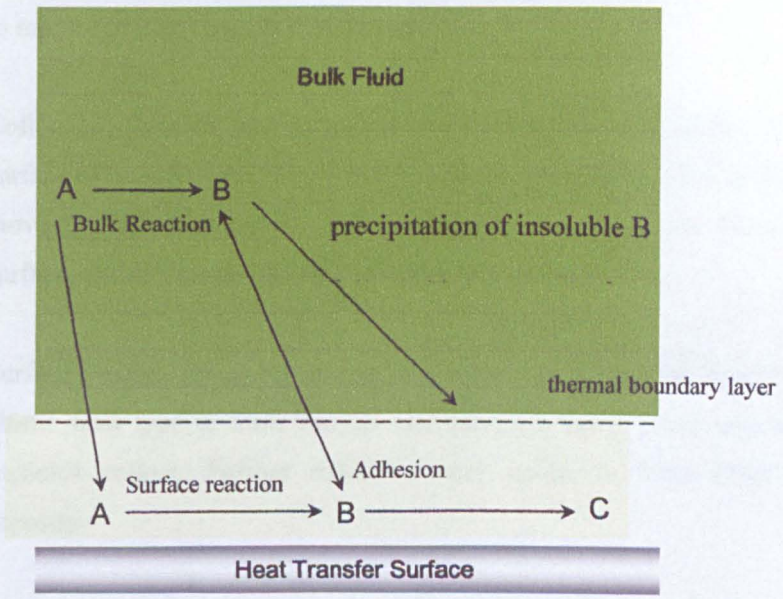

Figure 2-4: A general two stage model for carbon deposition on heated tube, see Bott (1995)

Although the autoxidation reactions have been broadly investigated, very little has been done on the subject of surface deposition. Epstein(1986) and Bott(1995) assumed that the arrival of the precursor species at a surface can occur by two

mechanisms, i.e. gravitational settlement and particle transport. However, in turbulent flow regimes, the gravity effect may be negligible as radial diffusion in bulk fuel is vigorous.

A combination of turbulent diffusion and Brownian motion must drive the precursor at the surface. The small size particles obey the Brownian and eddy diffusion while the large particles move according to momentum forces due to their greater mass. Another possibility for surface deposit formation is to assume that the deposit particles are initiated at the heated surface with little contribution form particles in the bulk fuel. The third possibility is that the surface deposition results from the contributions of both adhering bulk particles and deposits formed at the wall.

Regardless of the precursor migration to the wall, there are a multitude of complex physical interactions which can take place for deposition to occur.

The processes can be briefly highlighted as:, see Hazlett (1991)

i. The agglomeration of insoluble oxidation product molecules in jet fuel to micro spherical particles 500 to 3000 Å,

ii. Collection, through which the micro spherical particles settle on the surface of bulk fuel or collect on the surface after impingement from the moving fluid. Meanwhile, the more volatile species can leave the surface, and in that case heavier species may remain,

iii. Surface Fusion, during which particles may experience coalescence and plastic flow type to form varnish like substrate upon which additional particles collect. Further oxidation may occur to form coke like deposits.

Theses assumptions, however, are in the early stage of research and have not yet been justified.

In most of the design and engineering problems using the Computational Fluid Dynamics (CFD), surface deposition process is considered as a sub mechanism consisted of one-three reactions steps. These steps obey the Arrhenius law, characterised by an activation energy and a pre exponential factor, see Krazinski *et al* (1992), Katta and Roquemore(1993), Ervin *et al* (1996), Katta *et al* (1998), Ervin and

Zabarnick (1998), Ervin (2000) Ervin et al (2003), Wade *et al* (2004), Wade (2005) and Kuprowicz *et al* (2007).

2.2.4 Physical Feature of Deposits

Recent advances in instrumental analysis technology have provided the facilities for more detailed investigation of the carbonaceous deposits generated during the thermal stability. Particularly, the application of Scanning Electron Microscopy (SEM) has been widely applied to visualise topography of deposit.

Altin and Eser(2000) and Altin and Eser (2001) investigated the deposit structure in thermally stressed tubes utilising Temperature-Programmed Oxidation (TPO) and SEM. Combination of these two techniques was applied to investigate the stressed tube surfaces. This resulted in a number of practical information to depict the solid deposit morphology along with the formation mechanism.

TPO operates based on the carbon analyser detecting the oxidation of carbon constituent in deposit, in a furnace over a CuO catalyst bed. The generated CO_2 can then be quantified by a calibrated Infra Red(IR) detector as a function of furnace temperature. As the temperature steadily increases, various peaks in CO_2 production can be observed justifying the multiple" carbon phases" which have different oxidation reactivates. This can be described in terms of different levels of structural order, namely from amorphous to crystalline.

In the experiments carried out by Altin and Eser(2001), JP-8 was thermally stressed in the isothermal flow reactors employing nickel, stainless steel (316 and 304), silicosteel and glass-lined stainless steel tubes at 500°C in a pressurised system(P=34 atm) for a duration of 5 hours at a fuel flow rate of 1 ml/min. The experimental results showed that activity of the surfaces toward carbon deposition decreases in the order Ni > SS 316> Silicosteel> gas-lined stainless steel. This explains the catalytic reactions at the surface play a major role during the fuel thermal stability.

In the TPO analysis, increase of temperature results in well defined peaks in the carbon signal. This indicates that multiple deposition mechanisms occur throughout the thermal stressing. Peaks at lower temperatures were caused by deposit constituents that are highly reactive, such as amorphous carbon and fine filaments which were identified in the earlier work by McCarty and Wise(1979).They utilised temperature programmed surface reaction with hydrogen to characterise carbon

deposit formed on an alumina supported nickel methanation catalyst exposed to carbon monoxide at 227°C.

SEM micrographs of the surface deposited in Figure 2-5 and Figure 2-6 indicate that the presence of faceted crystallites in the deposits along the entire length of the reactor tubes proves that the initiation of deposition is the result of heterogeneous reactions. Smaller crystallites were found on the surfaces with lower catalytic activity, as confirmed by the lower amount of deposition identified on the surfaces which exhibited the least catalytic behaviour. The catalytic effects observed in the studies of Altin and Eser reported that differences exist between the application of untreated and passivated stainless steel tubing in thermal-oxidative flow experiments.

The TPO analysis of Altin and Eser(2001) for Silicosteel showed that the inert coating inhibits the formation of deposits with a high degree of structural order, or low reactivity in contrast to the results found for SS 316 and SS 304. Furthermore, the SEM images in Figure 2-5 and Figure 2-6 show the spherical deposit particles formed on the coated surface indicating that Silicosteel coating does not catalyse deposit formation.

Altin and Eser(2001) suggested that the presence of different carbon phases can be attributed to sequential processes of deposition using the assumptions of Albright and Marek(1988).They assumed that, firstly filamentous carbon is formed on the clean surface followed by thickening of the filaments and collection of tar droplets. Then non porous deposits are created away from the metal surface and gain additional non porous carbon thickness through the adsorption and reaction of micro species during the thermal stressing of liquid hydrocarbons.

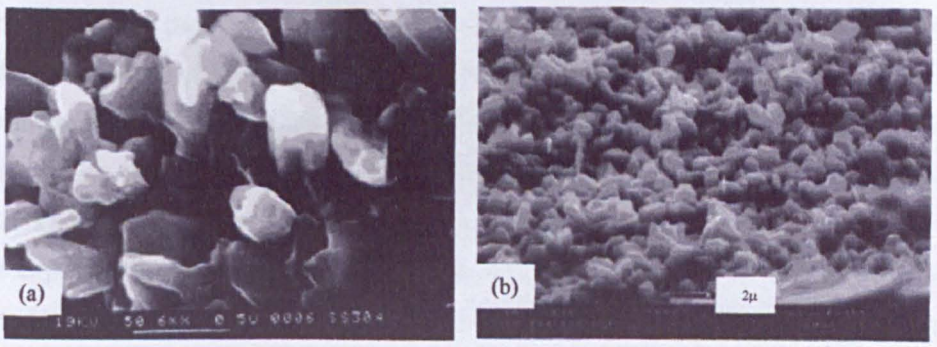

Figure 2-5:SEM micrographs of carbon deposits from JP-8 decomposition at 500°C and 34 atm with 1 mL/min flow for 5 hrs on SS 304 surface in (a) the initial 2.5-5 cm, and (b) the centre 12.5-15 cm sections of tubing used in the experiments of Altin and Eser(2000)

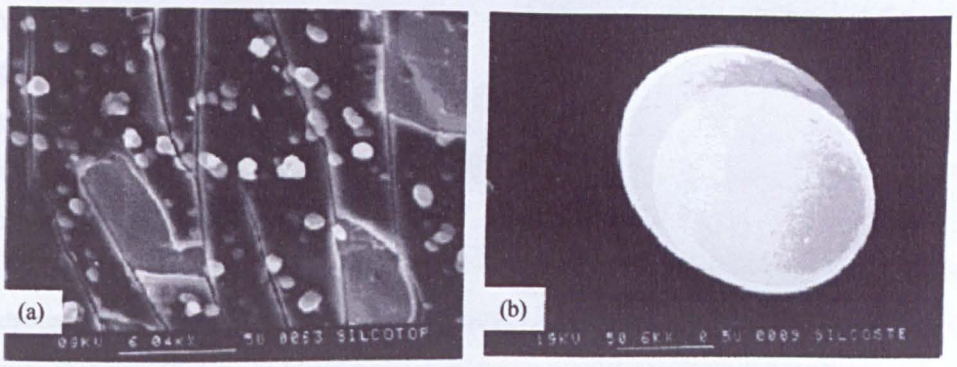

Figure 2-6: a) SEM micrographs of carbon deposits on Silicosteel centre segment (10-12.5 cm) of the 20 cm pipe, and (b) magnified spherical particles from the same piece, see Altin and Eser(2000)

2.2.5 Compositional Impact of Jet Fuel Constituents upon Thermal Degradation

The impact of heteroatomic compounds on jet fuel thermal stability has been the research subject for numerous investigators. Consequently, it was shown that in spite of considerably low concentration of these compounds in jet fuel, they are regarded as the most crucial species throughout the processes.

2.2.5.1 Impact of Various Classes of Hydrocarbons

The impact of hydrocarbons on liquid phase oxidation of hydrocarbons has been widely reviewed by Hogin and Clinkenbeard(1960), Mushrush and Hazlett (1984), Mushrush *et al*(1985), Hazlett (1991), Jones Balster (1993), and Hazlett *et al* (1977).
A general agreement indicates that fuel thermal stability increases in the order of normal alkanes, pure aromatics and naphtenes, see Fathoni and Batts(1991). Hogin and Clinkenbeard (1960) reported that the stability decreases in the order of paraffins, naphtenes, aromatics, olefins and diolefins. Similarly, Wallace observed that the hydrocarbon oxidation decreases in the order of alkyl aromatics, di olefins, mono olefins and paraffins, see Fathoni and Batts(1991).
The experimental results carried out by the department of "Fuel Science" in the Penn State University(1993) on the thermal stressing of straight-chain hydrocarbons proved that n-octane is the most thermally stable sample with no emergence of deposit until 450°C whereas n-dodecane and n-tetradecane were both less stable at 400°C. Additionally, in the condition where hydrocarbon experiences low temperature and short thermal exposure time, no deposit was formed. However, at the higher

temperatures where moderate formation of deposit was observed, alkyl benzenes, and naphatalenes were detected in the stressed liquid hydrocarbon. Eventually, at very high temperatures and long stress periods, where large amount of deposit were generated, alkylated naphatalenes, fluorenes, anthracenes, and pyrenes were found in the thermally stressed hydrocarbon.

A further observation states that when the largest compound present in the liquid hydrocarbon are naphatalenes, only negligible amounts of deposits is generated. This proves that naphthalene is likely to be precursor to solid deposit formation.

Malhotra *et al(*see Fathoni and Batts(1991)) showed that pure alkylnaphtalenes and other polynuclear aromatics are important sources of gum formation. The high proportion of these hydrocarbons results in the least stable hydrocarbons.

Other series of experiments performed by the department of "Fuel Science" in the Penn State University proved that for four isomers of butylbenzenes (normal, iso, and secondary and tertiary tetra butyl benzenes) the degree of branching in the side chain affects the reactivity of alkyl benzenes. The order of reactivity was found to be decreasing in order of normal, sec, iso and tert butyl benzene. Therefore, due to the variations in the reactivity order, their propensity to form carbonaceous solids is different.

2.2.5.2 Impact of Oxygenates

It has been generally agreed that during the period of thermal exposure, oxidised compounds are generated. These may participate in the processes that are responsible for surface deposition, see Schwartz (1962), Kendall and Mills(1986), Hazlett (1991) and Jones *et al* (1998).

Pickard *et al* (1998) reported that the rate of autoxidation process is a function of the trace quantities of hydroperoxides. Although insignificant rate of thermal degradation occurs in a non oxidising environment within the jet fuel, the presence of both oxygen and hydroperoxides increases the oxidative degradation. Under this situation, lower temperature is required for detrimental reactions to take place, see Watkins *et al* (1989). The secondary oxygen products during jet fuel thermal degradation are aldehydes. These oxygenate species are subject to further chemical transformations generating the carboxylic acids by the intervention of several oxidants such as alkaline hydroperoxides and dissolved oxygen, see Mushrush *et al* (1985).

2.2.5.3 Impact of Dissolved Metals

A number of metals in the form of solubles and/or insolubles are detected in petroleum products. It has been known for a long time that metals play significant role throughout the liquid phase autoxidation process, in the order of Cu>Al>Fe, see Fathoni and Batts(1991).

Pickard *et al* (1997) reported that the autoxidation is homogenously catalysed by cations of dissolved metals contributing to hydroperoxides decomposition. Hence, the accurate quantification of the metals in jet fuel is essential for the investigation of the processes.

Inductively Coupled Plasma(ICP) techniques in association with the Atomic Emission Spectroscopy (AES) and/or mass spectrometric detection can be applied for the identification and quantification of dissolved metals, see Kuprowicz *et al* (2007). The degree of accuracy in the quantification of dissolved metals is crucial as they can be active at very low concentrations. For instance, it is reported by Kuprowicz *et al* (2007) that dissolved copper (Cu) is active at a concentration of as low as 25 ppb. Although, Pande and Hardy (1997) reported that dissolved copper at approximately 25 μg/L can significantly increase the rate of autoxidation in some fuels.

While, some of the refining processes, such as Merox and hydrotreating have completely replaced the copper, this still can be detected in the jet fuel through contact with copper containing alloys in the fuel handling process.

All jet fuels contain measurable levels of Cu, Fe, Mg and Zn. Cu and Mn exhibit wide variation in concentration while the others show fewer changes.

It is believed that there is an inverse relationship between the amount of Cu and Mn in jet fuels in a sense that fuels with a high content of Cu tend to have low amount of Mn concentration and vice versa.

It has also been shown by Kuprowicz *et al (2007)* that Fe, Mg, and Zn usually become significant at levels greater than those presented in Table 2-4.

Fuel Sample	Cu (μgL^{-1})	Mn(μgL^{-1})	Fe(μgL^{-1})	Mg(μgL^{-1})	Zn(μgL^{-1})
F2747(JetA-1)	40	<10	93	33	89
F2959(Jet A)	<18	58	174	34	153
F3084(Jet A)	25	<10	142	34	101
F3166(Jet A)	111	13	142	34	100
F3219(Jet A)	58	<10	182	40	128
F3084(JP-8)	<18	<10	196	29	131
F4177(JP-8)	<18	88	144	26	69

Table 2-4 :Dissolved Metal Content of the Seven Fuels Studied (Via ICP-AES), see Kuprowicz(2007)

It was also reported by Pickard and Jones (1997) that the iron content in jet fuel might be detected in the forms of both iron oxides Fe_2O_3(hematite) and Fe_3O_4 (magnetite) at sizes 0-10 μm with hematite being the major component.

The following reaction scheme was suggested by Pickard and Jones for hematite showing the role of hydroperoxide decomposers.

$$RO_2H + Fe_2O_3 = [Fe_2O_3RO_2H]$$

$$[Fe_2O_3RO_2H] \rightarrow [(Fe_2O_3)_{1/2}R\dot{O}] + [(Fe_2O_3)_{1/2}H\dot{O}]$$

$$RH + [(Fe_2O_3)_{1/2}R\dot{O}] \rightarrow 0.5Fe_2O_3 + ROH + \dot{R}$$

$$RH + [(Fe_2O_3)_{1/2}H\dot{O}] \rightarrow 0.5Fe_2O_3 + H_2O + \dot{R}$$

In this scheme an intermediate species can form during the absorption of RO_2H on the surface of Fe_2O_3. The generation of the radical is assumed to proceed through the H-atom abstraction by RH from the surface absorbed radicals. Cu can be held in solution as chelated complex with natural fuel constituents. In this form, it is assumed to be able to catalyse the autoxidation process in the presence of dissolved oxygen.

2.2.5.4 Impact of Sulphur Compounds

There is a major disagreement on the effect of sulphur compounds on fuel thermal stability. It can be explained based on the fact that specific sulphur compounds in certain fuels exhibit different behaviour while exists alone rather than being

associated with others. In other word, the interaction between different classes of sulphur compounds can show positive, negative, or neutral consequences.

Organic sulphur compounds are identified and quantified in all petroleum samples, regardless of different sources. The sulphur concentration may vary from few ppm to several percent depending on the origin of the crude oil. These compounds appear in different types as presented in Table 2-5.

It was shown by Thompson *et al*(1949) that elemental sulphur, disulfides and polysulfides are active promoters in the course of autoxidation while aliphatic mercaptans and aliphatic sulphides have limited effect. In contrast, Kuprowicz *et al*(2007) reported that amongst all these classes, only sulphides and disulphides predominantly contribute to jet fuel thermal stability processes.

Schwartz *et al* (1962) reported that alkylmercaptans, sulphides and disulphides enhance the rate of gums formation particularly in the spec of gasolines produced through cracking. Mushrush *et al* (1991) stated that thiophenol is the most detrimental of the sulphur compounds while Fink and Nixon (1954) (see also Fathoni (1991)) showed thiophene to be equally deleterious.

The results of experiments carried out by Daniel *et al*(1991) exhibit that addition of thiol and thiophene at 121-135°C to jet fuel increases thermal stability, while addition of aliphatic sulphides and disulphides slightly decreases formation of carbon deposit. Conversely, it was considered by Loeffler(see Fathoni(1991)) that decreasing order of reactivity is thiophenol, tetrahydrothiophene and thiophene. The reactivity order by Mushrush *et al* (1991) was reported to be thiophenes, aromatic thiols, thiols and alkyl sulphides.

Class of Sulphur	Chemical Formula
Free, elemental sulphur	**S**
Hydrogen sulphide	**H_2S**
Organic sulphide	**R_1-S-R_2**
Organic disulphide	**R_1-S-S-R_2**
Sulphonic acid	**R-SO_3H**
Thiophenes	**C_4H_4S**
Mercaptans	**R-SH**

Table 2-5: type of sulphur compounds in jet fuels

The amount of different classes of sulphur compounds in the variety of military US jet fuels are presented in Table 2-6

Sample	Sulphides and Disulphides(ppm)	Thiphenes	Benzo-thiophenes	Dibenzo thiophenes	Total from adding classes (ppm)	Total from correlation Curve(ppm)
POSF-2959	1056	70	714	138	1978	1975
POSF-3459	985	54	234	56	1462	1445
POSF-3461	559	63	180	112	915	950
POSF-3684	253	18	163	73	507	526
POSF-3166	581	29	273	66	950	938
POSF-3084	588	7	199	109	909	947
POSF-2980	264	54	249	46	613	618
POSF-3084	544	18	310	94	978	993
POSF-3133	-27	12	14	-2	26	-6
POSF-2827	672	30	215	120	1056	1107
POSF-3219	352	16	117	47	535	560
POSF-3305	474	41	243	153	911	944
POSF-3444	-70	-8	29	12	79	12

Table 2-6: Sulphur Constituents in Selected Samples of Military Jet Fuels(2001)

2.3 A Literature Review of Experimental Methods Applied for the Investigation of Jet Fuel Thermal Degradation

Investigation of jet fuel thermal stability is generally based on three main aspects, namely chemistry of fuel thermal stability, materials and surface science, and engineering application. Regarding the mutual impact of chemistry and flow characteristics and considering the significance of metal surface on the processes, determination of one aspect requires the others being sacrificed.

Hazlett (1991), Taylor (2005) and Morris *et al* (2002) reported that for the study of many aspects of thermal stability including chemical kinetics of the processes, impact of homogenous and heterogeneous catalysis, fuel compositional effect, and deposit analysis, the impediments caused by the effect of fluid flow ought to be ignored through the application of " static method".

Depend on the significance of fluid flow on the processes, determination of reaction profiles can be examined by the application of "flow or dynamic devices". However, from an engineering point of view, component design, safety, performance and durability, requires the application of more realistic approach, capable of providing accurate representation of jet fuel thermal degradation in a close condition to the actual real jet fuel system.

2.3.1 Classifications of Thermal Stability Test Methods

The jet fuel thermal stability test methods can be classified as:

i. Static methods;
ii. Flowing methods;
iii. Simulator rigs;

2.3.1.1 Static Methods of Jet Fuel Thermal Stability

There are five main test methods used for the static determination of the jet fuel thermal stability presented in Table 2-7

Test	T(°C)	Duration	Fuel Volume	Analysis
QCM/Parr bomb	140	15h	60ml	Headspace O_2 by sensor
ICOT(ASTM 4871)	180	5h	100ml	Filtration and gravimetric analysis
Flask oxidation	140-190	1-4h	400ml	O_2 in exit gas; oxidation rate
Thin film oxidation	180-260	1-2h	2ml	O_2 , hydroperoxide concentrations
TSRT(GOST 11802)	150	4h	50ml	Filtration and gravimetric analysis

Table 2-7 :Classification of static methods of jet fuel thermal stability, see Hazlett (1991), Morris *et al* (2002) and Taylor(2005)

2.3.1.1.1 Quartz Crystal Microbalance (QCM)

During the test, jet fuel sample is saturated with the air and heated up to 140°C for duration of 15 hours. The QCM is employed to record the accumulated surface deposits. An oxygen sensor is used to detect the autoxidation process. Deposits form on the quartz crystal oscillator, lowering its characteristics frequency. The change of the frequency is then converted to a surface deposit in the units of microgram/cm^2 versus time.

Figure 2-7 represents the schematic of the QCM apparatus. The reactor includes a 100 ml 316 stainless steel pressure vessel, gas inlet/outlet tube, thermocouple, and pressure vent. The heating system is consisted of a clamp-on band heater with the temperature being controlled by a PID controller employing a thermocouple immersed in the sample. A magnetic stirrer is used to minimise spatial temperature

gradients. Autoxidation monitoring is applied to detect the level of dissolved oxygen in the reactor headspace. The oxygen sensor is capable of measuring oxygen level in the reactor headspace from zero to 100 percent with precision of ± 0.1%.

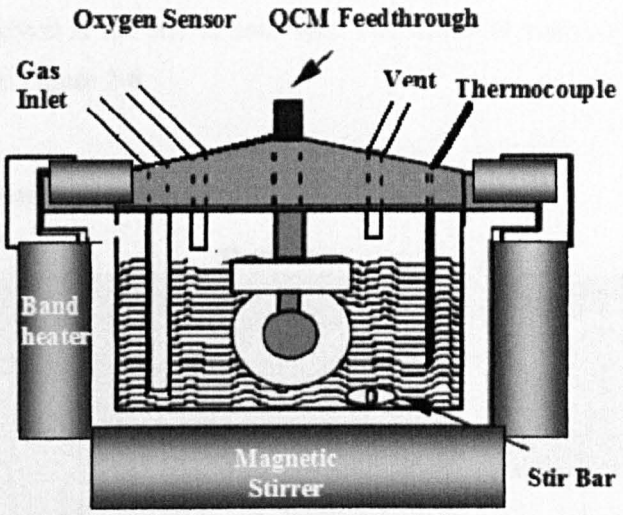

Figure 2-7: Quartz Crystal Microbalance(QCM) schematic, Taylor(2005)

2.3.1.1.2 Isothermal Corrosion Oxidation Tester (ICOT)

The ICOT is applied to measure the effectiveness of the thermal stability of additives by stressing the blend of baseline fuel with additive at a constant temperature in the situation of flowing saturating air. Thermal stability is determined by the amount of solids which remain on the filter. The filter is a glass micro fibber with a particle preservation of 0.7 to 1 μm.

This test method cannot be applied for all jet fuel types. Some fuels, for instance, JPTS do not produce measurable deposit at these testing conditions, although, other fuels produce higher amount of deposit. The most appropriate for this test are fuels with moderate propensity of deposit formation.

The complete description of this method is provided in ASTM method D4871-88, see Hazlett(1991), Morris *et al* (2002) and Taylor(2005).

2.3.1.1.3 TSRT (GOST 11802)

In this method, jet fuel is heated up to approximately 150°C over a period of 5 hours. Thermal degradation of sample occurs in the reaction vessel, in the presence of a copper block with a catalytic impact. The fuel quality is determined by the amount of deposit weighted at the end of each test. The different components of this apparatus are presented Figure 2-8.

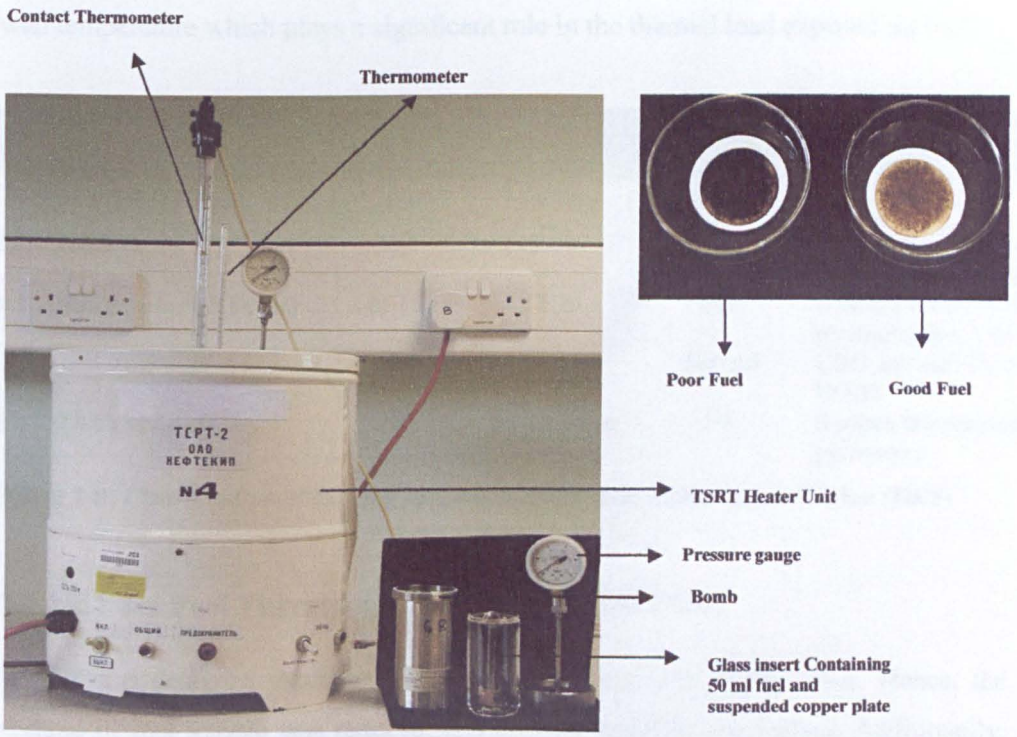

Figure 2-8 :GOST 11802 TSRT-2 apparatus, see Taylor (2005)

2.3.1.2 Flowing (dynamic) Thermal Stability Test Methods

Five test methods are applied for the investigation of fuel thermal stability when the effect of fluid flow is considered, as presented in Table 2-8.

The first developed flowing test method (not listed in the table) is CRC/ASTM Coker, see Hazlett (1991) and Morris *et al*(2002). This apparatus was developed as a dynamic test device in the 1950s through a joint military/industry group, under the

authority of the Coordinating Research Council, in response to the problems related to the thermal stability in US aircrafts. The test method was accepted as a tentative standard in 1959 by ASTM.

CRC/ASTM Coker was applied for the identification of fuel specifications for both military and civil aviation applications. However, it was soon replaced by the jet fuel thermal oxidation tester (JFTOT), due to a number of shortfalls. The major drawbacks were the large volume of sample (19 liter) and long duration of experiment. In addition, the controlling factor in this test method was fuel temperature rather than wall temperature which plays a significant role in the thermal load exposed on fuel.

Test	T(°C)	Duration	Fuel Volume	Analysis
JFTOT(ASTM D3241)	260	2.5h	600ml	Tube color and ΔP
gJFTOT(USN)	260	2.5h	450 ml	Gravimetric analysis of test strip and filter
Single-tube reactors(NIFTR)	140-150	72h	1-2L	Oxidation rate by O_2 measurement, CBO
HLPS	200	2-10h	600 ml	CBO and ΔP; O_2 and RO_2H
HiReTS(ASTM 6811)	290	65-125 min	5 L	Surface temperature by pyrometry

Table 2-8: Classification of flowing thermal stability test methods, see Taylor (2005)

2.3.1.2.1 Jet Fuel Thermal Oxidation Tester (JFTOT)

JFTOT was designed to overcome some of the shortfalls of the coker. Hence, the volume of fuel sample was reduced, and the test duration was halved. Additionally, the fuel stressing temperature is increased by the application of a Nitrogen pressurised system. The heating mechanism is provided by the resistance heating through the application of an electrical circuit. The temperature profile starts from the ambient at the fuel inlet to the control temperature (38.7 mm from the fuel inlet for the standard aluminium heater tube) as shown in the below diagram.

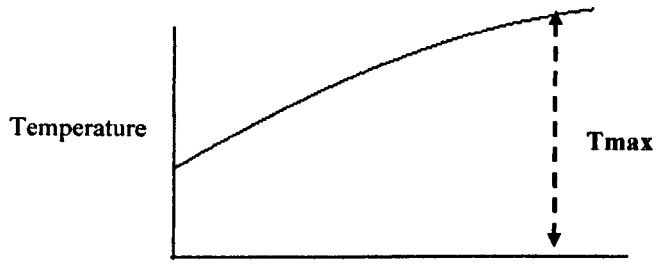

JFTOT is equipped with a filter located at the exit of tube housing which is at substantially lower temperature. The pressure drop limit for the filter is 3.3 kPa.

This test method has been accepted by the ASTM as D3241 since 1973. In this standard, JFTOT covers the procedure for rating the tendencies of a gas turbine fuel to form deposit within the fuel system. Therefore, jet fuel is rated at a minimum temperature to determine if it meets acceptance criteria.

The JFTOT test determines whether the fuel passes or fails the qualitative test based on the break point of the jet fuel. The breakpoint is defined as the highest temperature in degree°C at which the fuel receives a passing rating. For instance, the minimum JFTOT breakpoint for a stable jet fuel is 260°C. Therefore, JFTOT requires a heater tube control temperature of 260°C.

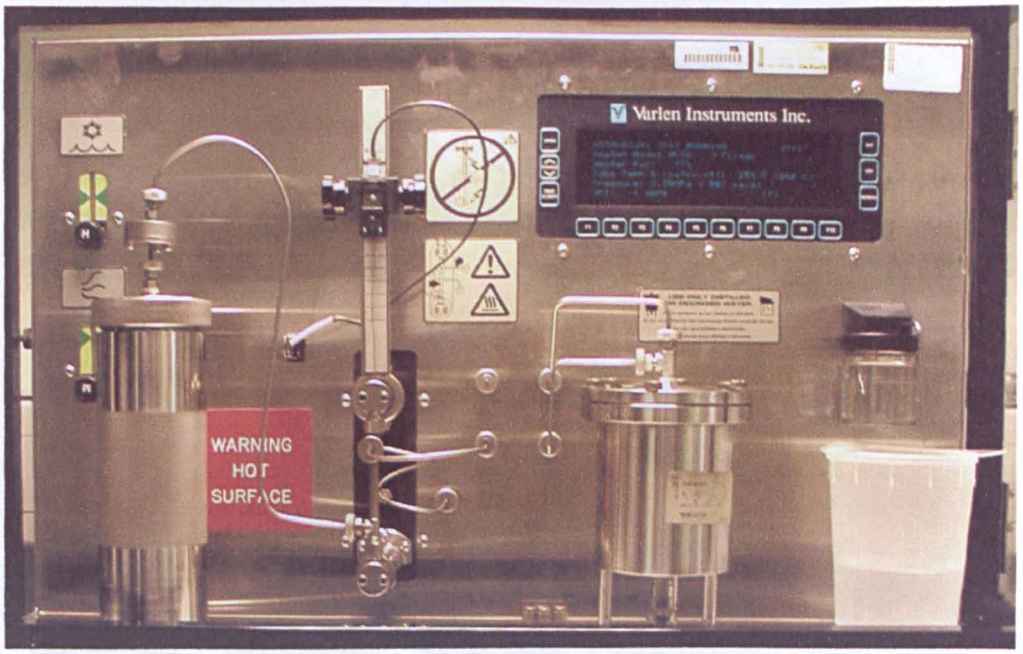

Figure 2-9: Jet Fuel Thermal Oxidation Tester(JFTOT) apparatus, see Taylor (2005)

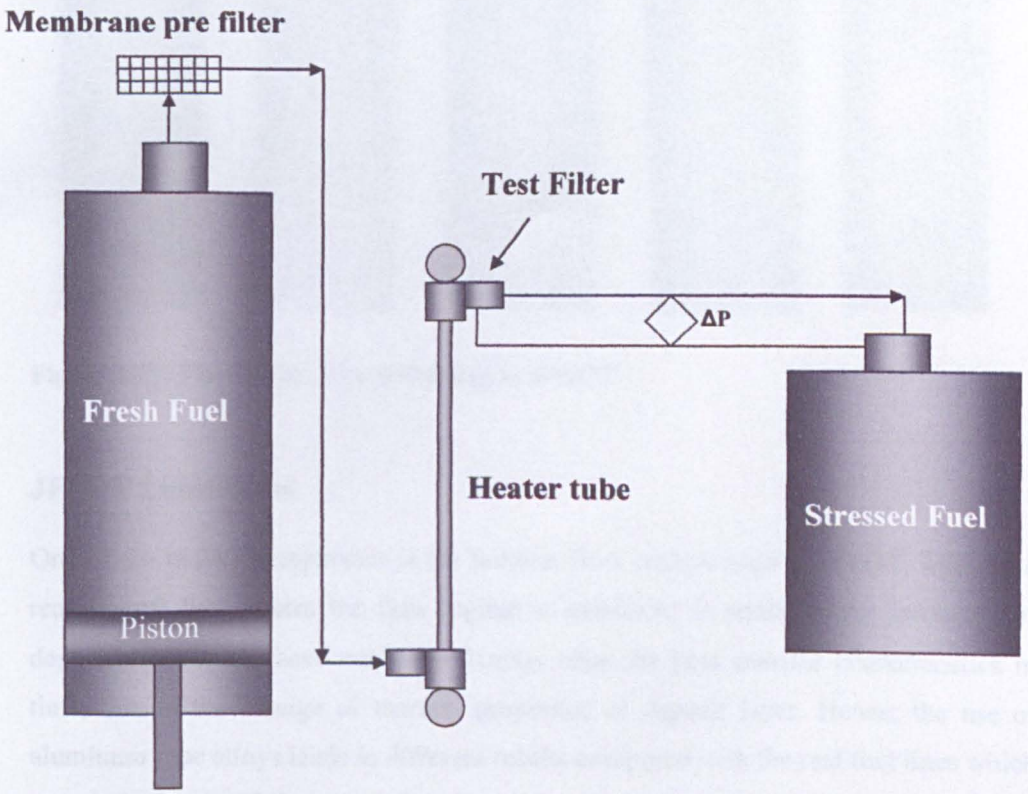

Figure 2-10: Jet Fuel Thermal Oxidation Tester(JFTOT) schematic, see Taylor(2005)

The value given by JFTOT is a qualitative measure and is not practical in terms of estimating the quantity of deposits that form in a real aircraft engine.

A few results of tube color analysis are presented in Figure 2-11. These results are based on the experiments using a pre aerated fuel, with a flow rate of 3 ml/min for a total duration of 2.5 hours thermal stressing. The JFTOT tubes were made from the 6061 aluminum tubes.

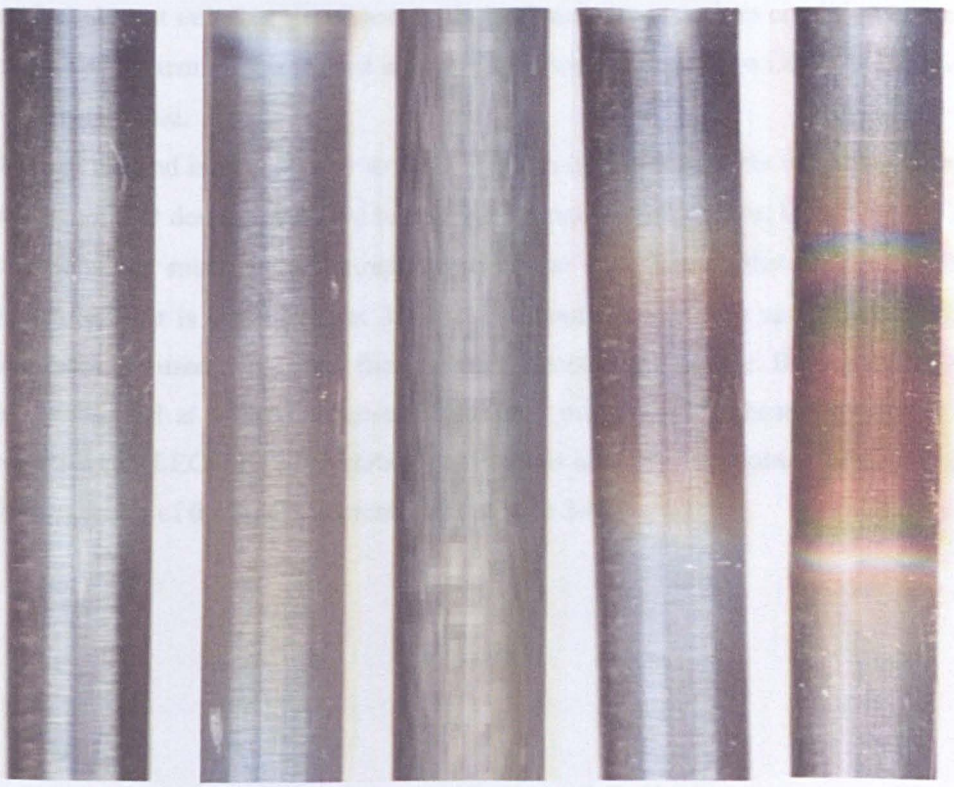

Figure 2-11: The results of jet fuel rating in JFTOT

JFTOT Limitations

One of the main discrepancies is the laminar flow regime used in JFTOT, while in a real aircraft fuel system the flow regime is turbulent. In addition, the formation of deposit on tube surfaces may significantly alter the heat transfer characteristics in time, due to the change of thermal properties of deposit layer. Hence, the use of aluminum tube alloys leads in different results compared with the real fuel lines which are made from stainless steel. Moreover, in the aircraft engine, the time space for

thermal degradation is the order of hundreds hours, while a specification test may take no more than a maximum of one day. In general, such a short experimental time space requires an increased temperature regime to accelerate the rate of chemical transformations.

2.3.1.2.2 Hot Liquid Process Simulator (HLPS)

The HLPS is designed and manufactured by Pratt & Whitney. This is an accelerated bench scale test unit that simulates the thermal stability at a close condition to the jet engine fuel system. When is used in association with Carbon Burn Off (CBO), deposit can be quantified.

This test method is very similar to the JFTOT in operational mode but differs from it on the modular design, extended temperature range, and flow rate. Moreover, the test conditions are much more stringent than those specified in the standard JFTOT procedure. Test is carried out at 335 °C for about 5 hours. The series 316 stainless steel tubes are used to consider the catalytic impact of the surface. During the test, jet fuel is pumped at a fixed volumetric rate of 3 ml/min over a heated tube. CBO is applied using LECO RC-412 carbon analyzer to quantify the amount of deposition. The schematic of the HLPS is presented in Figure 2-12.

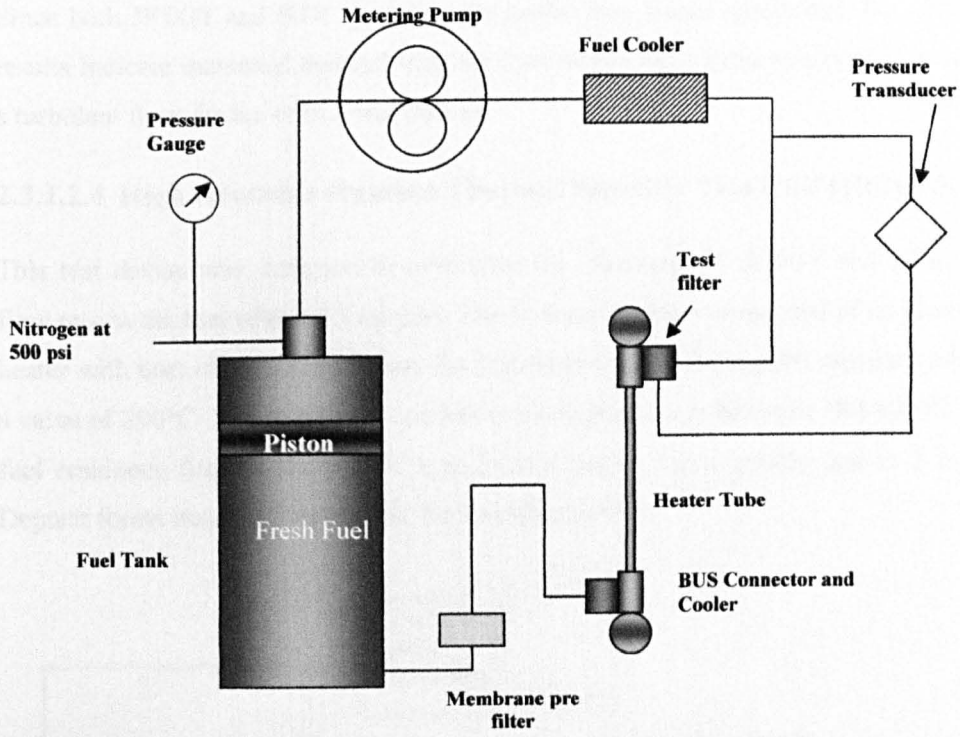

Figure 2-12: Hot Liquid Process Simulator(HLPS) schematic, see Taylor(2005)

2.3.1.2.3 Single Tube Reactor (STR)

This apparatus was developed by the U.S.Navy, aiming to quantify the deposit. The fuel flow through the STR is laminar with a rate of 10 ml/min and the corresponding Reynolds number at the fuel inlet is less than 2000.

The STR's heating system is consisted of two identical sections. The first is applied for the pre heating and the second is used to supply the heating for thermal stress. The ensemble heating system operates to maintain the bulk fuel temperature exiting the pre heater section to a value of approximately120°C and the exit of the main heating system to a value of 190°C.

The outside wall temperature for the main heater system ranges anywhere from 325-400 °C and the residence time of 0.82 sec/inch is estimated to produce a measurable amount of deposit in the test section. The total test duration will take up to 12 hours. This test unit is subject to CBO analysis.

Since both JFTOT and STR operation are under less severe conditions, the obtained results indicate increased thermal stability than would have been achieved if tested in a turbulent flow device or in a real aircraft.

2.3.1.2.4 High Reynolds Number Thermal Stability Test Unit (HiReTS)

This test devise was designed to overcome the shortages of JFTOT and STR. The flow rate in the fuel tube is 35 ml/min. The heating system is consisted of an electrical heater with bars clamps to maintain the bulk temperature exiting the capillary tube to a value of 290°C. The maximum outside wall temperature is between 380-400°C. The fuel residence time is about 0.01 s and the duration for a quality test is 2 hours. Deposit forms inside the tube at the fuel/metal interface.

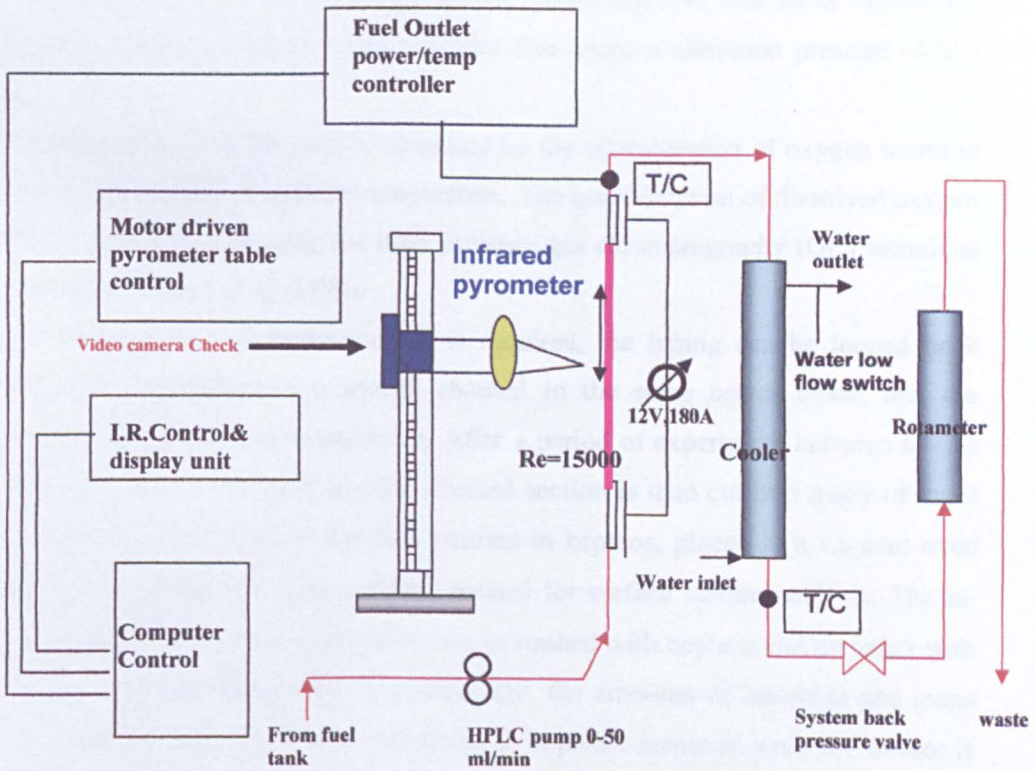

Figure 2-13: Schematic of High Reynolds Number Thermal Stability Test Unit (HiReTS)

2.3.1.2.5 Near Isothermal Flow Thermal Reactor (NIFTR)

This test rig was developed by Jones and Balster to create a reaction medium with the uniform distribution of temperature for the investigation of liquid phase autoxidation process. Using relatively low flow rate for long length of tube, the bulk fuel temperature and wall temperatures are kept at the same temperature, therefore chemical reactions occur under near-isothermal conditions.

The NIFTR is a dynamic test tube, made of the stainless steel, through which fuel passes with a relatively low velocity, thus providing high residence time. The temperature at the external wall of the tube remains constant during the test. This constant temperature is provided by surface contact within a heated copper block. This test devise is also consisted of a syringe pump which pushes fuel through a 32 inch long heater tube section, through a filter containing a 47 mm silver membrane, and finally through a backpressure regulator that keeps a minimum pressure of 350 psi.

The oxygen content at the inlet is estimated by the concentration of oxygen found in the air-saturated fuels at ambient temperature. The quantification of dissolved oxygen depletion occurs in-line using the high pressure gas chromatography (GC) technique developed by Rubey *et al* (1995).

When longer period of thermal stress is required, the tubing can be looped back through the application of a second channel in the same heater block, and the membrane filter is moved downstream. After a period of experiment between 6 – 72 h, the tube drained overnight and the stressed section is then cut into many of the 2 inch sections. These sections are then washed in heptane, placed in a vacuum oven (115°C) for a period of 12 h, and then treated for surface carbon analysis. The in-filters are then cut into two equal parts; one is washed with heptane and the other with mixture of heptane and acetone. Consequently, the amounts of insoluble and gums may be differentiated as both are insoluble in heptane, however, only the former is insoluble in acetone. Therefore, the amount of bulk insolubles caused by thermal stressing the fuel may be measured through the analytical chemistry methods.

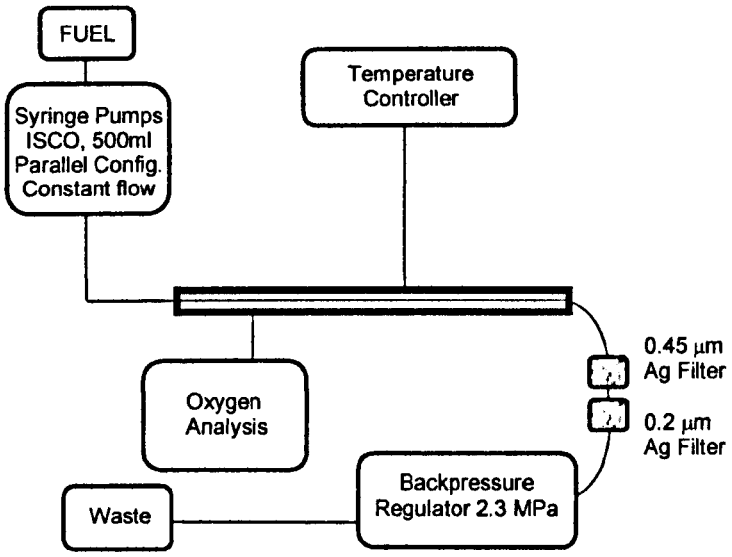

Figure 2-14: The schematic of NIFTR

2.3.1.3 Simulator Rigs

2.3.1.3.1 Aviation Fuel Thermal Stability Test Unit (AFTSTU)

This is described in Chapter 4.

2.3.1.3.2 Naval Aviation Fuel Thermal Stability Simulator (NAFTSS)

It was originally called as AFTSTU by the developers, Rolls Royce. Therefore the description of AFTSTU can be applied, see Chapter 4.

For the quantification of deposited carbon, there are three main methods explained below:

i. **Carbon Burn Off (CBO)** is based on the assumption that the total amount of deposit can be estimated from the carbon content. Despite high applicability, this method is not recommended for the aluminum heaters as the low melting point of aluminum precludes in a standard carbon, hydrogen, nitrogen analyser.

ii. **Dielectric Breakdown:** Measurements are restricted to the deposits which are thick enough to offer sufficient electrical insulation. The assumption with this technique is that all fuels under test conditions will generate thermal insulative deposits with the same value of dielectric constants.

iii. **Optical Methods Including Ellipsometry and Interferometry:** This is based on the polarisation of light passing through a thin reflective surface, for instance, thermal deposits on JFTOT tube surface. Therefore, it is not appropriate for the cases of very thick deposits.

2.4 Application of Computational Fluid Dynamic Modeling on Jet Fuel Thermal Degradation

It was addressed that the formation of surface deposition is, to some extent, influenced by flow characteristics. Besides, convective heat transfer through the wall as well as from the deposit to the fluid (and also throughout the bulk fuel) is also the important parameter in the course of thermal degradation. Therefore, the predictive methods capable of accurately imitating the heat transfer within the tube are essential for the investigation of processes.

Although, the empirically based fouling models can potentially be used to a number of engineering problems, they are usually limited to the specific experimental configurations. In contrast, Reynolds Averaged Navier Stockes (RANS) models in association with different chemical models have been applied by various researchers to investigate thermal degradation behaviour of the jet fuels for a broad range of test conditions and geometries. In spite of applicability, RANS models are limited to the thin deposit layer problems, when fuel boundary does not noticeably modify the heat transfer and flow pattern.

The real time evolution of deposit in the fuel passage is a complex task. Firstly, the physics of surface deposition is not well understood. The complexity of surface deposition, in almost all of the CFD models, is disguised by a sub mechanism of Arrhenius type. Correspondingly, instead of inclusion of more stages of deposition such as agglomeration, collection, fusion, and nucleation, it is assumed that the interaction of surface and precursor species is described in one, two, or three step,

each characterised by the reaction rate parameters. The appropriateness of such parameters can be improved through the adjustment and optimisation techniques once the experimental results are provided. Secondly, the accuracy of real time evolution of deposit is constrained by the lack of information about thermal properties of deposit as the functions of time and temperature. It is evident that the change of thermal conductivity and density affects the heat transfer rate from the wall towards the bulk fuel.

The purpose of this subsection is to review the most of the CFD modeling attempts for the investigation of jet fuel thermal degradation.

2.4.1 Early CFD/Chemistry Models

Due to the simplicity and the lack of more descriptive chemistry models, global chemistry was used in CFD calculations by Krazinski *et al* (1992), Katta and Roquemore (1993), Ervin *et al* (1996) and Katta *et al* (1998).

The global chemistry considers only one reaction for the autoxidation step as following:

$$\text{Fuel} + O_2 \rightarrow \text{products}$$

In this case, the overall reaction of autoxidation can be represented by one rate equation. This is a product of a rate constant and the concentration of oxygen with simple reaction order as presented in Eq 2-1

$$-\frac{d[O_2]}{dt} = k[RH][O_2]^n \qquad \text{Eq 2-1}$$

The CFD models based on the global chemistry usually assumes that the O_2 consumption proceeds through a reaction order of unity, see Ervin and Zabarnick(1998). In some cases, however, is assumed that the overall reaction order is zero until the concentration of dissolved oxygen reaches an arbitrary value and then the order is set to unity.

Katta and Roquemore (1993) used a four step chemistry for the simulation of the real time evolution of deposit in a cylindrical passage. In this chemistry model, it was assumed that the precursor is produced from the reaction between fuel and dissolved oxygen. Another global reaction step was included to limit the concentration of the

precursor at higher temperature which considers precursor transforms to the soluble species. It was further assumed that the longer period residence time that occurs in the wall adjacent layer causes the autoxidation reaction to underpredict the chemical reaction rate for the laminar sub layer. Therefore, another step was included in the model as wall reaction which accounts for the emergence of deposit from the direct reaction of fuel and oxygen. The precursor species formed in the bulk fuel are transported to the wall through the combination of convective fluid motion, molecular and turbulent diffusion processes. For the precursor sticking on wall, a model was suggested. However, the lack of a fundamental understanding of the processes contributed in sticking caused this aspect to be excluded from their model and a simple model based on the homogeneity of the wall was suggested which considers a direct conversion of the precursor to the deposit.

Reaction Index	Reaction	A[1]	Ea[2]
1	fuel + oxygen → precursor	1E8	30000
2	precursor → soluble	3E15	35000
3	fuel + oxygen → deposit	6.34E-8	8000
4	precursor → deposit	1E20	0

Table 2-9: rate parameters and units for the global chemistry model, see Krazinski *et al* (1992)

The chemical kinetic parameters used by Katta and Roquemore are presented in Table 2-9 that initially were suggested by Krazinski *et al*(1992). Their model however, underpredicted the total amount of deposit, therefore the rate parameters were modified as presented in the following table.

xliii

[1] the units for the pre exponential factor in this mechanism is not the same for all reaction steps, the unit m^3/mole.s was used for the reaction 1, 1/s for reaction 2, m^4/mole.s and 1/s.

[2] as for activation energy, the unit of cal/mole.k was used for the first three reaction steps and the unit for reaction 4 was m/s

Reaction Index	Reaction	A	Ea
1	fuel + oxygen → precursor	3E8	27000
2	precursor → soluble	1E18	40000
3	fuel + oxygen → deposit	6.34E-8	8000
4	precursor → deposit	1E20	0.1

Table 2-10 : modified rate parameters for the global chemistry model

In Katta and Roquemore models the deposit was allowed to grow on the wall surface in a way that after each time step the geometry of the fuel deposit interface is subject to change. The experimental results of Hardy *et al* (1992), Jones *et al* (1993), Jones *et al* (1995), Heneghan *et al* (1994) and Heneghan *et al* (1996) proved that the rate of autoxidation in the most of the liquid hydrocarbons is more or less independent from the dissolved oxygen concentration. Therefore, it was concluded that formation of precursor is due to the chemistry of hydroperoxide and not directly from reactions involving molecular oxygen. The global chemistry schemes are, however, unable to address these aspects. Accordingly, Katta *et al* (1998) employed a semi detailed scheme on the basis of a general free radical mechanism, involving a number of steps in a similar manner with the experimental observations of Jones *et al*(1993).

Reaction Index	Reaction	Pre-exponential Multiplier, A	Activation Energy, E_a (kcal/mol)
	Bulk Fuel Reactions		
1	$Fuel + O_2 \rightarrow RO_2H$	2.5×10^{13} (mol $m^{-3}s^{-1}$)	32
2	$RO_2H + Fuel \rightarrow Solubles$	1×10^{4} (s^{-1})	10
3	$RO_2H + F_S \rightarrow P$	8×10^{9} (s^{-1})	15
4	$RO_2H + Fuel \rightarrow D_{bulk}$	200 (s^{-1})	10
5	$P + Fuel \rightarrow Solubles$	3.2×10^{12} (s^{-1})	30
6	$D_{bulk} + Fuel \rightarrow 2D_{bulk}$	1×10^{-3} (s^{-1})	0
	Wall Reactions		
7	$O_2 + Fuel \rightarrow P$	5.2×10^{-3} (ms^{-1})	12
8	$P\|_{wall} \rightarrow D_{wall}$	260 (ms^{-1})	17
9	$D_{bulk}\|_{wall} \rightarrow D_{wall}$	0.8 (ms^{-1})	18

Table 2-11: Global kinetic model2 of Katta

In the mechanism presented above

Table 2-11, RO_2H represents both hydroperoxides and peroxy radicals, the species F_S represents the heteroatom-containing compounds in jet fuel, P is considered as deposit precursor, D_{bulk} represents the bulk insolubles species and D_{wall} is the wall deposited species. In addition, F_S also represents non depleting sulphur compounds present in the fuel which usually advances the deposition process. Moreover, this term also considers any other trace metals which may exhibit the catalytic role on some reactions. This model considers the general formulation addressed by Jones *et al* (1995); however, such a scheme does not provide information about the initiation and propagation reactions in order to control the autoxidation phase.

The first step in the model represents the initiation step in general mechanism of Jones *et al.* (1991). The reaction steps 1-4 represent the generation of non-radical species, insoluble gums, and solids. The reaction step 5 depicts the precursor removing reaction generating soluble products. Reaction step 6 is the chemical representation of the agglomeration process.

The modelling attempts of Katta *et al* (1998) showed that when the appropriate Arrhenius reaction rate parameters are used, the six bulk phase reactions are capable of imitating the thermal stability of jet fuels. It was assumed that the reactions are elementary, that is, they follow law of the mass action.

For fitting the autocatalysis- behaviour of the aviation fuels, the rate of reaction1 is assumed to be independent of the oxygen concentration. Therefore, a zero order reaction was suggested until the concentration of oxygen reaches to the value of 10 ppm, and then the order of reaction is changed to 1. For the surface deposition, three wall reactions were applied in the model to simulate the sticking processes of O_2, P, and D_{bulk} which are finally transformed into surface deposits, D_{wall}, after attaching to the walls.

In spite of the capability of Katta's approach for prediction of different experimental conditions, this model is unable to predict the concentrations of RO_2H and D_{bulk} due to the lack of further hydroperoxide thermal decomposition chemistry path.

The results of Zabarnick (1993) was used by Katta *et al* (1998) to modify the rate expressions for the bulk reactions to account for the inadequacy of the prediction for intermediate species. The modifications were mainly based on the effect of sulphur on the rate of reactions. For instance, it was assumed that the consumption of RO_2H with contribution of dissolved metals reduces the rate of initiation step, hence

retarding the autoxidation within the fuel. At the same time, dissolved metals advance the initiation of radicals through catalytic reactions and therefore promote deposition. Besides, the role of dissolved metals in the fuel is similar to that of the antioxidants in that the overall effects of antioxidants decreases the RO_2H while deposition is increased. Correspondingly, the modifications in the reaction rate expressions are presented as following:

$$k_1 = \left[\frac{1}{F_S}\right]^{0.4} A_1 \exp\left(\frac{-E_1}{RT}\right) \quad (1)$$

$$k_2 = [F_S]^{0.4}[RO_2H]A_2 \exp\left(\frac{-E_2}{RT}\right) \quad (2)$$

$$k_3 = [F_S][RO_2H]A_3 \exp\left(\frac{-E_3}{RT}\right) \quad (3)$$

$$k_4 = \left[\frac{[O_2]_{in} - [O_2]}{[O_2]}\right][P][F_S]^{-1} A_4 \exp\left(\frac{-E_4}{RT}\right) \quad (4)$$

$$k_5 = [F_S][RO_2H]A_5 \exp\left(\frac{-E_5}{RT}\right) \quad (5)$$

$$k_6 = [D_{bulk}]^{0.4} A_6 \exp\left(\frac{-E_6}{RT}\right) \quad (6)$$

In the modified mechanism $[O_2]_{in}$ represents the initial concentration of dissolved oxygen in the fuel and FS represents the concentration of dissolved metals and antioxidants. The reaction step 1 permits the rate of oxygen consumption to be decreased in an opposite trend with the increase of the concentration of FS. This indicates, for instance, for a hydrotreated fuel, including relatively low concentration of dissolved metals and antioxidants, oxidation depletion occurs quickly.

The fast formation of RO_2H with drop of F_S caused by the modification of reaction rate 1 is controlled by the acceleration of the conversion of RO_2H into solubles during reaction rate 2, hence permitting model to reach to the steady state concentration of RO_2H which has been observed experimentally. The rate expression 3 is the same as the one used in the original mechanism of Katta *et al* (1993).Eventually, the surface deposition rate due to the reactions 7 and 9 was suggested as:

$$\frac{d[D]}{dt} = [O_2]_{Wall} A_7 \exp\left(\frac{-E_7}{RT}\right) + [P]_{Wall} A_8 \exp\left(\frac{-E_8}{RT}\right)$$

A number of experimental investigations proved that the surface deposition rate decreases to a near-zero value as the oxygen in the fuel is entirely used up. This indicates that the products of autoxidation have the tendency to remove the precursor species. Accordingly, the nine-step model of Katta was modified to take this behaviour in consideration by adjusting the rate expression of reaction step 4 for the precursor-destruction reaction. The production of bulk particles was further modified in the new nine-step model by adjusting it proportional to the concentration FS, and their agglomeration is limited by replacing power 1 with 0.4, as presented in the reaction rate expression 6.

Ervin *et al*(1998) used another modification on scheme of Katta and Roquemore for a CFD simulation to imitate the blockage in cooled regions within a flowing system. In this approach, a particular attention was paid to the cooled region where the prediction of Katta and Roquemore was poor. The new global model contains 11 reactions and three additional species, i.e. P_1, Dwallc and. P_1 is a precursor species which results in the formation of deposits in the cold region. The wall deposit, Dwallc, was assumed to be generated when the wall temperature reaches to a critical value around 97°C. Dbulkc represents bulk insolubles species which form when certain bulk solubles within the thermally stressed fuel become insoluble as the bulk temperature goes below the critical temperature.

Experimental results of Ervin *et al* (1998) showed that the impact of additives at high temperatures are less important in prevention of deposition in cooled regions. The application of new model proved reasonably good improvement in prediction of the peak of deposition in the cooled section compared to the old model. Moreover, it was observed that the rate of deposition in cooled regions is an order of magnitude higher than that of heated regions. This observation indicates that surface fouling in cool sections could be a serious issue in aircraft

Goel and Boehman(2000) attempted to develop a mathematical model for the calculation of jet fuel thermal degradation in the heated flow environment by the application of accurate description of the transport phenomena when a global chemistry is employed. This model solves for coupled, non linear, parabolic PDEs of energy and mass balance using a commercially available code named as 'stiff'. For the validation, it was assumed that thermal stability is characterised in terms of the

amount of unreacted fuel remaining after stressing fuel in a flow reactor. The hydrocarbon used for their experiment was n-dodecane.

The predicted results for unreacted dodecane were observed to have a low accuracy due to the extreme sensitivity of dodecane degradation to the kinetic parameters. In their investigation, the Arrhenius parameters were adjusted from batch reactor experiments for the fuels, and therefore intrinsic uncertainties in the estimation of the kinetic parameters had a large impact on predicted unreacted fuel.

2.4.2 CFD Models Based on Multi Step Chemistry

The most descriptive scheme for the aviation fuel autoxidation suggested by Taylor and Wallace(1968) and Mill and Hendry(1980) involves hundreds of reactions, hence, computationally expensive to implement. Accordingly, the majority of CFD researchers attempted to reach to a compromise between the oversimplified models and the computationally expensive mechanisms. Correspondingly, the recent CFD models rely on the application of "pseudo-detailed" scheme, see Zabarnick(1993).

One of the most comprehensive CFD models, to date, is the one developed by Ervin *et al* (2000). This is a simplified one-dimensional model that accounts for both fuel autoxidation and surface deposition in a cylindrical passage. In this model, it is assumed that the sticking probability vary inversely proportional with the shear stress at the fuel-deposit interface and the rate of deposition is described by an Arrhenius-type expression on the heated wall in a similar manner with Epstein(1986). It was also assumed that after each time step the geometry of the fuel-deposit interface changes, and one dimensional grid is regenerated after every time step to capture changes in the solid boundary following the model used by Katta and Roquemore(1993).

The surface sub mechanism in one dimensional approach consists of two reaction steps presented as following:

$O_2 + RH \rightarrow P$	1E3(ms^{-1})	19(kcal/mol)
$P \rightarrow$ Deposit	5E-3	10

This CFD model was further used for the prediction of fuel oxidation employing pseudo-detailed mechanism suggested by Zabarnick(1998).The Arrhenius parameters were estimated by the comparison with the measured rate constant and theory.

In spite of capability of this model in reproducing the experimental results, there are some limitations for its practical applications. Firstly, in this model the change of the boundary is valid just in radial direction. Secondly, as deposit forms the axial thermal conduction within the deposit layer becomes significant. Therefore, the appropriate time dependent values of thermal properties ought to be provided for prediction of accurate unsteady state temperature distribution within the wall, deposit layer, and bulk fuel.

The NIFTR experiments were used for seven different fuels at identical conditions of flow rate (0.25 mL/min), temperature (185°C), and total duration of thermal exposure (72 hours), see Jones *et al* (1995) and Kuprowicz *et al* (2007). The experimental results exhibited differences in deposition profiles and magnitude among fuel samples. This is caused by varying chemical composition of samples and changes in oxidation rate and deposit forming tendencies. For instance, it was shown that measured peak deposition varies by over an order of magnitude from 10-160 $\mu g/cm^2$. Moreover, the axial locations in the NIFTR tube corresponding to the peak of deposition may vary significantly from 0.08-0.48 m and seems to be function of autoxidation rate. Accordingly, fuel samples that oxidise quickly tend to form peak deposition further upstream than the fuels that do more slowly. Furthermore, slow oxidising fuel samples showed the tendency of broader deposition peaks than fast oxidising fuels. On the basis of these experimental results, Kuprowicz *et al* (2007) adjusted a new sub mechanism for the surface deposition reactions presented as following:

Sub mechanism	Reaction Type	Reaction	Pre exponential factor	Activation Energy
a	wall	ProductsAH → deposit	Not reported	Not reported

Table 2-12: sub mechanism a for the surface reaction deposition

This global sub mechanism is a single, direct reaction of AH reaction products at the wall surface and/or fuel-deposit interface to form deposit. This sub mechanism is capable of producing reasonable results of peak axial location corresponding to the peak deposition for the NIFTR experimental results, however, showed inaccurate in prediction of magnitude of deposition.

Sub mechanism	Reaction Type	Reaction	Rate constant
b	wall	$ProductsAH + O_2 \rightarrow deposit$	5E-4 L mol^{-1} s-1

Table 2-13: sub mechanism b for the surface reaction deposition

Sub mechanism b was created to overcome the deficiencies in sub mechanism a by adding oxygen as a reactant to the wall reaction of ProductsAH. This change resulted in lower deposition rate downstream of the peak of the oxygen consumption. This sub mechanism proved good capability for simulation of deposit magnitude for higher peak deposit fuel samples than the fuels with the lower deposition rate.

Sub mechanism c was created to overcome the discrepancies in sub mechanism b. This sub mechanism is consisted of three steps including two bulk reactions and a single wall reaction. Accordingly, ProductsAH can react to yield either soluble or insoluble precursor species. For the surface reaction, the insoluble can react to yield deposits. The key point in sub the mechanism c is that it creates a concurrent scheme in which only a fraction of the each products may react at wall providing more opportunities for the calibration.

Sub mechanism	Reaction Type	Reaction	Pre exponential factor	Activation Energy(kcalmol^{-1})
c1	bulk	ProductsAH → soluble	1E9 S^{-1}	0
c2	bulk	ProductsAH → insoluble	3.8E10 S^{-1}	6.5
c3	wall	insoluble → deposit	3E3 $S^{-1}m^{-1}$	16.3

Table 2-14: sub mechanism c for the surface reaction deposition

In this sub mechanism the axial location corresponding to the deposit peak is mainly a function of the oxidation and the reaction rates, whereas the deposit magnitude is a function of the competition between two bulk reactions.

Wade *et al* (2004) and Wade *et al*(2005) employed Genetic Algorithm(GA) technique for the optimisation of pseudo detailed mechanism in both zero and multi dimensional modelling. In his first study, the 9-step global model using the Fould2D code, a purpose-built FORTRAN code which employs finite different technique to solve the Navier-Stockes, energy, and species conservation equations was used and linked with the GA. The results indicate that the single step expression of the extremely complex deposition process in the 9-step model produces simulated results which cannot imitate all characteristics showed by the experimental deposition.

In the second investigation, the GA inversion procedure was used in conjunction with an integrator code. Employment of this technique for the 19 step pseudo detailed mechanism proved a good success in optimisation of rate parameters as well as the initial concentrations of the species at the beginning of process. This technique seems practical for the application in AFTSTU heated nozzle module when the determination of species concentrations at the nozzle inlet is not straight forward and the history of fuel varies with time and temperature.

CHAPTER 3

ZERO DIMENSIONAL MODELLING OF JET FUEL THERMAL OXIDATIVE STABILITY

3.1 Overview

It was previously discussed that the autoxidation of liquid hydrocarbons proceeds through the multitude of elementary reactions involving radicals. Quantitative description of this process requires the employment of appropriate rate coefficients for all significant reaction steps.

In general, there are essentially four ways to obtain the rate coefficients as following, see Laidler(1987) :

i. From the literature based on the previous investigations;
ii. From the experiment(reliable data but expensive);
iii. From the molecular orbital calculation(complicated);
iv. From the empirical estimation(less reliable) ;

The values of rate coefficients when proved reliable are used in the kinetic analysis of other systems. However, these are often evaluated through a simplified and direct method where a reaction is isolated from the rest of competing steps. The individually validated rate constants when combined together usually do not accurately imitate the experimental observations, hence associated with the uncertainties, see Young and Boris (1977) and Elliot *et al* (2003).

In fitting the rate parameters to a set of experimental data, it is important to know the sensitivity of model predictions on the parameters , see Rabitz *et al* (1983), Leis and Kramer(1988) and Turyani (1990). From the stand point of chemical kinetics, sensitivity refers to a mathematical method capable of describing the degree of dependency of system solution (concentrations) on the input parameters including the rate constants, temperature, and pressure. Results of sensitivity analysis are practical in reduction of the detailed mechanism, see Laidler (1987) Swihart (2006).

Solution of chemical kinetic is usually carried out by considering the ensemble of reaction steps as a set of coupled, non linear, and first order ordinary differential equations where the effect of fluid dynamics is neglected. Accordingly, by the integration of such system in either analytical or numerical approach over an

appropriate time space, with the right initial conditions, the rate coefficients are adjusted to obtain the best fit with the experimental data, see Rabitz *et al* (1983) and Swiheart (2006).

In general, a necessary condition for any chemical transformation to take place is that the atoms or molecules involved in the reaction scheme come together to form an activated complex. This complex is assumed to be situated at the top of an energy barrier lying between the initial state (reactants) and the final state (products). In this way, the reaction rate is controlled by the rate at which the complex travels onto the top of the barrier, see Benson (1970) and Laidler (1987).

In a bimolecular reaction, it is assumed that the rate of reaction between two molecules of gaseous reactant is proportional to a parameter, named α that is a fraction of the rate at which two reactants collide. This parameter is divided into two factors. The first one is Boltzman factor ($e^{\frac{-E}{RT}}$) representing the fraction of collision pairs of reactants. The second is the steric factor (p) which states solely a fraction of properly recognised collisions would have the suitable geometry for reaction.

From the view point of collision, the bi molecular rate constant is written as in Eq 3-1

$$k = pZ(e^{\frac{-E}{RT}}) \qquad \text{Eq 3-1}$$

Where Z is the frequency of collisions between the two reactants in some standard concentration units.

According to the kinetic theory of gases Z is calculated from the Eq 3-2.

$$Z = \pi\delta^2\left(\frac{8RT}{\pi\mu}\right)^{\frac{1}{2}} \qquad \text{Eq 3-2}$$

Where δ is the distance between the centres of mass of two molecules of the reactants in the collision complex, and μ is the reduced molecular weight of the colliding pairs. The concept of molecules assumes a relatively unambiguous meaning only for the case of dilute gas where the individual molecules spend relatively long periods of time isolated from each other. For simplicity, in the case of liquid phase autoxidation of hydrocarbons, the ensemble of chemical reactions is assumed to occur in such a dilute and gas phase. In this way, the molecular concepts take direct and simple application.

Therefore, both thermodynamic and kinetic parameters can be expressed in terms of simple molecular parameters.

In reality, chemical reaction between two molecules proceeds through three distinct stages:

i. Diffusion of molecules to each other;
ii. The actual chemical transformation;
iii. Diffusion of products away from each other;

In a classical kinetic expression this can be expressed as inserting the diffusion rate into the chemical kinetic equation, so in the case of one dimensional diffusion the kinetic equation becomes as Eq 3-3

$$\frac{\partial C}{\partial t} = D\frac{\partial^2 C}{\partial X^2} - kf(C) \qquad \text{Eq 3-3}$$

where C is the concentration, D is the diffusion coefficient, X denotes the distance between the two molecules, and kf(C) is the rate of reaction due to pure chemical transformation, see Walte(1957) and Benson (1968).

Diffusion in liquid like any other process has activation energy but its magnitude is generally not greater than 5 kcal. At the same time, many of chemical reactions have their activation energies more than 5 kcal thus cannot involve diffusion as the slow step. This conclusion is supported by the fact that the rate of these reactions do not depend on the viscosity of the solvent, as they would if the diffusion were significant, see Walte (1957) and Benson (1968).

The purpose of this chapter is to investigate the sensitivity of oxygen profile as well as the hydroperoxide species on the rate parameters of the pseudo-detailed mechanism presented in Table 2-3.

3.2 Mathematical Modelling for the Solution of Multi Step Chemical Kinetic Schemes

For each independent, stoichiometric chemical equation that can be written for a system such as Eq 3-4, all species in equations are related to each other by the stoichiometric coefficients as illustrated in Eq 3-5, see Laidler (1987)

$$aA + bB + \cdots = pP + qQ + \cdots \qquad \text{Eq 3-4}$$

$$\frac{1}{p}\left[\frac{dP}{dt}\right] = \frac{1}{q}\left[\frac{dQ}{dt}\right] = -\frac{1}{a}\left[\frac{dA}{dt}\right] = -\frac{1}{b}\left[\frac{dB}{dt}\right] = R_l \qquad \text{Eq 3-5}$$

Where R_l is the molar rate of reactions, a, b, p and q denote the stoichiometric coefficients for the species A, B, P and Q.

In general, R_l is a function of external variables such as volume, temperature, electric, magnetic, or gravitational fields and chemical composition of the system. Accordingly at a fixed temperature and pressure, the reaction rates for the system of reactions can be calculated through the solution of the ordinary differential equations.

$$\frac{d\mathbf{C}}{dt} = f(\mathbf{C},\mathbf{k}) \qquad \text{Eq 3-6}$$

Where $\mathbf{C}$ is the matrix of species and $\mathbf{k}$ is the matrix of rate constant.

In order to arrange the ordinary differential equations in a solvable mathematical form the Eq 3-7 is established.

$$\frac{d\mathbf{C}}{dt} = \boldsymbol{\alpha}^T\mathbf{r} \qquad \text{Eq 3-7}$$

Where $\boldsymbol{\alpha}$ is the matrix of stoichiometric coefficients and $\mathbf{r}$ is the matrix of reaction rates.

It is assumed that chemical reactions in pseudo-detailed scheme proceed through the elementary steps. A necessary condition for each reaction to be elementary is its rate follows the law of mass action, see Swihart (2006). This means that the reaction order with respect to each reactant is absolute value of its stoichiometric coefficients. For that reason, Eq 3-8 is applied for the calculation of the rate of transformations for each of the elementary reaction steps.

$$r_i = k_i \prod_{j=1}^{N} C_j^{vij} \qquad \text{Eq 3-8}$$

Where k_i is the rate constant for the i^{th} reaction; C_j is the j^{th} species in the species matrix and ν_{ij} is the order of the i^{th} reaction with respect to j^{th} species.

3.3 Numerical Solution Methods

3.3.1 The Explicit Euler Method

This method is the simplest technique for the numerical solution of an initial value problem. The reason why this method is called explicit is because the time derivative at a given time step is explicitly evaluated in terms of the value of the function at previous time steps, see Leis and Kramer (1988) and Swihart(2006).
For the first order ordinary differential equation such as Eq 3-9 when the size of Δt is small enough; the derivatives are approximated as Eq 3-10.

$$\frac{dy}{dt} = f(y) \qquad \text{Eq 3-9}$$

$$\frac{dy}{dt} \approx \frac{\Delta y}{\Delta t} = \frac{y(t+\Delta t) - y(t)}{\Delta t} \qquad \text{Eq 3-10}$$

Then it can be solved for $y(t+\Delta t)$ to get to Eq 3-11

$$y(t+\Delta t) = y(t) + f(y(t))\Delta t \qquad \text{Eq 3-11}$$

The main advantage of this method is its simplicity; however, it is relatively inaccurate compared to more sophisticated methods, hence, requires small value of time step for the integration, although, small value of time step may result in longer computational expenses.

3.3.1.1 Stability of Solution

For a time step larger than some critical value, the explicit method becomes unstable and diverges from the true solution, see Swiheart (2006).
For instance, for the simple cases such as those similar with the Eq 3-12 for which at least one analytical solution exists (presented in Eq 3-13), applying the explicit Euler method yields Eq3-14.

$$\frac{dy}{dt} = -ay \qquad \text{Eq 3-12}$$
with $y(t=0)=y_0$

$$y = y_0 \exp(-at) \qquad \text{Eq 3-13}$$

$$y_{i+1} = y_i - ay_i(\Delta t) = y_i(1 - a(\Delta t)) \qquad \text{Eq3-14}$$

The numerical solution after two steps is:

$$y_1 = y_0(1 - a(\Delta t)) \qquad \text{Eq 3-15}$$

$$y_2 = y_1(1 - a(\Delta t)) = y_0(1 - a(\Delta t))(1 - a(\Delta t)) = y_0(1 - a(\Delta t))^2$$

Therefore the numerical solution after i^{th} can be written as Eq 3-16

$$y_i = y_0(1-a(\Delta t))^i$$

Eq 3-16

If the values of Δt and a are such that in Eq 3-17; a physical solution exists that decays smoothly to 0 at longer times. It can be shown that in this condition solution converges to the true solution as the time step size is reduced.

$$0 < (1-a(\Delta t)) < 1$$

Eq 3-17

If the relationship between Δt and a follows the condition of Eq 3-18 then a will be negative, and both true and the approximate solutions go to infinity at long times. This situation is never encountered for a chemical system as the concentration cannot go to infinity without violating conservation of mass and other physical laws.

$$\text{If } (1-a(\Delta t)) > 1$$

Eq 3-18

In relation to the Eq 3-19 the solution will oscillate between positive and negative values.

$$(1-a(\Delta t)) < 0$$

Eq 3-19

In order to get a reasonable physical solution (one without unphysical oscillation), it is required that $(1-a(\Delta t)) > 0$ or equivalently $\Delta t < \frac{1}{a}$.Therefore for large values of a, the size of time step would be very small.

It can be shown that for a system of non linear equations, a similar condition applies provided that the above condition is replaced by Eq 3-20, see Swihart (2006)

$$\Delta t < \frac{1}{f'(y)} \qquad \text{Eq 3-20}$$

Where f(y) denotes the first derivative of rate equation with respect to time.
Euler's method can be extended for the solution of equations denoting the solution after i time steps by $\mathbf{y}_i$ and the vector of initial conditions by $\mathbf{y}_0$ as expressed in Eq 3-21.

$$\mathbf{y}_{i+1} = \mathbf{y}_i - \mathbf{A}\mathbf{y}_i(\Delta t) = (\mathbf{I} - \mathbf{A}(\Delta t)\mathbf{y}_i \qquad \text{Eq 3-21}$$

Consequently the numerical solution after i time step can be calculated by Eq 3-22

$$\mathbf{y}_i = (\mathbf{I} - \mathbf{A}(\Delta t))^i \mathbf{y}_0 \qquad \text{Eq 3-22}$$

According to the linear algebra, if $\mathbf{\Lambda}$ is the diagonal matrix with the eigenvalues of $(\mathbf{I} - \mathbf{A}(\Delta t))$ on its diagonal, and $\mathbf{T}$ is the matrix whose columns are the corresponding eigenvectors the Eq 3-23 can be established.

$$(\mathbf{I} - \mathbf{A}(\Delta t))^i = \mathbf{T}(\mathbf{\Lambda})^i \mathbf{T}^{-1} \qquad \text{Eq 3-23}$$

Accordingly, the diagonal matrix raised to a power is equal to

$$(\Lambda)^i = \begin{bmatrix} \lambda^i_1 & 0 & 0 & 0 \\ 0 & \lambda^i_2 & 0 & 0 \\ 0 & 0 & \lambda^i_3 & 0 \\ 0 & 0 & 0 & \text{etc} \end{bmatrix}$$

In order to have a well-behaved physically meaningful solution the following condition for all of the eigenvalues of $(\mathbf{I} - \mathbf{A}(\Delta t))$ must exist, see Numerical Recepies(1992).

$$0 \leq \lambda_i \leq 0$$

It can be shown that if μ_i is an eigenvalue of **A**, then the corresponding eigenvalue of $(\mathbf{I} - \mathbf{A}(\Delta t))$ is given by Eq 3-24

$$\lambda_i = 1 - \mu_i(\Delta t) \qquad \text{Eq 3-24}$$

Accordingly, the stability condition for the above equation can be expressed by Eq 3-25

$$\Delta t < \frac{1}{\mu} \qquad \text{Eq 3-25}$$

Where μ_B is the largest eigenvalue of **A.**

For a non linear system of equations, the same condition holds except that instead of the largest eigenvalue of A, the largest eigenvalue of J, namely the Jacobian matrix of the equation, can be used. The elements of the Jacobian matrix are given by partial derivatives of the elements of f with respect to the independent variables(y) as presented in Eq 3-26.

$$J_{ij} = \frac{\partial f_i}{\partial y_j} \qquad \text{Eq 3-26}$$

For the situations where there is only one equation, or if all of the eigenvalues of the Jacobian are comparable in magnitude, the concept of stability is not an important issue. Accordingly, only by taking time steps small enough to resolve the solution, the stability criterion is automatically satisfied. On the other hand, if the eigenvalues vary over a wide range, then stability will be a serious concern, see Swihart (2006).

3.3.2 The Implicit Euler Method

The stiffness occurs when there are physical processes that proceed at vastly different rates. In general, the stiffness problem can be avoided by using an implicit method instead of the explicit approach. This means that the derivatives are evaluated at the end of each time step rather than the beginning. In other word, in the implicit Euler method, the function f(y) is evaluated at time $t + \Delta t$ instead of t. Hence, this and its solution become as Eq 3-27 and Eq 3-28.

$$y(t + \Delta t) = y(t) + f(y(t + \Delta t)))\Delta t \qquad \text{Eq 3-27}$$

$$y_{i+1} = y_i + f(y_{i+1})\Delta t \qquad \text{Eq 3-28}$$

For cases such as Eq 3-12, applying the implicit Euler method yields the numerical solution after i time step as presented in Eq 3-29, see Numerical Recepies (1992) and Swihart (2006)

$$y_{i+1} = y_i - ay_{i+1}(\Delta t) \qquad \text{Eq 3-29}$$

Solving for y_{i+1} gives the Eq 3-30

$$y_{i+1} = y_i\left(\frac{1}{1 + a(\Delta t)}\right) \qquad \text{Eq 3-30}$$

If y (t=0) $=y_0$, then the numerical solution after i time steps is given by Eq 3-31

$$y_i = y_0\left(\frac{1}{1 + a(\Delta t)}\right)^i \qquad \text{Eq 3-31}$$

It can be shown that the approximate solution converges to the true solution as the time step size is reduced. Therefore, with the implicit Euler method the time step size can be used based on the accuracy and not based on stability considerations. This remark is also true for non linear equations as well as for the systems of non linear equations provided that the eigenvalues of the Jacobian are all positive.

3.3.2.1 Stability of Solution

From the stand point of stability, application of the implicit method is much more complicated. This results in Eq 3-29.
This set of non-linear algebraic equations cab rewritten as Eq 3-32.

$$\mathbf{g}(\mathbf{y}_{i+1}) = \mathbf{y}_{i+1} + \mathbf{f}(\mathbf{y}_{i+1})\Delta t - \mathbf{y}_i = \mathbf{0} \qquad \text{Eq 3-32}$$

The iterative Newton's method can be applied for solving the set of non linear algebraic equations as expressed in Eq 3-32.The solution for the next iteration can be obtained from the Eq 3-33.

$$y_{i+1,j+1} = y_{i+1,j} - J^{-1} g(y_{i+1,j}) \qquad \text{Eq 3-33}$$

Where $y_{i+1,j}$ denote the approximate solution to the non linear equations for y_{i+1} after j iteration of Newton's method.
To obtain the Eq 3-33 by the application of implicit method $\mathbf{g}(\mathbf{y}_{i+1,j+1})$ must be approximated by the Eq 3-34.

$$\mathbf{g}(\mathbf{y}_{i+1,j+1}) \cong \mathbf{g}(\mathbf{y}_{i+1,j}) + \mathbf{J}^{-1}(\mathbf{y}_{i+1,j+1} - \mathbf{y}_{i+1,j}) \qquad \text{Eq 3-34}$$

Where the Jacobian matrix **J** contains the partial derivatives of the element g with respect to the elements of **y.**
Solving the Eq 3-35 for $y_{i+1,j+1}$ results in :

$$\mathbf{g}(\mathbf{y}_{i+1,j}) + \mathbf{J}^{-1}(\mathbf{y}_{i+1,j+1} - \mathbf{y}_{i+1,j}) = 0 \qquad \text{Eq 3-35}$$

$$\mathbf{y}_{i+1,j+1} = \mathbf{y}_{i+1,j} - \mathbf{J}\mathbf{g}(\mathbf{y}_{i+1,j}) \qquad \text{Eq 3-36}$$

Alternatively it can be written as Eq 3-37

$$\mathbf{J}(\Delta \mathbf{y}) = -\mathbf{g} \qquad \text{Eq 3-37}$$

Where $\Delta y = y_{i+1,j+1} - y_{i+1}, j$

In Newton's method, for each iteration, this set of equations is solved .Accordingly, at each chosen time step as many as iterations that is required for the convergence need to be performed, however, compare to the explicit approach, the implicit method requires the use of larger time step.

3.3.3 Higher Order Methods

There are more accurate methods for integrating the ordinary differential equations rather than those presented so far. For instance, predictor-corrector methods use information from the previous time steps to calculate the solution at the new time. Gear's method of integration is a predictor-corrector approach that is very effective for the solution of stiff systems. This is widely used in different software libraries. This multistep implicit integration method usually results in significant reduction in execution time. It requires the construction, handling, and inversion of matrices, hence, storage requirements for the matrices.

3.4 Mathematical Formulation for the Calculation of Sensitivity Analysis

Sensitivity analysis provides a method to determine the dependence of model predictions on input parameters, see Rabitz *et al* (1983), Turanyi (1990) and Swihart (2006).

If in model presented in Eq 3-38, **y** represents the vector of species concentrations that is supposed to be fitted to the experiment, and **p** denotes the vector of rate coefficients, the dependence of the i^{th} species on the rate coefficient of reaction j as a function of time can be calculated by the Eq 3-39, see Turanyi(1990) and Swihart (2006).

$$\mathbf{y} = \mathbf{f}(\mathbf{p}, t) \qquad \text{Eq 3-38}$$

$$Z_{ij} \equiv \frac{\partial y_i}{\partial p_j} \qquad \text{Eq 3-39}$$

Where Z_{ij} denotes the sensitivity coefficients of y_i to p_j. Eq 3-39 signifies that an infinitesimal change in the value of p_j results in the change of the amount of y_i.

Another quantity that is often more practical than the sensitivity coefficient is the scaled sensitivity coefficient which can be calculated from the Eq 3-40, see Turanyi (1990) and Swihart (2006)

$$\sigma_{ij} \equiv \frac{p_j}{y_i} Z_{ij} = \frac{p_j}{y_i} \frac{\partial y_i}{\partial p_j} = \frac{\partial(\ln(y_i))}{\partial(\ln(p_j))} \qquad \text{Eq 3-40}$$

Eq 3-40 indicates that an infinitesimal fractional change in the value of p_j results in the fractional change of the amount of y_i.

Although, there are more efficient methods for the calculation of sensitivity coefficients; the simplest is brute force method. In this method, the model prediction is computed based on the modification of one parameter by a tiny amount and

continuing with the calculation of model prediction again. In this case, the sensitivity coefficients is defined as the amount of prediction divided by the change in the parameter as expressed in Eq 3-41, see Turanyi(1990)

$$Z_{ij} = \frac{\partial y_i}{\partial p_j} \approx \frac{\Delta y_i}{\Delta p_j} \qquad \text{Eq 3-41}$$

As was previously discussed in this chapter, the mathematical formulation illustrating the chemical models is the set of ordinary differential equations which can be re written as Eq 3-42. In this equation, vector of **y** changes in time but the vector of **p** does not.

$$\frac{\mathbf{dy}}{dt} = \mathbf{g(y,p)} \qquad \text{Eq 3-42}$$

An additional differential equation can be written for the calculation of the sensitivity coefficients that need to be integrated simultaneously with the rate equations. To do this, the derivative of the sensitivity coefficients can be written as Eq 3-43 in which the order of differentiation has been reversed. Since **y** depends on **p**, the partial derivatives of **g** with respect to **p** must be expanded out as Eq 3-44.

$$\frac{dZ_{ij}}{dt} = \frac{d}{dt}\left(\frac{\partial y_i}{\partial p_j}\right) = \frac{\partial}{\partial p_j}\left(\frac{dy_i}{dt}\right) = \frac{\partial}{\partial p_j}(g_i(y,p)) \qquad \text{Eq 3-43}$$

$$\frac{\partial}{\partial p_j}(g_i(y,p)) = \frac{\partial g_i}{\partial p_j} + \sum_{l=1}^{N} \frac{\partial g_i}{\partial y_l} Z_{lj} \qquad \text{Eq 3-44}$$

According to the Eq 3-39, the mathematical model for the calculation of the sensitivity coefficients can be written as Eq 3-45, see Turanyi (1990) and Swihart (2006)

$$\frac{dZ_{ij}}{dt} = \frac{\partial g_i}{\partial p_j} + \sum_{l=1}^{N} \frac{\partial g_i}{\partial y_l} Z_{lj} \qquad \text{Eq 3-45}$$

3.5 Results and Discussion

A computer code was created in MATLAB 7.1 using the Taylor series expansion based on the work published by Kennealy and Moore(1977). In spite of applicability of this method in the solution of very simple scheme (up to 4-5 reaction steps), solution of pseudo detailed mechanism is computationally expensive. Therefore, this approach was excluded for further applications. The scripts of the code along with the associated functions are included in Appendix A.

Another computer program was written in MATLAB 7.1 in response to the shortfalls with the initial integrator code. In the second code, the solution of coupled system of ordinary differential equations expressed in Figure 3-1 was carried out by the application of the MATLAB build-in functions, namely ode 15s or ode 45s which are typically designed for the solution of such systems based on Gear's method, see MATLAB help(2005).

Solution of energy balance was not considered in this calculation as the change of the enthalpy of reaction is not significant during the fuel degradation reactions.

The code requires the following input information: reaction mechanism including the rate parameters (activation energy and pre exponential factor), initial concentrations at the reaction onset for each species involved in mechanism and time intervals together with a range of tolerances for the accuracy of the computation. This program yields the individual species concentrations at each time interval along with the scaled sensitivity coefficients of the species of concern for the same time interval of the integration. The main integrator code, functions for the calculation of sensitivity analysis are presented in Appendix B.

The initial species concentrations were employed in the integrator code in accordance with those corresponding to the sample named as F2959, see Kuprowicz *et al* (2007). The result of dissolved oxygen depletion within the bulk fuel was compared with the experimental outcomes tested in NIFTR.

$$\frac{d}{dt}\begin{bmatrix} C_I \\ C_R \\ C_{O_2} \\ C_{RO_2} \\ C_{RH} \\ C_{ROOH} \\ C_{Termination} \\ C_{R_2} \\ C_{RO} \\ C_{OH} \\ C_{ROH} \\ C_{Rprime} \\ C_{Carbonyl} \\ C_{H2O} \\ C_{ROterm} \\ C_{alkane} \\ C_{AH} \\ C_A \\ C_{AQ} \\ C_{AQH} \\ C_{ProductsAH} \\ C_{SH} \\ C_{ProuctsSH} \end{bmatrix} = \begin{bmatrix} -1 & 1 & 0 & 0 & 0 & 0 & 0 & 0 & 0 & 0 & 0 & 0 & 0 & 0 & 0 & 0 & 0 & 0 & 0 & 0 & 0 & 0 & R1 \\ 0 & -1 & -1 & 1 & 0 & 0 & 0 & 0 & 0 & 0 & 0 & 0 & 0 & 0 & 0 & 0 & 0 & 0 & 0 & 0 & 0 & 0 & R2 \\ 0 & 1 & 0 & -1 & -1 & 1 & 0 & 0 & 0 & 0 & 0 & 0 & 0 & 0 & 0 & 0 & 0 & 0 & 0 & 0 & 0 & 0 & R3 \\ 0 & 0 & 0 & -2 & 0 & 0 & 1 & 0 & 0 & 0 & 0 & 0 & 0 & 0 & 0 & 0 & 0 & 0 & 0 & 0 & 0 & 0 & R4 \\ 0 & 0 & 0 & -1 & 0 & 1 & 0 & 0 & 0 & 0 & 0 & 0 & 0 & 0 & 0 & 0 & -1 & 1 & 0 & 0 & 0 & 0 & R5 \\ 0 & 1 & 0 & 0 & -1 & 0 & 0 & 0 & 0 & 0 & 0 & 0 & 0 & 0 & 0 & 0 & 0 & 0 & -1 & 1 & 0 & 0 & R6 \\ 0 & 0 & -1 & 0 & 0 & 0 & 0 & 0 & 0 & 0 & 0 & 0 & 0 & 0 & 0 & 0 & 0 & -1 & 1 & 0 & 0 & 0 & R7 \\ 0 & 0 & 0 & 0 & 0 & 0 & 0 & 0 & 0 & 0 & 0 & 0 & 0 & 0 & 0 & 0 & -1 & 1 & -1 & 1 & 0 & 0 & R8 \\ 0 & 0 & 0 & 0 & 0 & 0 & 0 & 1 & 0 & 0 & 0 & 0 & 0 & 0 & 0 & 0 & 0 & 0 & -2 & 0 & 1 & 0 & 0 & R9 \\ 0 & -2 & 0 & 0 & 0 & 0 & 0 & 0 & 0 & 0 & 0 & 0 & 0 & 0 & 0 & 0 & 0 & 0 & 0 & 0 & 0 & 0 & R10 \\ 0 & 0 & 0 & 0 & 0 & -1 & 0 & 0 & 1 & 1 & 0 & 0 & 0 & 0 & 0 & 0 & 0 & 0 & 0 & 0 & 0 & 0 & R11 \\ 0 & 1 & 0 & 0 & -1 & 0 & 0 & 0 & -1 & 0 & 1 & 0 & 0 & 0 & 0 & 0 & 0 & 0 & 0 & 0 & 0 & 0 & R12 \\ 0 & 0 & 0 & 0 & 0 & 0 & 0 & 0 & -1 & 0 & 0 & 1 & 1 & 0 & 0 & 0 & 0 & 0 & 0 & 0 & 0 & 0 & R13 \\ 0 & 1 & 0 & 0 & -1 & 0 & 0 & 0 & 0 & -1 & 0 & 0 & 0 & 1 & 0 & 0 & 0 & 0 & 0 & 0 & 0 & 0 & R14 \\ 0 & 0 & 0 & 0 & 0 & 0 & 0 & 0 & -2 & 0 & 0 & 0 & 0 & 0 & 1 & 0 & 0 & 0 & 0 & 0 & 0 & 0 & R15 \\ 0 & 1 & 0 & 0 & -1 & 0 & 0 & 0 & 0 & 0 & 0 & -1 & 0 & 0 & 0 & 1 & 0 & 0 & 0 & 0 & 0 & 0 & R16 \\ 0 & 0 & 0 & 0 & 0 & -1 & 0 & 0 & 0 & 0 & 0 & 0 & 0 & 0 & 0 & 0 & 0 & 0 & 0 & 0 & -1 & 1 & R17 \\ 0 & 1 & 1 & -1 & 0 & 0 & 0 & 0 & 0 & 0 & 0 & 0 & 0 & 0 & 0 & 0 & 0 & 0 & 0 & 0 & 0 & 0 & R18 \end{bmatrix}$$

Figure 3-1: Coupled system of ordinary differential equations

Figure 3-2 shows that the predicted results can reasonably imitate the experimental data.

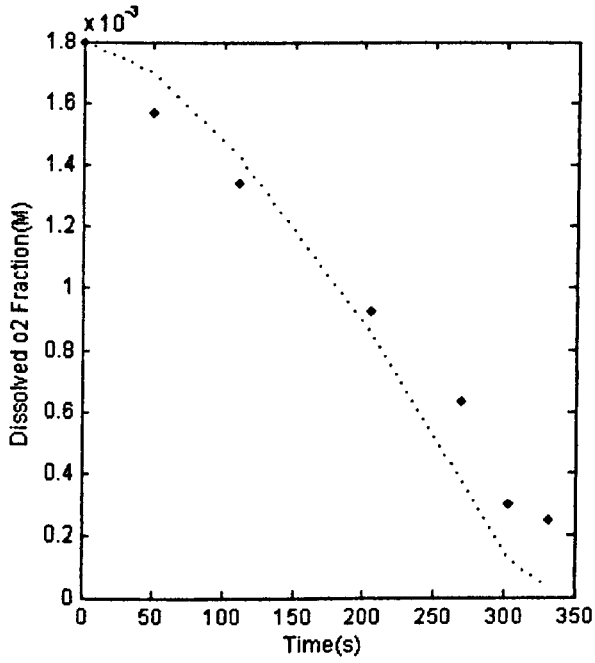

Figure 3-2: Comparison of measured and calculated dissolved oxygen consumption for F2959 thermally stressed at 185°C.Symbols represent measurements. Dotted curve represents chemical kinetic simulations

After the code validation, the sensitivity coefficients of hydroperoxide species and dissolved O_2 depletion were computed as presented in Figure 3-4.

Considering the initial step (I→R˙) is extremely slow reaction, it supplies a very low level of alkyl radicals (R˙). These are not enough to interfere with the overall oxidation process; hence, this step can be removed from the mechanism. It is assumed that hydroperoxides species in the jet fuels are sufficient to initiate the chain without including the "fake" initiation step.

To prove this computationally, pre exponential factor and/or the initial concentration of "Initiator" were set to zero. As was expected, no differences were observed in the concentration profile of the alkyl radicals (R˙) throughout the process.

By exerting small perturbation to the rates of the hydroperoxide decomposition steps, it was shown that the alkyl radical is significantly sensitive to the reaction step 9 and 18 as presented in the Figure 3-3 and Figure 3-4.

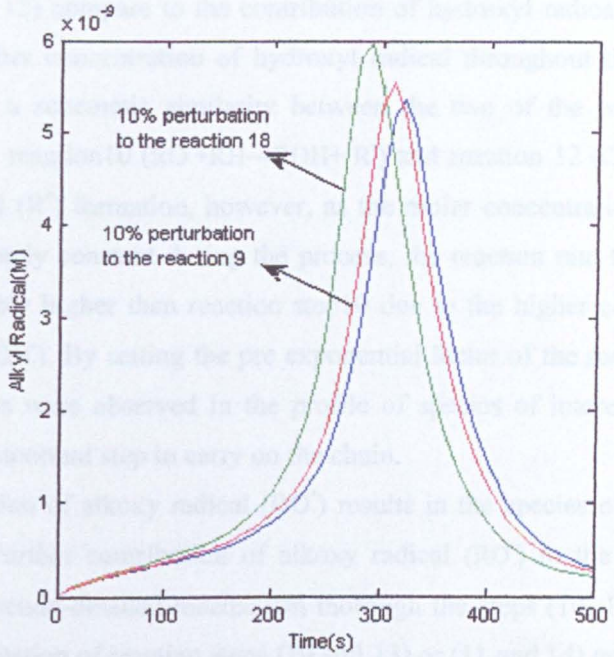

Figure 3-3 Alkyl radical with and without reaction rates perturbation

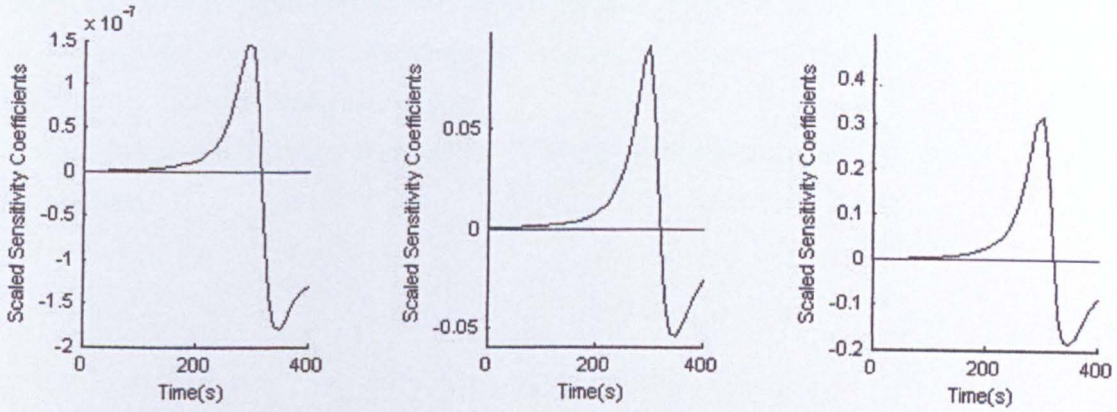

Figure 3-4: Sensitivity of alkyl radical to the reaction 1, reaction 9 and reaction18 in pseudo-detailed mechanism

According to the pseudo detailed mechanism, equal number of moles of alkoxy radical ($RO^{\bullet}$) and hydroxyl radical ($OH^{\bullet}$) are generated through the hydroperoxide

decomposition steps. However, further participation of alkoxy radical ($RO^{\bullet}$) in more reactions (10, 11, 13) compare to the contribution of hydroxyl radical (only reaction 12) results in higher concentration of hydroxyl radical throughout the autoxidation process. There is a schematic similarity between the two of the propagation step reactions, namely, reaction10 ($RO^{\bullet}+RH \rightarrow ROH+ R^{\bullet}$) and reaction 12 ($OH^{\bullet}+RH \rightarrow H_2O+ R^{\bullet}$) in alkyl radical ($R^{\bullet}$) formation, however, as the molar concentration of bulk fuel (RH) is approximately constant during the process, the reaction rate for the reaction step 12 is noticeably higher than reaction step10 due to the higher concentration of hydroxyl radical ($OH^{\bullet}$). By setting the pre exponential factor of the reaction 10 equal to zero no changes were observed in the profile of species of interest. In contrast, reaction 12 is an important step to carry on the chain.

Complete elimination of alkoxy radical ($RO^{\bullet}$) results in the species of interest to be under predicted. Further contribution of alkoxy radical ($RO^{\bullet}$) to the mechanism is described in the pseudo-detailed mechanism thorough the steps (10, 11, 13 and 14). However, by elimination of reaction steps (10 and 13) or (11 and 14) no changes were observed in the profile the species of interest. Insignificance of these reactions for the entire process of O_2 depletion and deposit precursor formation can be justified from the values of sensitivity coefficients presented in the Figure 3-6 - Figure 3-8.

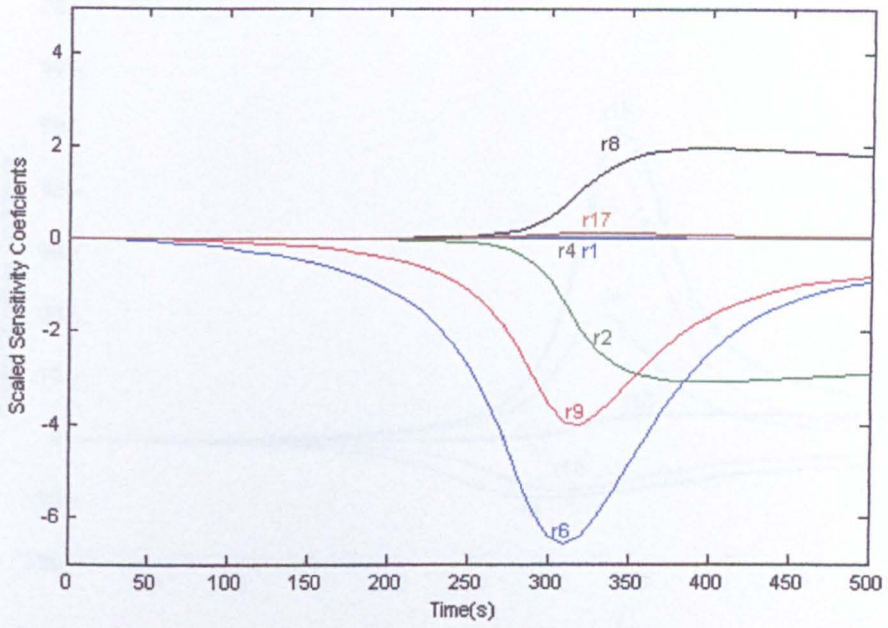

Figure 3-6 : Low sensitive reaction steps for dissolved oxygen

To sum up, calculation for both species (dissolved O_2 and hydroperoxide species) indicate that with respect to the sensitivity, the reaction steps can be divided to the high sensitive and low sensitive categories for both species. There are also some other steps which are very low and no sensitive.

The sensitivity calculation was repeated for different temperature and similar results were observed.

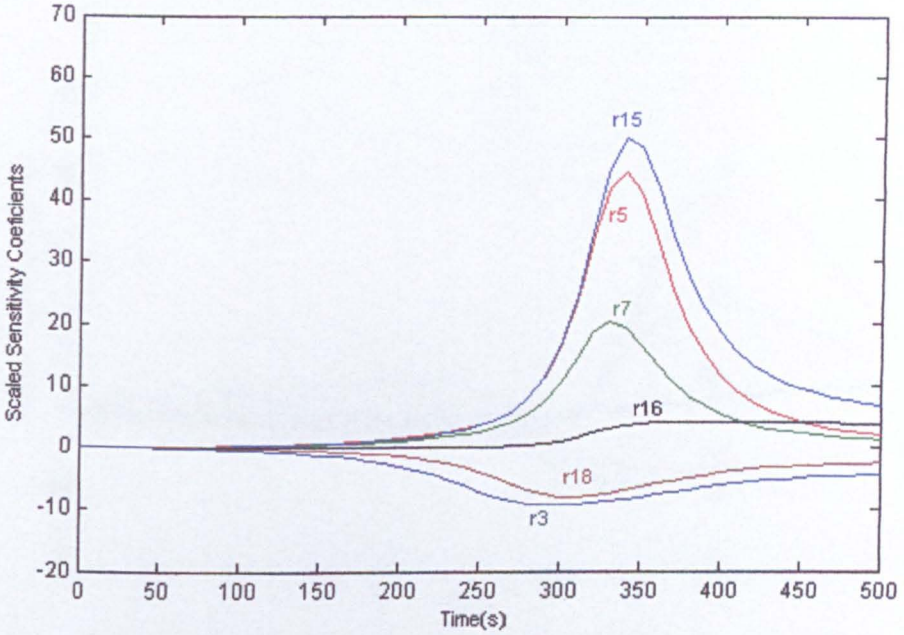

Figure 3-5: High sensitive reaction steps for dissolved oxygen

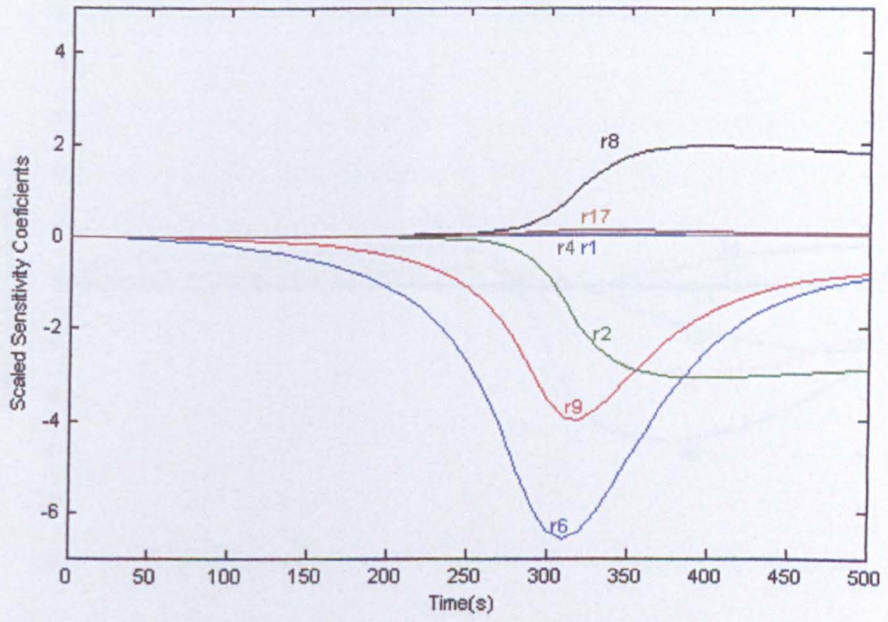

Figure 3-6 : Low sensitive reaction steps for dissolved oxygen

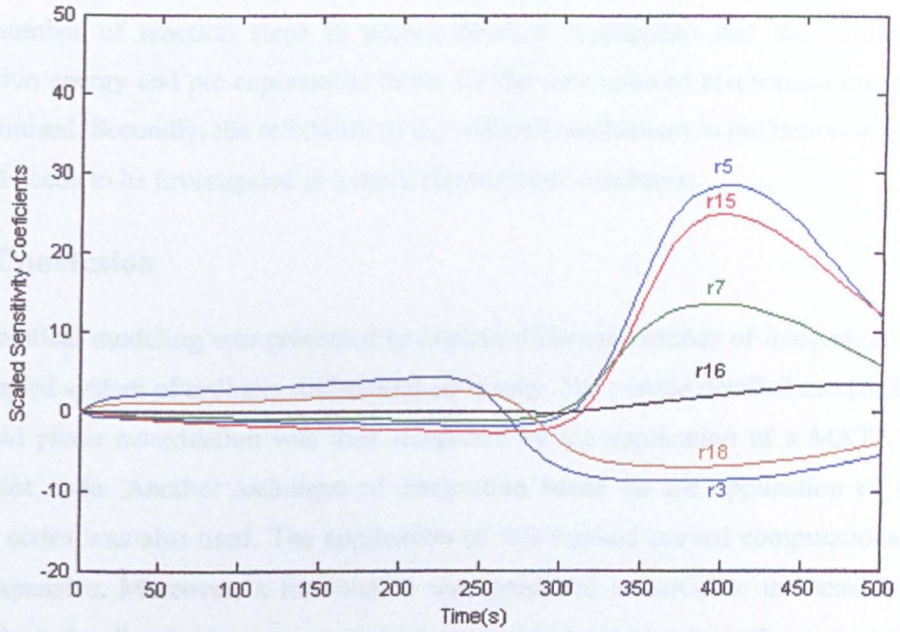

Figure 3-7 : High sensitive reaction steps for hydroperoxide species

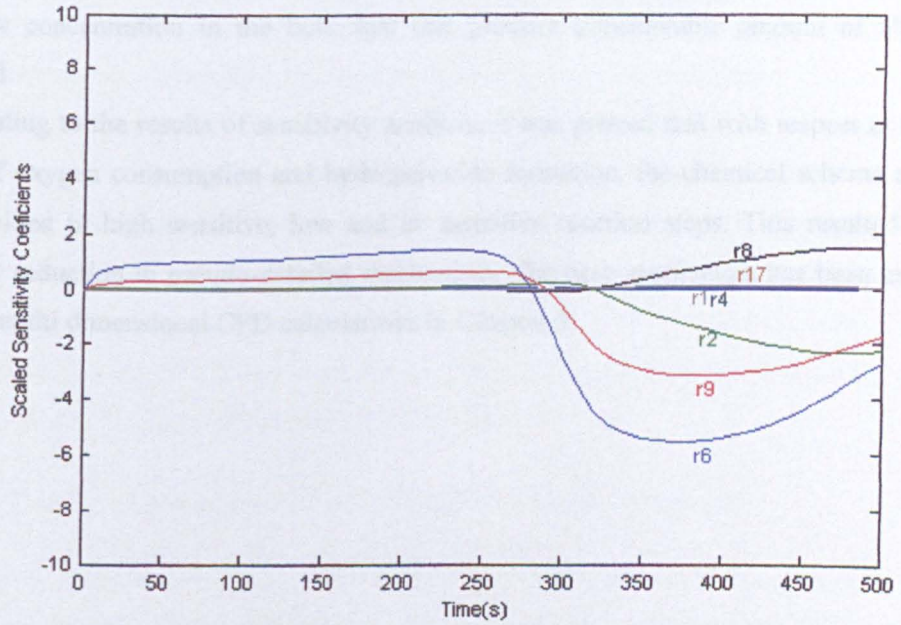

Figure 3-8 : Low sensitive reaction steps for hydroperoxide species

Results of sensitivity analysis also indicate further reduction can be performed in the total number of reaction steps in pseudo-detailed mechanism and the values of activation energy and pre exponential factor for the new reduced mechanism ought to be optimised. Secondly, the reliability of the reduced mechanism in prediction of total deposit needs to be investigated in a multi dimensional simulation.

3.6 Conclusion

Mathematical modeling was presented to explain different methods of integration for the coupled system of ordinary differential equations. The pseudo detailed mechanism of liquid phase autoxidation was then integrated by the application of a MATLAB integrator code. Another technique of integration based on the application of the Taylor series was also used. The application of this method proved computationally very expensive. Moreover, a formulation was presented to calculate the sensitivity coefficients for dissolved oxygen and the hydroperoxide species to each reaction rate constants. It was observed that the first reaction step in pseudo detailed mechanism, namely the production of alkyl radical is insignificant to the oxygen consumption as well as creation of hydroperoxide. It was also shown that hydroperoxide species, even in low concentration in the bulk fuel can produce considerable amount of alkyl radical.

According to the results of sensitivity analysis, it was proved that with respect to the rate of oxygen consumption and hydroperoxide formation, the chemical scheme can be divided in high sensitive, low and no sensitive reaction steps. This resulted in further reduction in pseudo-detailed mechanism. The new mechanism has been used in the multi dimensional CFD calculations in Chapter 5.

CHAPTER 4

EXPERIMENTAL INVESTIGATION OF CARBON DEPOSITION IN A HEATED NOZZLE OF AFTSTU

4.1 Overview

There are a number of concerns indicating that the application of conventional chemical specification tests is not a realistic approach for determination of jet fuel thermal degradation. One major limitation is described in terms of the thermal and flow conditions that fuel faces in the real aircraft fuel system. These vary with the aircraft, engine design and flight conditions. Accordingly, a stability test must guarantee that jet fuel faces with the most stringent thermal and flow conditions that may encounter during the flight, see Hazlett (1991), Morris *et al* (2002) and Taylor (2005).

Additional limitation can be expressed in relation to the test time and volume of the fuel. Formation of deposit in the aircraft fuel system occurs in a time frame of hundreds of hours while a specification test must be completed rapidly, not more than a day maximum. Therefore, the compensation for this time disparity causes fuel temperature to be increased in order to accelerate the rate of autoxidative reactions.

It was previously discussed that a number of influencing parameters contribute to the jet fuel thermal degradation processes. These are fuel type, bulk fuel temperature, fuel residence time, metal wall temperature, surface roughness, flow characteristics and etc. In view of all these influencing factors, Aviation Fuel Thermal Stability Test Unit(AFTSTU) is designed to includes most of these parameters for simulation, see Dagget *et al* (1995) and Hobday and Lewis(1995).

4.2 Thermal Management in Aircraft Turbine Engines

The major components of the aircraft fuel system are schematically presented in Figure 4-1. This figure shows that in an actual fuel system, energy is added to the fuel in the low pressure firs stage fuel pump that is a centrifugal pump, secondly in the high pressure second stage pump which is a gear pump in most engines, and finally in the reheat pump, namely a special type of centrifugal pump. Heat generation of the

fuel system is determined by the pump speed, the fuel flow rate; pump efficiencies, the pressure rise through the pumps and deposited carbon layer.

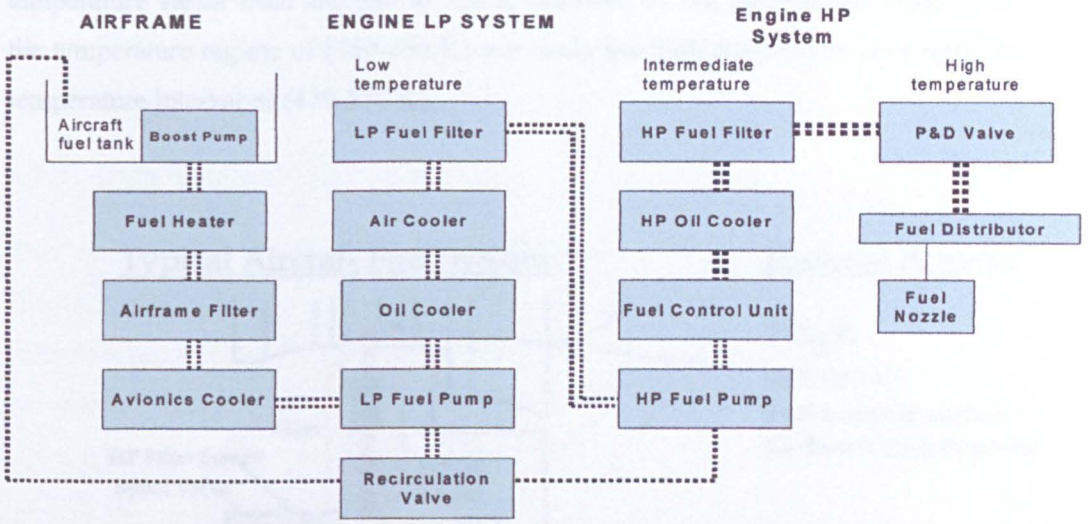

Figure 4-1:Aircraft Fuel System Components, see Dagget *et al* (1995) and Rolls Royce (2000)

Another generic diagram of the fuel/oil system in jet engine is presented in Figure 4-2. This depicts that fuel from the tank to the injector passes through the various sections, hence changes its temperature.

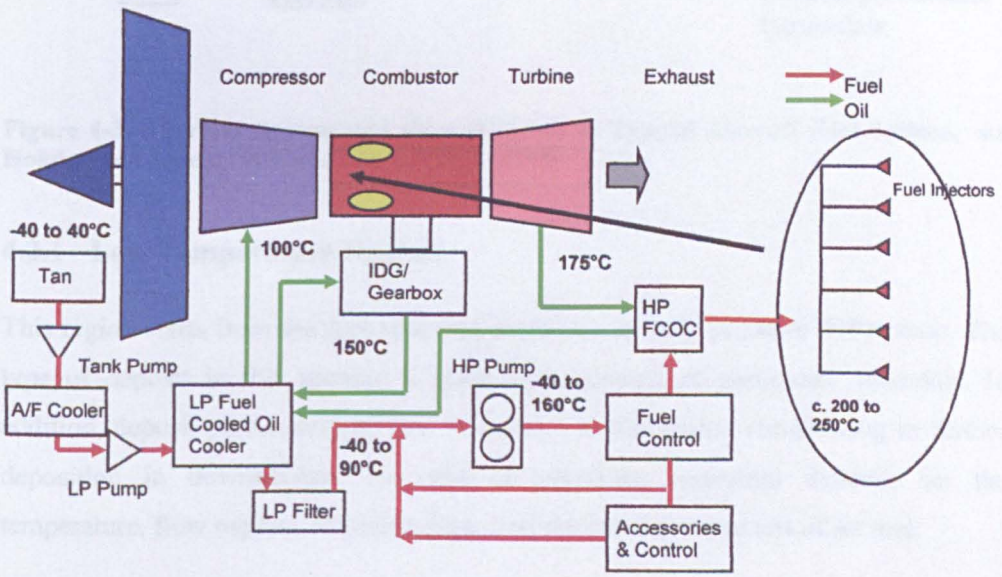

Figure 4-2: Generic Fuel and Oil System, see Rolls Royce (2000)

Three major thermal regimes are identified in the aircraft fuel system as schematically presented in Figure 4-3. First stage represents the low temperature region whose temperature varies from ambient to 350 K followed by the intermediate region with the temperature regime of (350-450 K) and lastly the high temperature zone with the temperature interval of (470-570 K).

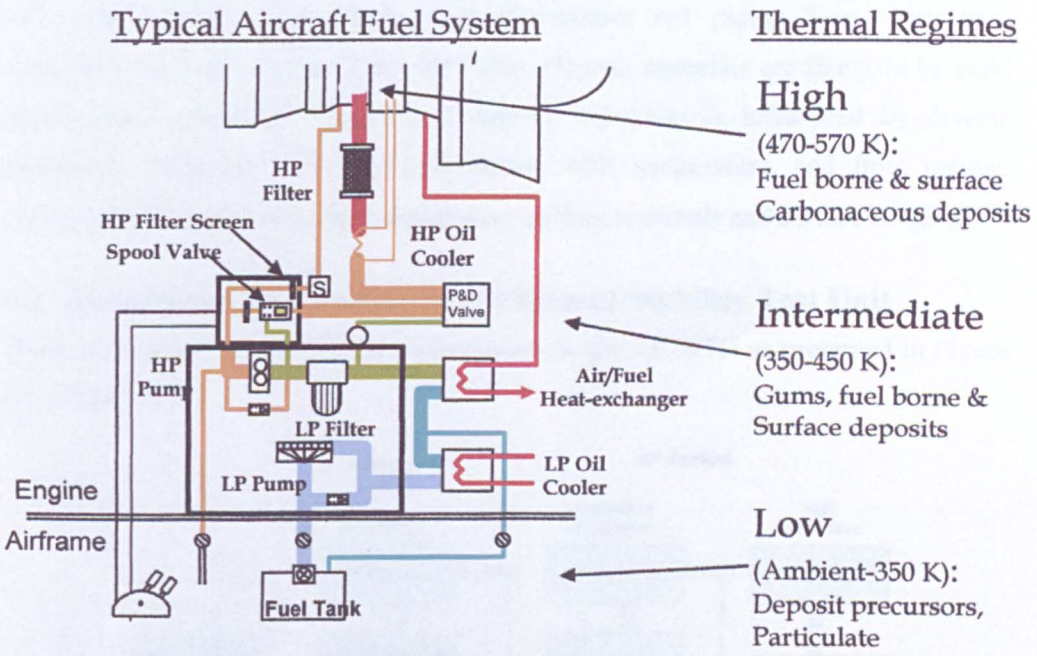

Figure 4-3: Thermal Regime and Flow Diagram in Typical Aircraft Fuel System, see Hobday and Lewis(1995) and Dagget *et al* (1995)

4.2.1 Low Temperature Regime

This region starts from the fuel tank and continues up to hi pressure (HP) pump. The type of deposit in this section is generally consisted of particulate materials. In addition, deposit precursors can also be formed in this region contributing in further deposition in downstream. The rate of precursor formation depends on the temperature, flow regime, residence time, and chemical constituents of jet fuel.

4.2.2 Intermediate Temperature Regime

This regime is met within the aircraft fuel system after the high pressure pump (HP) and prior to the fuel nozzle. Deposits in this region are likely to be gums, fuel borne, and surface particulates. The rate of deposition is governed by fuel temperature, flow regime and chemical constituents of jet fuel.

4.2.3 High Temperature regime

This zone includes fuel nozzle, fuel distributors and piping lines. The main characteristic of this region is the hot walls. Deposit materials are likely to be solid carbonaceous materials. The rate of deposit formation is influenced by diverse parameters including fuel inlet temperature, wall temperature, and flow regime, chemical constituents of jet fuel, component surface materials and surface roughness.

4.3 Description of Aviation Fuel Thermal Stability Test Unit

There are similarly three fuel thermal regimes in the AFTSTU as presented in Figure 4-4 - Figure 4-6.

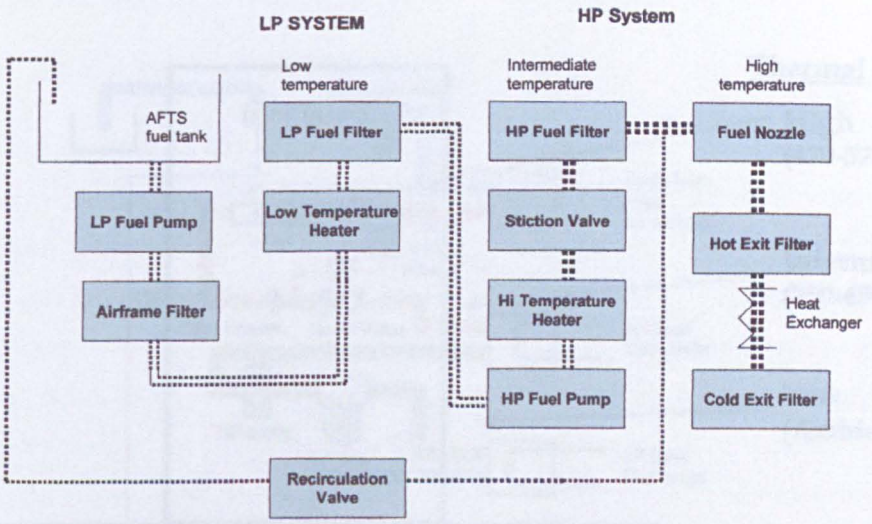

Figure 4-4 : Aviation Fuel Thermal Stability Test Unit (AFTSTU) Main Components, see Dagget (1995) Rolls Royce (2000)

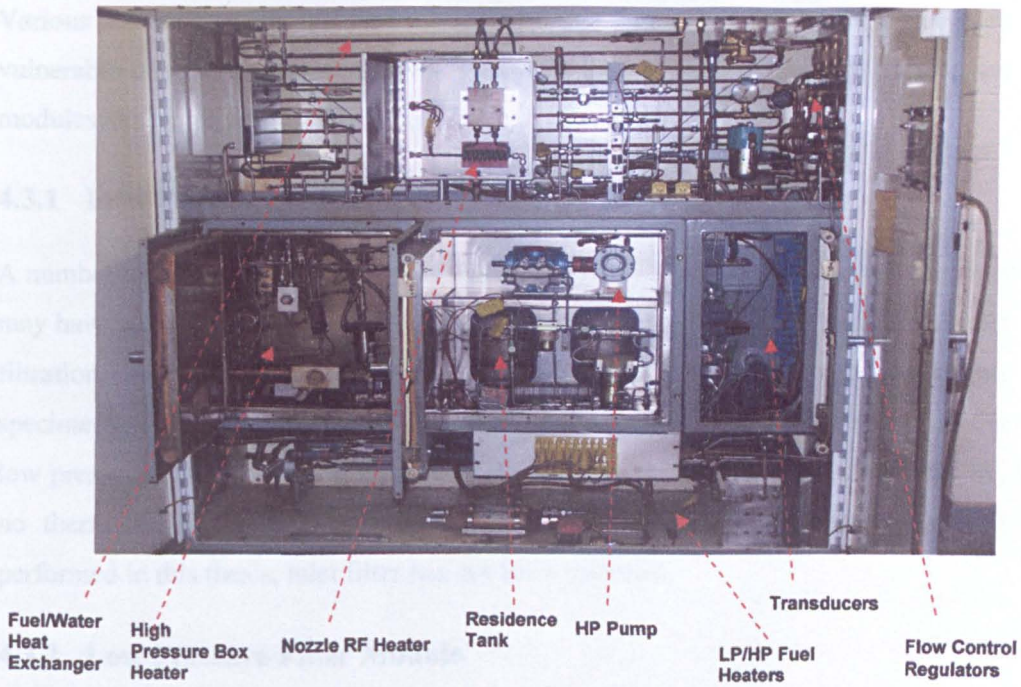

Figure 4-5: The AFTSTU Test cabinet with the Main Components

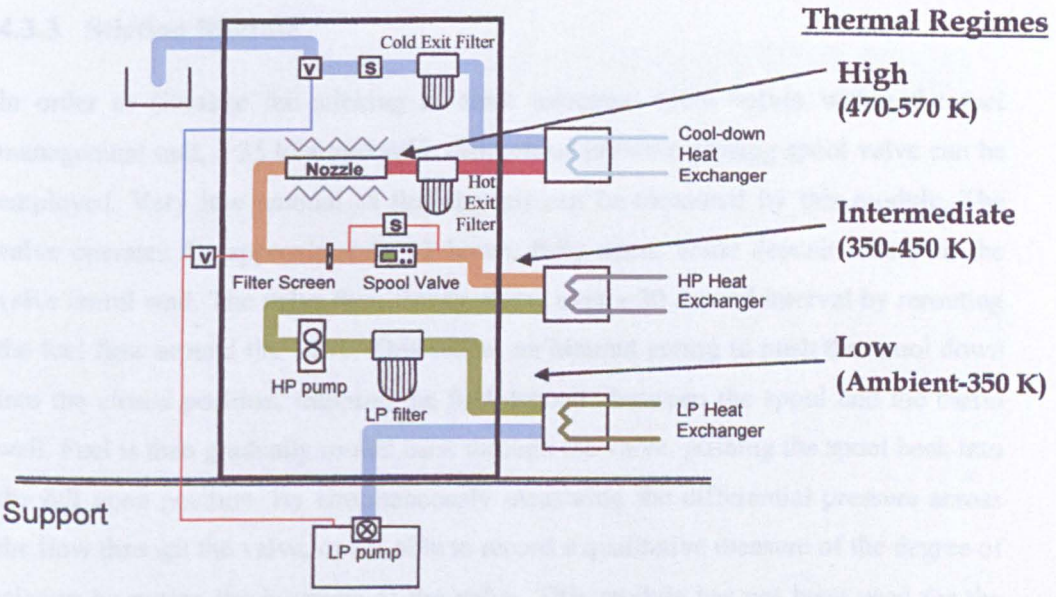

Figure 4-6: Thermal Regime in Aviation Fuel Thermal Stability Test Unit and Flow Diagram

Various test modules are included within the thermal regimes to characterise the most vulnerable aircraft components in the course of jet fuel thermal stability. These test modules are highlighted as following:

4.3.1 Inlet Filter

A number of tests performed by Rolls Royce proved that the degree of initial filtration may have an impact on deposit formation see Dagget *et al* (1995). Therefore, the inlet filtration can condition jet fuel prior to reach to the fuel heating section and test specimens. This also serves to remove any waste that may be generated through the low pressure fuel pump. However, as the thermal operation for the filter is ambient, no thermally related deposition is expected to be detected. For the experiment performed in this thesis, inlet filter has not been included.

4.3.2 Low Pressure Filter Module

This module includes the main LP filter operating at the low temperature regime from ambient to 350 K. In the experiments used in this research a modified 10 μm aircraft LP filter was used.

4.3.3 Stiction Module

In order to simulate the sticking in close tolerance spool valves within the fuel management unit, a 35 kPa hydraulic differential pressure sensing spool valve can be employed. Very low amount of fuel deposit can be measured by this module. The valve operates for approximately 12 hours, fully open, while deposit forms on the valve barrel wall. The valve then slowly closes over a 30 second interval by rerouting the fuel flow around the valve. This causes an internal spring to push the spool down into the closed position, trapping the fuel deposits between the spool and the barrel wall. Fuel is then gradually routed back through the valve, pushing the spool back into the full open position. By simultaneously measuring the differential pressure across the flow through the valve, one is able to record a qualitative measure of the degree of stiction by noting the hystresis of the valve. This module has not been used for the experimental work of this thesis.

4.3.4 High Pressure Filter Module

This module represents the high pressure region by the application of a 70 μm, 304 stainless steel woven mesh screen. The screen is sized to simulate a small last chance filter permitting for 0.85 m/s fuel velocity in the mesh open area. The filters are weighted prior to the test and reweighed afterwards. Discrete test data are gathered from deposit weight while real time data are obtained from recording the differential pressure across the filter. The results from this module were not used for the work performed here.

4.3.5 Heated Nozzle Module

Nozzles and nozzle feed arms operate within the highest temperature envelopes and have some of the smallest flow path dimensions, hence, very short fuel residence in the engine fuel system. Thermal loads on jet fuel are of the highest value in this component; therefore, fuel atomisers and feed arm injectors are considered as the most critical components in the engine fuel system. Figure 4-7 shows a typical fuel feed arm injector employed during the AFTSTU operation.

Figure 4-7: Typical Jet Fuel Feed Arm Injector Used for Heated Nozzle Module in AFTSTU

Deposits are formed on inner surface of feed arm injector or on the fuel wetted hot metal surfaces with the catalytic activity. This occurs during the engine operation, as fuel passes over the hot metal surfaces for relatively large periods of time. The tube heating mechanism is based on the constant thermal energy generation in the volume of metal by the application of an induction heating system. This includes the use of an electrically conducting material through the electromagnetic induction. Accordingly, currents are induced in the material causing the heating. The frequency used may vary from 50/60 Hz to more than 10 MHz. Induction heating is generally a non-contact process. It consists of a coil surrounding the material subject to the heating (usually a metal). In this case, due to the constant energy generation rate in the volume of

metallic wall, during the deposition, temperature increases on the tube's wall. This is schematically presented in Figure 4-8.

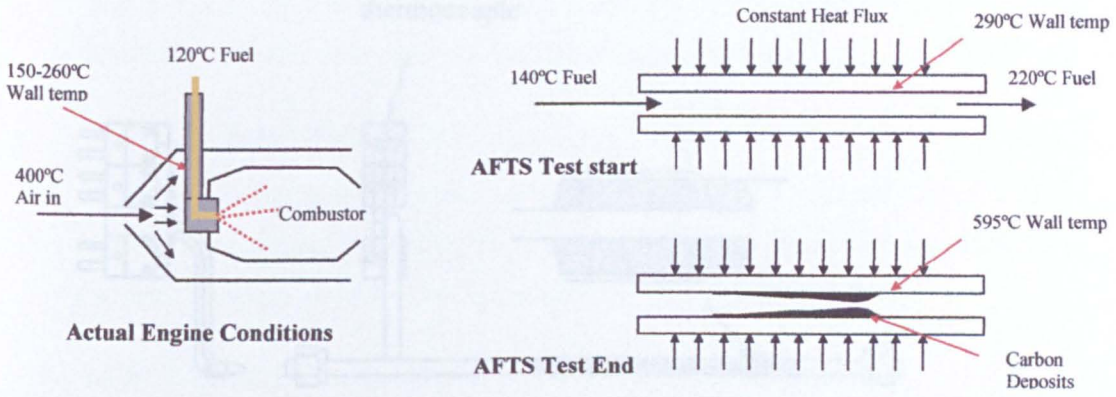

Figure 4-8 a: Aircraft Nozzle Heating, b: Nozzle Module Heating Mechanism

High pressure (HP) system assures that jet fuel is maintained above its vapor pressure to prevent the formation of two phase flow. The tube consists of three segments and two end attaching pieces. The middle segment is exposed to the thermal load. For the temperature rise detection along the tube's wall, there are three pairs of thermocouple. Each pair records the temperature from two different radial distance one approximately from the external wall and the second from slightly deeper point on to wall which is close to the deposit layer. This is schematically presented in Figure 4-9. The technical drawing of the heated tube and the location of thermocouples can be found in the Appendix C.

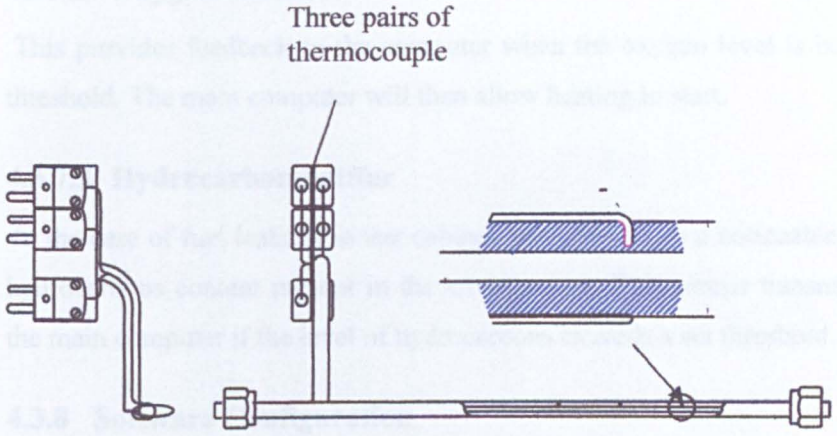

Figure 4-9 Heated Nozzle Tube Assembly

4.3.6 Instrumentation and Control

Independent process controllers are able to communicate with the main computer for set-point information control and the sub system temperatures within the AFTSTU. The entire instrumentation is placed in one cabinet which includes central safety barriers to decrease the risks of sparks in the main enclosure. The main controlling part consists of the control valves, six control loops, data logging, graphical user interface, alarms, and paging actions.

4.3.7 Safety of the System

To ensure that the test area meets health and safety requirements, five independent safety systems are included in AFTSTU:

4.3.7.1 Nitrogen purge

Prior to the test, all mechanical cabinets are purged with nitrogen, so oxygen is completely removed form the test cabinet. This assures that a fire will not ignite in the

case of fuel leakage over a hot component. Nitrogen passes continuously through the cabinets during the test.

4.3.7.2 Oxygen Sniffer

This provides feedback to the computer when the oxygen level is below a required threshold. The main computer will then allow heating to start.

4.3.7.3 Hydrocarbon Sniffer

In the case of fuel leakage in test cabinet, there would be a noticeable increase in the hydrocarbons content present in the environment. This sensor transmits feedback to the main computer if the level of hydrocarbons exceeds a set threshold.

4.3.8 Software Configuration

The graphical user interface allows the user to input the set points and displays the information on screen.

Once the software is loaded the first user screen is available as presented in Figure 4-10.

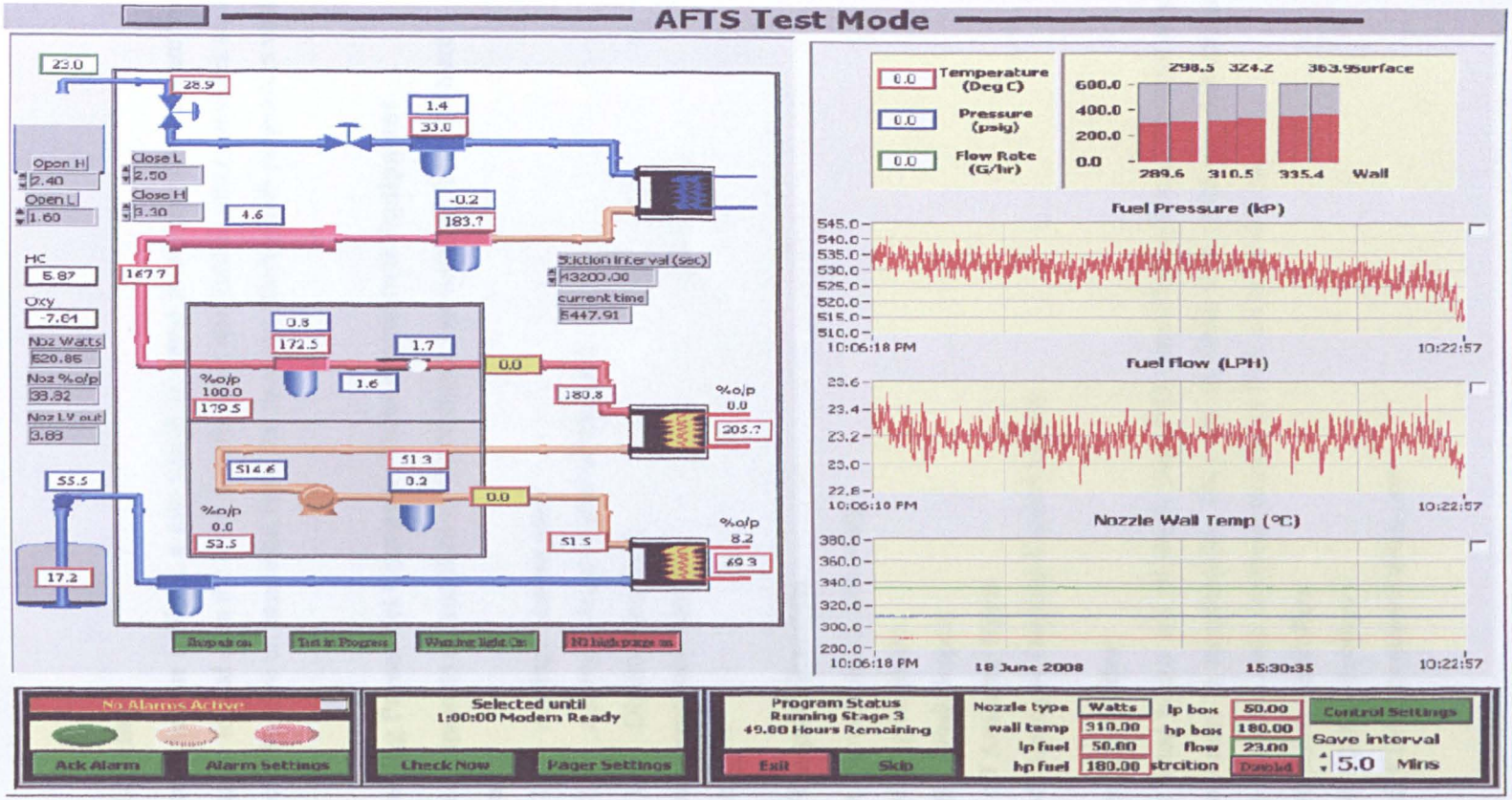

Figure 4-10: First user screen once the controlling software is loaded, see White (2000)

4.3.8.1 Data Logging

The software saves data in a file at a rate which is stated in set up. The data are tab separated and can be loaded onto the input devices to be analysed in other packages such as Microsoft Excel. To save on execution time, the user can select which parameters wish to save to file.

4.3.8.2 Controlling Personnel Computer Data acquisition Equipment

Data acquisition equipments are supplied by the National Instruments Plc™ which are listed as following:

i. PCI Analogue output card
ii. PCI Analogue Input/Digital output card
iii. PCI Digital Input Card
iv. Data interconnect cables
v. Hub units

4.3.8.3 Input/Output Channels

The input/output channels are as following:

i. 8 off Digital Inputs
ii. 8off Digital Outputs
iii. 64 off Analogue Inputs
iv. 8 off Analogue Outputs(Control Loops)

4.3.8.4 Process Controller

The instruments listed below are all single loop PID controllers which can control any process from flow rates to temperatures. They are all fitted with serial communication boards. This will allow the main computer to pass on their set point information.

i. 6 off safety controllers
ii. 2 off 2016 controllers
iii. 1 off KD485 communication port
iv.

4.4 Description of Test Method

The baseline tests were performed to investigate the operation of the AFTSTU after relocation and recomissioning at the University of Sheffield. The test procedure is discussed in the internal report by Blakey and Wilson (2008).

The AFTSTU ran for a total duration of 300 hours per test. This was divided into 4 stages allowing four different burner feed arm conditions to be investigated. All components prior to the nozzle operate under the steady state conditions excluding inter stage warm up and cool down times. Each stage ran to a different initial nozzle wall temperature at the corresponding power input. The nozzle was initially heated up to a fixed temperature and once steady state achieved, for that temperature, the heating power was fixed.

The temperature rise along the external wall was recorded by the three pairs of thermocouples. For each stage, a new nozzle was used to permit comparison between deposition rates at different initial wall temperatures. The difference between the two baseline tests was the operating temperature of the HP system with 160°C in the first, and 180°C in the second. The specifications required for the AFTSTU are shown in Table 4-1

	Normal Range	Baseline test			
Test time(h)	300	300			
Fuel flow rate(l/min)	23	23			
Low Pressure System(psi)	50-100	50			
LP bulk fuel temperature(°C)	50-100	50			
LP cabinet (°C)	500-100	50			
High Pressure System(psi)	500-1000	500			
HP bulk fuel temperature(°C)	50-200	160			
HP cabinet(°C)	50-200	160			
Stages	4	1	2	3	4
RF Heater Power(W)		480	510	600	630
Time(hrs)	<300	150	75	50	25
Inlet Feed Arm Temperature Baseline1 (°C)		150	150	150	150
Outlet Feed Arm Temperature Baseline1(°C)		163	167	171	172
Stages	4	1	2	3	4
RF Heater Power		450	460	520	580
	<300	150	75	50	25
Inlet Feed Arm Temperature Baseline2 (°C)		167	167	167	167
Outlet Feed Arm Temperature Baseline2(°C)		178	180	183	186
RF Box Temperature(°C)		51	51	53	53

Table 4-1: AFTSTU test parameters

Table 4-2 indicates the measurements made during the test. These measurements are normally recorded at every 10 min intervals.

Measurement	Description	Units
Temperature	Supply	°C
Pressure	LP System	Psi
Temperature	LP bulk fuel	°C
Temperature	LP cabinet	°C
Temperature	LP filter	°C
Diff.Pressure	Across LP filter	Psi
Pressure	HP system	Psi
Temperature	HP bulk fuel	°C
Temperature	HP cabinet	°C
Diff.Pressure	Spool flow across orifice plate	Psi
Diff.Pressure	Spool pressure drop	Psi
Temperature	HP filter	°C
Diff.Pressure	Across HP filter	Psi
Power	Feed arm heater	W
Temperature	Feed arm In	°C
Temperature	Feed arm A	°C
Temperature	Feed arm B	°C
Temperature	Feed arm C	°C
Temperature	Feed arm D	°C
Temperature	Feed arm E	°C
Temperature	Feed arm F	°C
Diff.Pressure	Across feed Arm	Psi
Temperature	Feed arm out	°C
Diff.Pressure	Across hot filter	Psi
Temperature	Cold filter	°C
Diff.Pressure	Across cold filter	Psi
Flow	Flow	L/min
Temperature	Exit	°C

Table 4-2: AFTSTU test measurements

Table 4-3 presents the residence time of jet fuel in low pressure and high pressure system.

Thermal Region	Temperature(k)	Residence Time(s)
LP System	323	1200
HP System	433-453	60

Table 4-3: The residence time of jet fuel in LP and HP system

The aviation fuel used in the experiments was the product of Merox and Hydrotreatment processes. The quality test result for this fuel was carried out in Shell Thornton and presented in Table 4-4 and Table 4-5.

Specification	Standard	Result	Units
Appearance			
Appearance	D 4176	Satisfactory	
Saybolt Colour	D158		
Colour		28	
Particulate Contaminant		D 5452/IP 243	
Total Contaminant		0.02	mg/L
Composition			
Acid, total	D 3242/ IP 354	0.002	mg KOH/g
Hydrocarbon types(FIA)	D 1319/ IP 156	18.5	%V
FIA Aromatics			
Sulphur, total	IP 336	0.07	%m/m
Mercaptan Sulphur	D 3227/ IP 342	0.0011	%m/m
Hydroprocessing Details	Calc		
Hydroprocessed Components		36.2	% V/V
Severely Hydroprocessed Components			
Volatility			
Distillation	D 86/IP 123		
IBP		149.8	°C
10% recovered		168.9	°C
20% recovered		178.2	°C
50% recovered		197.0	°C
90% recovered		239.2	°C
FBP		262.2	°C
Residue		1.5	% V/V
Loss		0.0	% V/V
Flash point	IP 170	40.5	°C
Density at 15	D 4052/ IP 365	801.9	Kg/m^3
Fluidity			
Freezing point	D 5972/ IP 435	-51.2	°C
Viscosity at -20	D 445/IP 71	3.778	cSt
Combustion			
Specific Energy net	D 3338	43.21	MJ/Kg
Smoke point	D 1322	210	mm
Naphthalene content	D 1840	15	% V/V
Corrosion			
Copper Corrosion	D 130/IP 323	1A	
(Thermal) Stability			
JFTOT(default 260	D 3241/ IP 323		
Pressure drop		<1	mmHg
Visual lubo rating		1	
Contaminants			
Existent gum	IP 540	<1	Mg/100 mL
MSEP with SDA	D 3948	96	
Other Tests			
Conductivity	D 2624/IP 274	285	pS/m
Conductivity Temperature		210	°C

Table 4-4: Aviation fuel quality test result

Specification	Standard	Result	Units
Appearance			
Appearance	D 4176	Sediment	
Saybolt Colour	D 156		
Colour		30	
Particulate Contaminant	D 5452/IP 423		
Total Contaminant		0.33	mg/l
Composition			
Acid, total	D 3242/IP 354	0.002	mg KOH/g
Hydrocarbon types(FIA)	D 1319/IP 156		
FIA Aromatics		18.3	%V
Mercaptan Sulphur(potentiometer)	D 3227/IP 342		
Mercaptan Sulphur		0.0014	% m/m
2D-GC composition	Thornton		
Carbon range		5-20	None
n paraffin		19.98	%w
iso paraffin		25.80	%w
naphtenics		22.24	%w
di naphtenics		7.38	%w
mono aromatics		18.42	%w
naphtenics mono aromatics		4.45	%w
di aromatics		1.92	%w
naphtenic di aromatics		0.03	%w
Volatility			
Distillation	D 86/IP 123		
IBP		151.6	°C
10% recovered		168.9	°C
20% recovered		176.4	°C
50% recovered		197.2	°C
90% recovered		239.5	°C
FBP		263.9	°C
Residue		0.9	% V/V
Loss		0.8	% V/V
Recovery at 200		53.7	% V/V
Recovery at 210		65.2	% V/V
Recovery at 240		90.3	% V/V
Flash point	IP 170	40	°C
Density at 15	D 4052 /IP 365	802.4	Kg/m^3
Fluidity			
Freezing point	D 2386/ IP 16	-53.5	°C
Viscosity at -20	D 445/ IP 71	3.793	cSt
Combustion			
Specific Energy net	0.3338	43.2	MJ/Kg
Smoke point	D 1322	20.5	mm
naphtalene content	D1840	1.3	% V/V
Corrosion			
Copper Corrosion	D 130/IP 154	1A	

Contaminants			
Existent gum	IP 540	<1	mg/100 mm
MSEP	D 3948		
MSEP with SDA		95	
Metals	TMS 573/08		
Copper	ICP-AES	<50	ppb
Iron		<10	Ppb
Tin		<100	ppb
Others		Nothing significant	
Other Tests			
Conductivity	D 2624/IP 274	89	pS/m
Conductivity Temperature		22	°C
Peroxide number	SMS 359-95	0.285(av)	ppm
Lubricity			
BOCLE	0.5001		
Mean WSD		0.61(av)	mm
Additives			
RED/A/610	18.95		mg/L
RED/A/621	0.92		mg/l

Table 4-5: Aviation fuel analytical test result

During the experimentation, Carbon Burn off was not available, therefore, quantification of deposit has not been included in this research.

4.5 Experimental Results

4.5.1 Baseline Test 1

For the stage1 of baseline test1, AFTSTU was expected to run for duration of 150 h with a power of the RF heater corresponding to a fuel temperature rise from 423°C (at inlet) up to 163°C (at outlet). The data recorded by the thermocouples indicates that temperature was increased throughout the test. Experiment was carried on normally up to 64 h and at this time, a leakage problem occurred and the system was shut down, fixed, and restarted. The results of temperature rise for the next 45h showed the same trend as for the first 64 h test.

Due to the LP heater malfunction, the system was shut down again. Then after the problem was fixed, the test was carried on for another 65 h. In spite of the fact that, the latter test run resulted in the same trend of the temperature rise for the thermocouples (A

and D) and (B and E) as for the first 64h, the results of the third thermocouples (C and F) were unexpectedly below. These are shown in Figure 4-11.

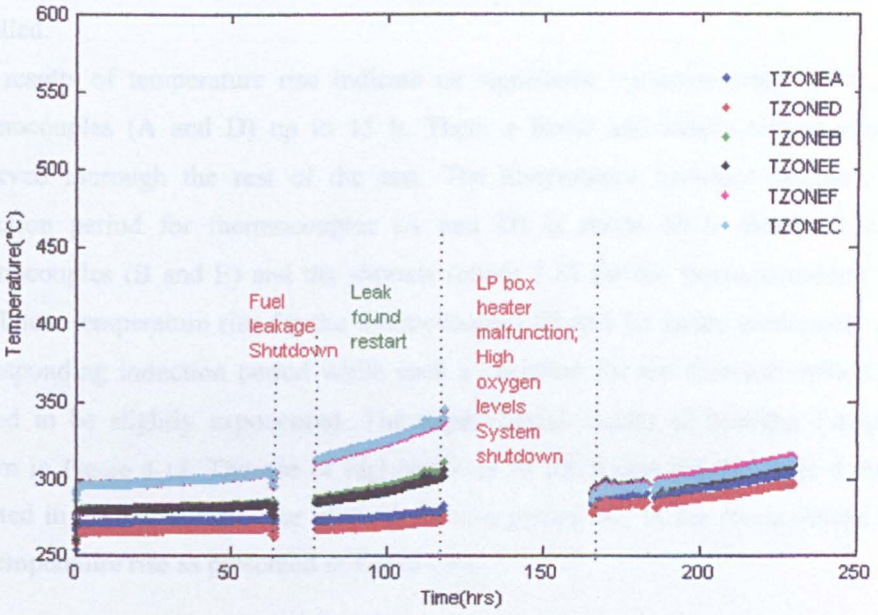

Figure 4-11: Results of temperature rise for the three sets of thermocouple for baseline 1, stage1

For the stage 2 of baseline test 1, total duration of 75 h was planned. A power was fixed in the RF heater corresponding to a rise from 150°C of inlet up to 167°C of the outlet for the entire duration of the test.

The test was carried on normally up to 20 h. At this instant malfunction was noticed on HP pump and the system was shut down. Once the problem was fixed, the system was restarted. The test was run again for about 40 h. The monitored temperature rise data for all three pairs of the thermocouples showed the same trend for the first 20 h with the lowest values for the nearest thermocouples to the inlet(A and D) and the highest for the thermocouples(C and F).

After approximately 60h, the system control computer was shut down automatically while the RF heater remained on. Then the system was manually restarted and run for another 10 h. The experimental results of baseline 1 stage 2 are shown in Figure 4-12.

For the stage3, baseline test1, the test was carried on for a total duration of 50 h without any malfunctions. A power by the RF heater corresponding to a rise in the jet fuel form inlet temperature (150°C) up to the outlet (171°C) for the entire duration of the test was supplied.

The results of temperature rise indicate no significant variation (only 2-3°C) for the thermocouples (A and D) up to 15 h. Then, a linear and steady temperature rise is observed thorough the rest of the test. The temperature invariant segment, namely induction period for thermocouples (A and D) is about 10 h shorter than of the thermocouples (B and E) and the shortest (about 7 h) for the thermocouples(C and F). The linear temperature rise for the thermocouples (B and E) varies moderately after the corresponding induction period while such a variation for the thermocouples(C and F) tended to be slightly exponential. The experimental results of baseline 1-stage 3 are shown in Figure 4-13. The use of higher power of RF heater for the stage 4, baseline1 resulted in the same behaviour of the induction period and in the characteristic form of the temperature rise as presented in Figure 4-14.

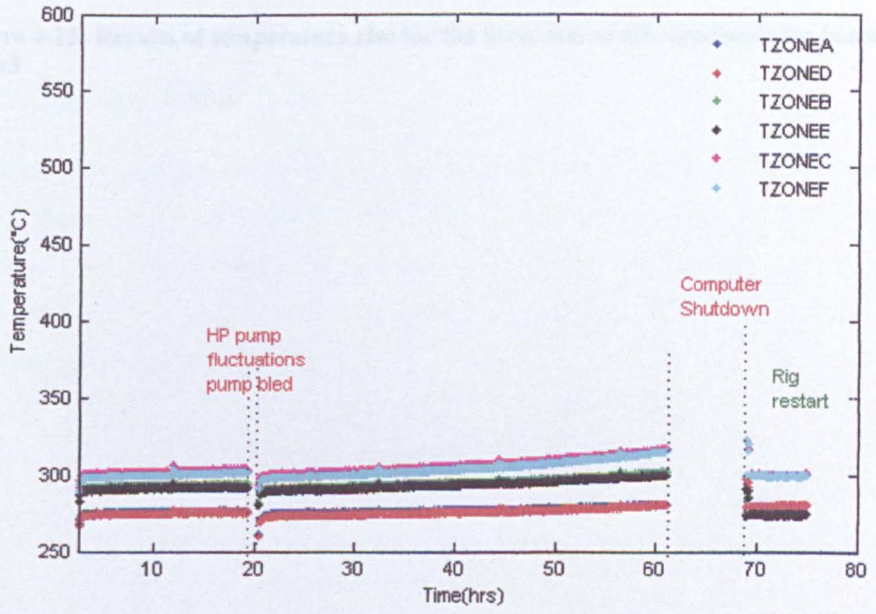

Figure 4-12: Results of temperature rise for the three sets of thermocouple for baseline 1, stage 2

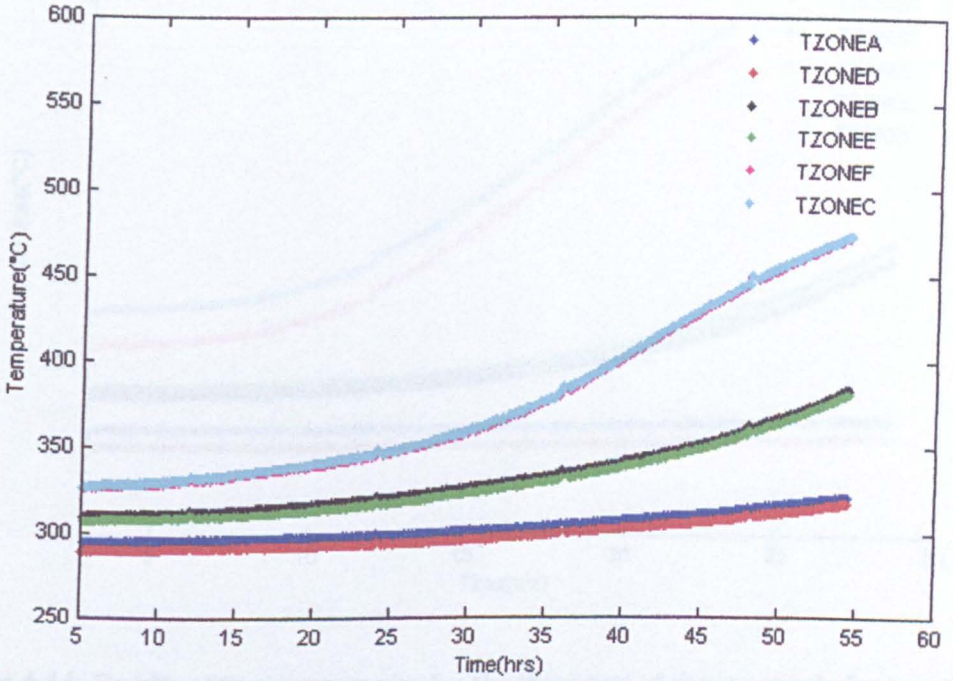

Figure 4-13: Results of temperature rise for the three sets of thermocouple for baseline 1 stage3

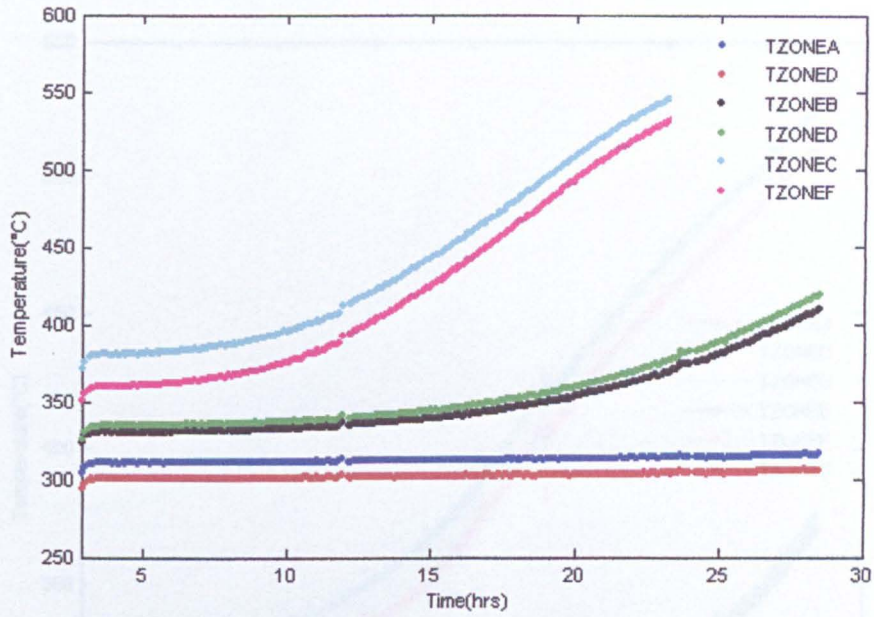

Figure 4-14: Results of temperature rise for the three sets of thermocouple for baseline 1 stage4

4.5.2 Baseline Test 2

Similarly, the experimental results of baseline test 2, prove that the use of different power of RF heater yield the typical temperature profile starting with an induction period followed by a rise corresponding to the each stage. For this baseline test, however, the fuel temperature at nozzle entrance was increased by the application of High pressure heater as presented in Table 4-1.

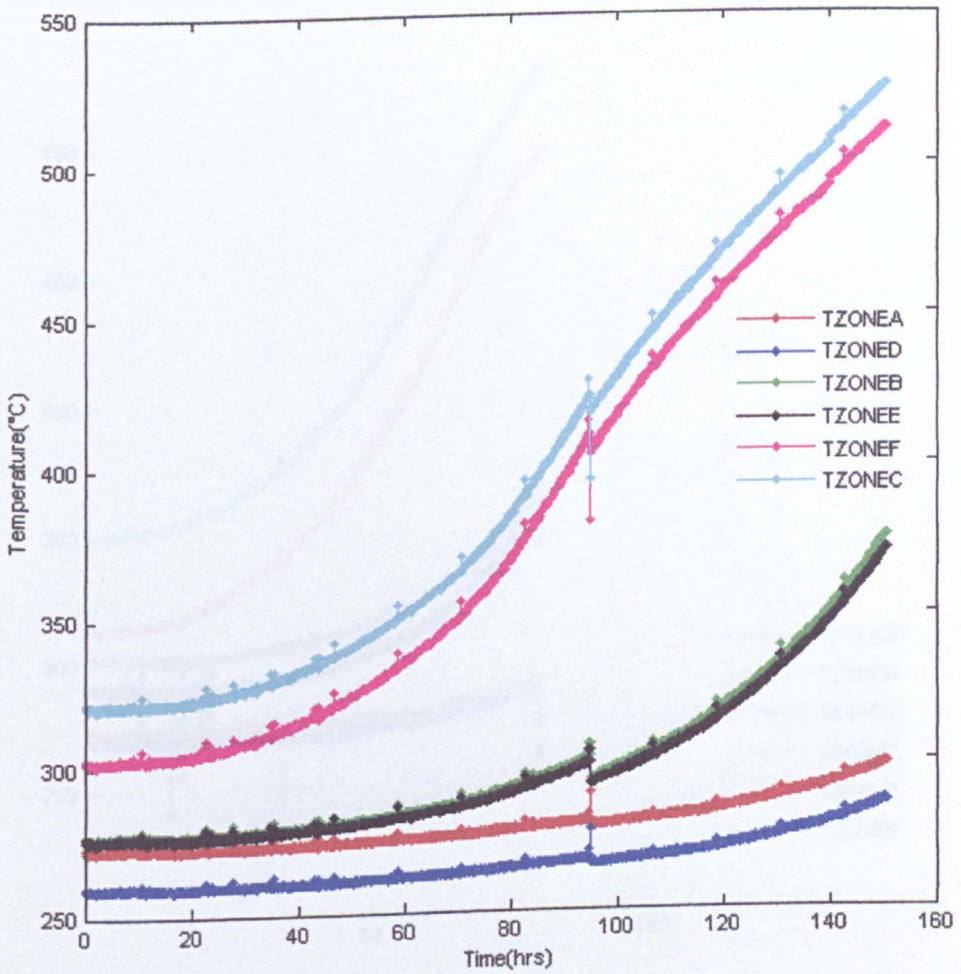

Figure 4-15: Results of temperature rise for the three sets of thermocouple for baseline 2 stage 1

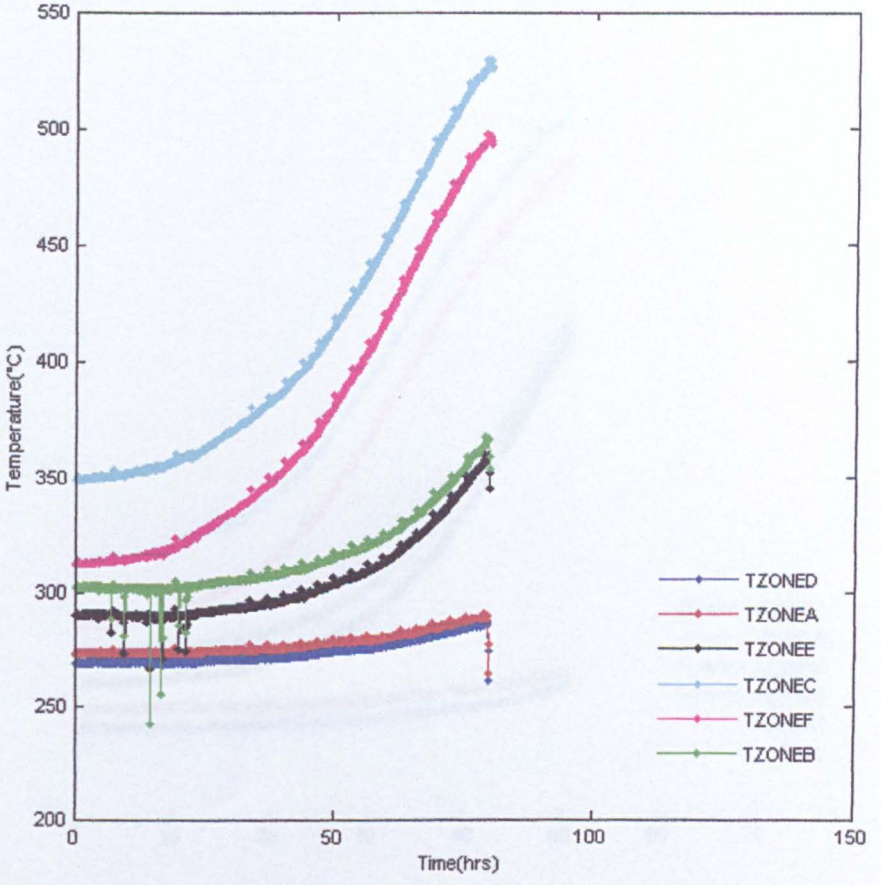

Figure 4-16: Results of temperature rise for the three sets of thermocouple for baseline 2 stage2

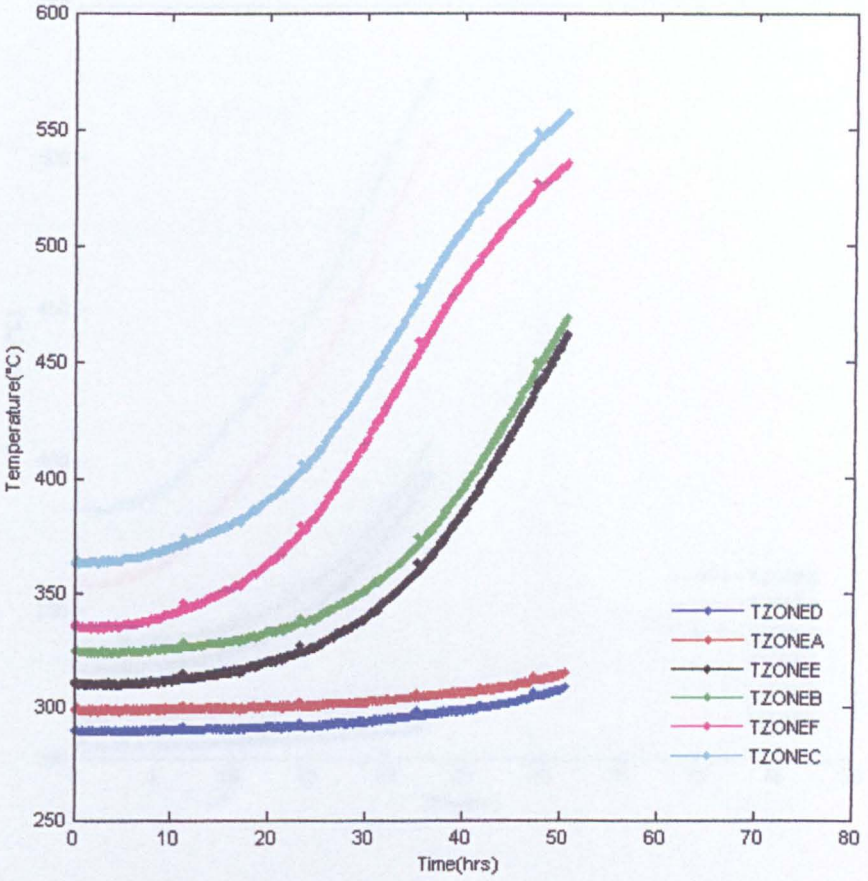

Figure 4-17: Results of temperature rise for the three sets of thermocouple for baseline 2 stage3

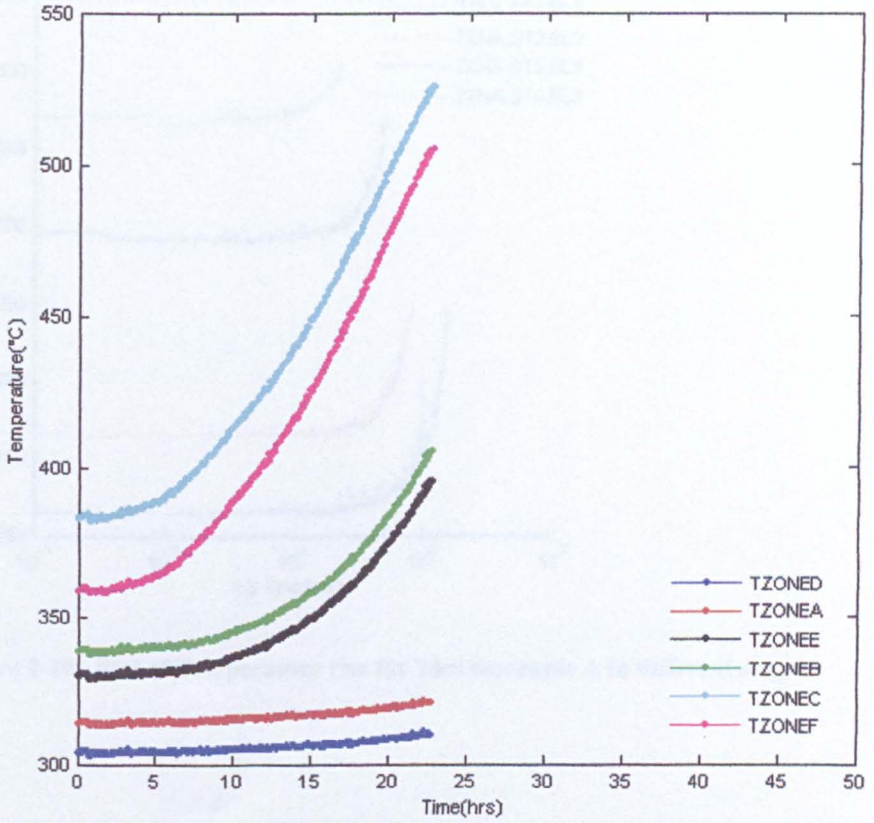

Figure 4-18 : Results of temperature rise for the three sets of thermocouple for baseline 2, stage4

The experimental results of thermocouples A, B, and C for all of the four stages in baseline test 2 are plotted in Figure 4-19, Figure 4-20 and Figure 4-21. These three figures indicate that the length of the induction period is inversely proportional with the power supplied by RF heater in all stages. It has also been observed that for each data point, regardless of the amount of power supplied, after the induction period, an accelerating and non linear temperature rise occurs that takes until the end of the test run.

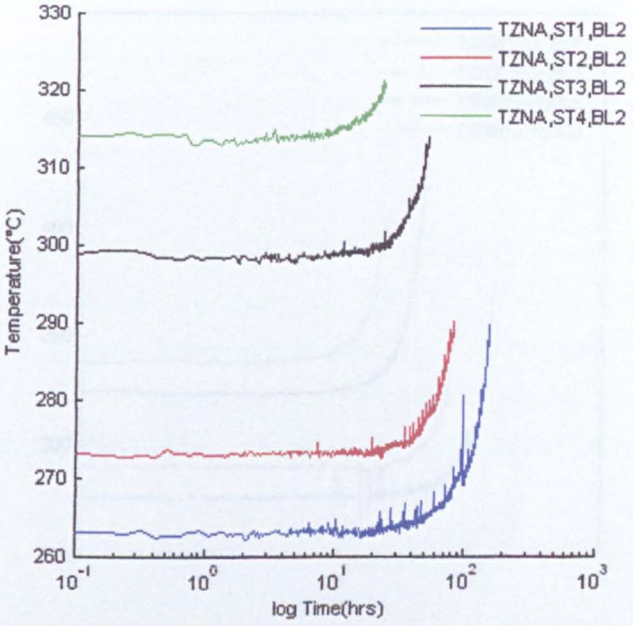

Figure 4-19: Plot of Temperature rise for Thermocouple A in different stages

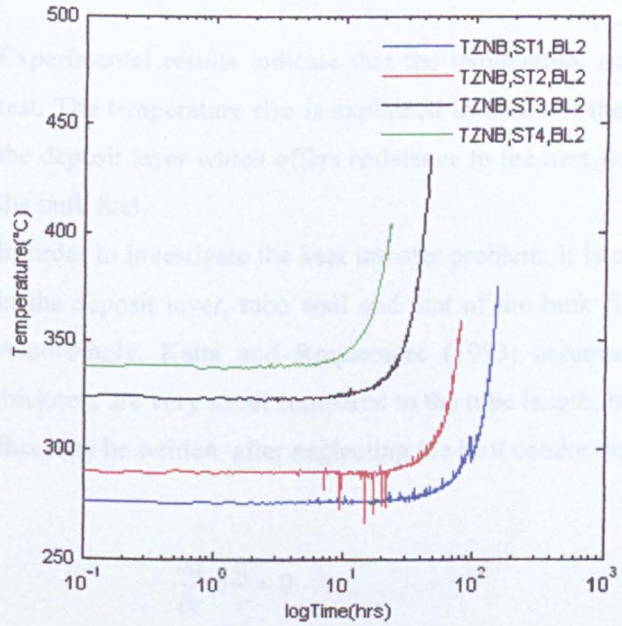

Figure 4-20 : Plot of Temperature rise for Thermocouple B in different stages

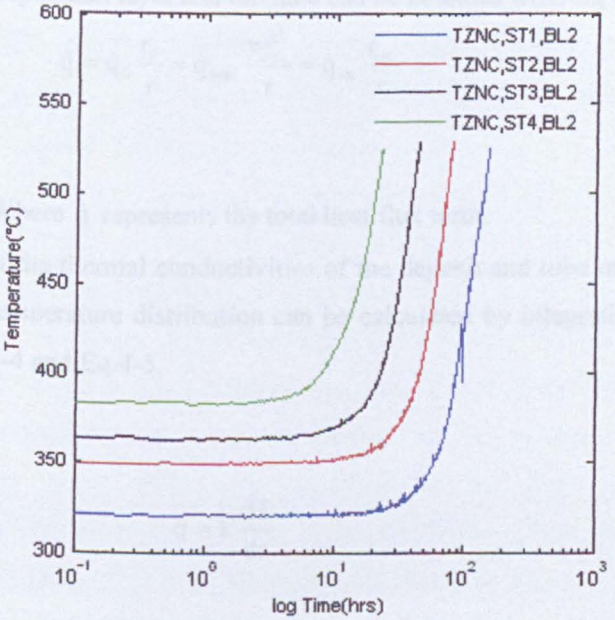

Figure 4-21: Plot of Temperature rise for Thermocouple C in different stages

4.6 Discussion

Experimental results indicate that the temperature across the wall increases during the test. The temperature rise is explained in terms of thermally insulative characteristics of the deposit layer which offers resistance to the heat flow from the stainless steel towards the bulk fuel

In order to investigate the heat transfer problem, it is considered that the heat distribution in the deposit layer, tube wall and that of the bulk flowing fuel occurs simultaneously. Accordingly, Katta and Roquemore (1993) assumed that the deposit and tube-wall thickness are very small compared to the tube length, hence, the heat equation for the heat flux may be written, after neglecting the heat conduction in the axial direction as Eq 4-1

.

$$\frac{\partial \dot{q}}{\partial r} + \frac{\dot{q}}{r} = 0 \qquad \text{Eq 4-1}$$

By integration of Eq 4-1 the analytical expression for the heat-flux distributions in the deposition layer and the tube can be obtained from Eq 4-2

$$\dot{q} = \dot{q}_0 \frac{r_0}{r} = \dot{q}_{wall} \frac{r_{wall}}{r} = \dot{q}_{int} \frac{r_{int}}{r} \qquad \text{Eq 4-2}$$

Where $\dot{q}$ represents the total heat flux term.

If the thermal conductivities of the deposit and tube metal are denoted by k_d and k, their temperature distribution can be calculated by integration of Eq4-3 Which results in Eq 4-4 and Eq.4-5.

$$\dot{q} = k \frac{dT}{dr} \qquad \text{Eq4-3}$$

$$T = T_{int} + \int_{r\,int}^{r} \left(\frac{\dot{q}_{int} r_{int}}{k_d}\right)\frac{1}{r}dr \qquad \text{Eq 4-4}$$

$$T = T_{wall} + \int_{rwall}^{r} \left(\frac{\dot{q}_{wall} r_{wall}}{k_t}\right)\frac{1}{r}dr \qquad \text{Eq.4-5}$$

If k_t is independent of temperature, and the tube wall is assumed to have homogenous properties, then an expression for the tube outer wall temperature can be calculated by solving Eq.4-5 which yields Eq.4-6

$$T_0 = T_{wall} + \frac{\dot{q}_{wall} r_{wall}}{k_t} \ln\left(\frac{r_0}{r_{wall}}\right) \qquad \text{Eq.4-6}$$

For a given constant heat-flux at boundary in each time step, Eq 4-2 can be solved for the value of $\dot{q}_{int}$ and then flow calculations can be performed using this value at the corresponding boundary condition (deposit layer for instance).

However, with respect to the operational mode of RF heater which is based on the induction heating, the problem is slightly different. That is, the temperature rise within the AFTSTU tube can be expressed in terms of an energy accumulation on a time basis approach. Although the inflow and outflow terms are both surface phenomena and are associated with the processes occurring at the control surface, RF unit operation is based on the energy generation for the piece of the metal when is placed inside the coil. Hence, there is no inflow term in the form of heat to enter in the control volume through the surface. In fact, energy generation term is a volumetric phenomenon and occurs within the control volume and is associated with the conversion from a form of energy (electromagnetic) to heat. Consequently, on a time basis, the rate of temperature rise in AFTSTU tube is equal to the rate at which thermal energy is generated within the tube minus the sum of the rate at which thermal energy leaves the control volume due to heat lost and the amount of energy required for deposit to be built up.

Figure 4-22 indicates that extremely low amount of bulk fuel is converted to the intermediate and product species, throughout the jet fuel autoxidation. In this case the enthalpy of reaction during the autoxidation process and deposition stager is negligible, therefore the energetic of carbon build up can be neglected from the energy balance, and hence the temperature rise is a net result of energy generated in the wall minus heat lost from the surfaces of AFTSTU tube.

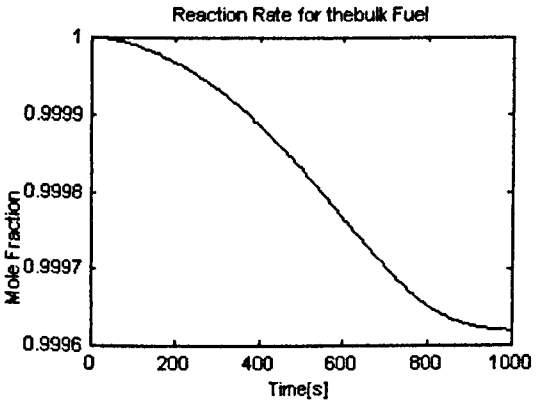

Figure 4-22: Conversion of bulk fuel during the carbon deposition process based on zero dimensional calculation using the integrator code

Although the temperature rise can be expressed in terms of first law of thermodynamics, the existence of induction period and also interpretation of the profile of the temperature rise is not very straight forward.

It was briefly discussed in chapter 2 that prior to the deposition stage a multitude of physical interactions can take place including the agglomeration of insoluble products (precursors) to the micro spherical particles, the settlement of the micro spherical particles to surface after impingement form the liquid and eventually particles coalescence and plastic flow to form the varnish like layer upon which additional particles can occur followed by the further oxidation to form coke. A realistic interpretation of surface deposition necessitates that ensemble of these "less clearly understood" to be considered.

Katta and Roquemore (1993) stated that temperature for the fuel interface region within a cylindrical passage remains more or less unchanged while the tube is exposed to a constant heat flux that is a similar condition with AFTSTU heated nozzle. Unfortunately there is no data recorded for this region. Although the temperature at the fuel exit shows no change throughout the entire test, the thermocouple reads these data form the tube centreline.

4.7 Conclusion

The experimental attempts were carried out to investigate the surface deposition on inner surface of the heated nozzle of the AFTSTU. The test was performed in two baselines; each consisted of four different thermal loads. In the baseline 2, the fuel inlet temperature for every stage was higher than the stage 1. The duration of experiment for each baseline was in the order that the larger test duration to be for the lowest thermal load.

The results of both baseline tests indicate that temperature increases along the tube's wall in a non linear manner as function of time. A closer look at the results of temperature reading for each thermocouple exhibits a similarity for all of the experiments. Accordingly, in each graph, a temperature invariant region is observed at the beginning of the test which can be continued up to the 15 hours. The length of this region is different for each stage of test depending on the amount of thermal load. The slope of the temperature rise profile can be function of location of thermocouple and the thermal load exposed on fuel. Hence, regardless of the amount of thermal load supplied for each test stage, the lowest is for the position of the first thermocouples which is the one closest to the fuel inlet and the highest is monitored for the farthest thermocouple. For the same position of thermocouples, the slope of the temperature rise varies with the amount of thermal load, in the way that, the application of higher thermal loads results in a higher slop.

The third region of the graph which is best manifested for the data taken from the farthest thermocouple indicate that the temperature rise is followed by a level off zone. As an overall trend, it can be concluded that the temperature reading graphs manifest as a sigmoid shape.

It is rather important to mention that, as was proved by Siouris(2009) the values of temperature reading by the thermocouple are highly dependent on the location of thermocouples.

CHAPTER 5

APPLICATION OF COMPUTATIONAL FLUID DYNAMICS FOR JET FUEL THERMAL DEGRADATION MODELLING

5.1 Introduction

It is essential for both aircraft engine manufacturers and jet fuel producers to gain a fundamental knowledge of fuel thermal stability. Such knowledge will be applicable in creation of predictive methods for the evolution of deposit and its rate of accumulation in fuel lines. For this reason, jet fuel thermal stability has been the area of research for many years by different sections and great deals of experimental data and empirical correlations have been created.

Computational fluid dynamic approach is the ensemble of different knowledge and techniques developed to solve partial differential equations representing the mass, momentum, energy and turbulence. Generally, analysis of a chemical process and its interaction with transport phenomena is quite complicated and is intimately connected to the fundamental of fluid dynamics. For the investigation of jet fuel thermal degradation process, however, such a combined analysis, at the first stage, necessitates to comprehend a realistic chemical scheme of jet fuel thermal degradation along with the subsequent deposition sub mechanism. It is, however, important to understand that such mechanism is an intrinsic property of a given system and is not a function of any physical process such as mixing or heat and mass transfer. Once the chemical mechanism is available, the production rate and composition of the products can be related to the transport equations for the deposition modelling in various geometries.

Discussions about the chemical mechanism have been provided in chapter 2 and chapter 3 of this thesis. Although, a number of attempts have been carried out over the years to employ various chemical schemes in CFD models, to date, very little is known about the reliability of these schemes for the case of more severe situations similar to those

occurring in real aircraft jet fuel system. The kinetics parameters for these surface deposition sub models will not assure universality since they have been adjusted for the particular cases. In addition, these sub mechanisms contain only two or three reactions describing the surface process. Such complex phenomenon ought to be more descriptive. Furthermore, the most recent CFD models are based on the application of pseudo detailed mechanism whose validation was performed using less realistic boundary conditions. For instance, there are a number of models validated against the NIFTR experimental conditions aiming to predict the surface deposition rate as well as the axial location of the peak deposition. Although, near isothermal condition provide a simplified temperature distribution in reaction medium, in actual aircraft jet fuel system, the environment is subject to the rigorous temperature changes which may have significant impacts on fuel chemistry.

Due to the complex flow pattern and high cost of computation, it is not yet practical to model the entire aircraft fuel system. Correspondingly, as the first step of modelling, it is essential to begin with the simulation of deposition in a simple geometry such as the heated nozzle module of the Aviation Fuel Thermal Stability Test Unit (AFTSTU). This is assimilated with the feed arm injector in a real aircraft fuel system.

The purpose of chapter 5 is to describe a formulation for real time growth of deposit on inner surface of a cylindrical tube. Accordingly, a moving boundary technique based on the surface deposition in radial direction has been presented. This has been used in Fluent 6.3.26 to imitate two different experiments, firstly NIFTR and then the heated nozzle module of the AFTSTU.

5.2 Computational Fluid Dynamics (CFD)

Advances in the capacity of digital computers to store data and to perform algebraic equations representing the fluid mechanic have been significantly facilitated the solution of numerical techniques. These resulted in the progress of CFD models with wide applicability in different engineering areas.

Having less cost, with lower risk and much shorter time than experiment, CFD techniques proved to be quite practical for the detailed analysis at the early stage of engineering design. However, solution of partial differential equations can be quite complicated for

the most of engineering applications. Although, flow pattern in a cylindrical fuel passage like NIFTR and AFTSTU heated nozzle are relatively straight forward, even in such simple flow regimes, numerical simulations will always be approximated and hence accompanied with the errors due to a number of reasons. First and foremost, the capabilities of CFD models are limited to the accuracy of the solution of partial differential equations which in turn depends on various factors. The major constraint in the use of partial differential equations is the complexities associated with the physical model. Moreover, the following items are also important in creating the errors, see Ranade (2002)

i. Fluid dynamic equations as such ;
ii. Input data and boundary conditions;
iii. Numerical methods and convergence criteria;
iv. Computational limitations;
v. Interpretation of results

In order to reduce the errors, it is essential to develop an appropriate methodology to combine the potential of CFD for engineering analysis. The methodology that has been used in this thesis is presented in the chart presented in Figure 5-1.

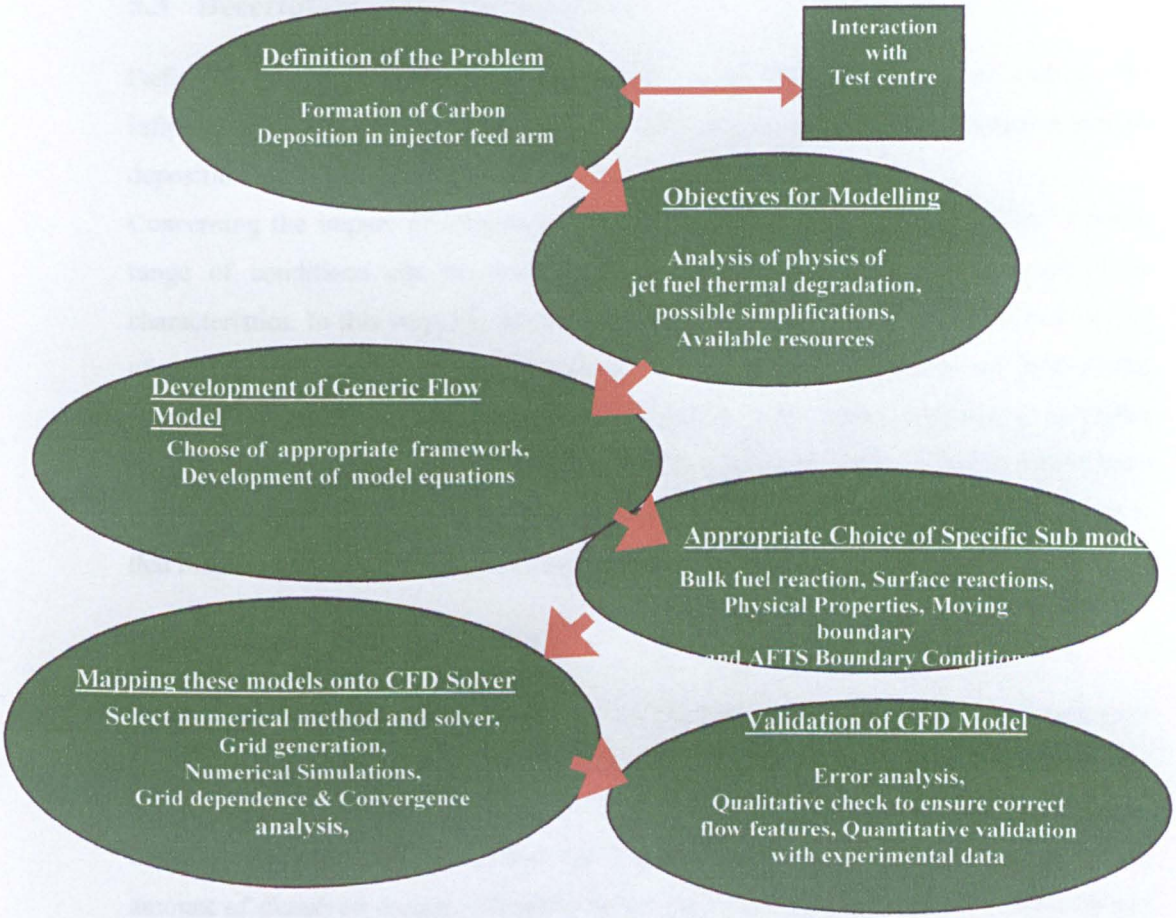

Figure 5-1: Methodology used for the computational fluid dynamic for the investigation of carbon deposit process.

5.3 Description of the Methodology

Definition of jet fuel thermal stability and its favourable situation as well as the influencing parameters on the emergence of deposit precursor and the subsequent surface deposition are addressed in chapter 2.

Concerning the impact of influencing parameters on jet fuel thermal stability, a broad range of conditions can be encountered in terms of temperature, time, and flow characteristics. In this way, the process has been observed to proceed over a long period of time and relatively low temperature in a laminar fluid flow system or even whilst stagnant during the storage, as well as a shorter time where exposed to a higher temperature. Similarly, in AFTSTU, since bulk fuel faces with different temperature regimes within the fuel pipe lines, it undergoes a number of physico chemical interactions that may result in the change of its chemical compositions.

5.3.1 Objectives for Modelling

The primary purpose of the simulation in this chapter is to develop a numerical technique for the investigation of real time growth of deposit on inner surface of a cylindrical passage subject to heating.

It was discussed in chapter 2 that the previous investigations indicate under certain amount of dissolved oxygen (70 ppm) in jet fuel and in presence of heat, autoxidation reactions are initiated within the bulk fuel. It was also reviewed that the simplest model which accounts for the entire process of carbon deposition on the tube wall surface is simply divided in a two path process including bulk and surface reactions. Bulk fuel reactions in the form of liquid phase autoxidation have been formulated and validated for a wide range of experimental conditions. This resulted in a comprehensive chemical mechanism known as pseudo detailed. Regardless of practicability of this mechanism in simulation of deposition for NIFTR, very little is known about it's viability in prediction of deposit in real jet fuel systems where the thermo fluid characteristics are far from the isothermal and laminar conditions.

From the stand point of chemical kinetics, increasing the residence time of thermally stressed jet fuel in heated tubes would be expected to boost the total quantity of carbon deposition, however, it has been shown by Marteney and Spadaccini (1986) Chin and Lefebvre(1993) and Spadaccini *et al* (2001) that the total amount of carbon deposition changes in an inversely proportional trend with respect to the Reynolds number modification for the same diameter of the tube. A possible explanation for such an ambiguous observation is to consider that the increase of radial diffusion acts as a controlling factor for the migration of deposit precursors.

The concepts of residence time distribution and mixedness have been extensively applied in the past to gain an insight into the interaction of flow, mixing and chemical reactions especially for the combustion problems. It is well postulated that when the characteristic time scale of chemical reactions is comparable with or lower than the characteristic time scale for mixing, effective reaction rate is a complex function of mixing and chemical kinetics. Therefore, several models such as micro mixing models have been developed to treat these situations. These models require information about local turbulent kinetic energy and energy dissipation rates. However, the results of jet fuel autoxidation indicate that the time scale for 70 ppm of dissolved O_2 in bulk fuel to be completely consumed is in the order of minutes, hence, it is assumed that the thermal degradation of jet fuel is governed only by chemical kinetics.

In any reactive flow process, molecular diffusion, which brings molecules of different species into close contact, is essential for chemical reaction to initiate. Consequently, reactive flow processes are therefore controlled by the combination of fluid mechanics, mixing, diffusion and chemical reactions. The interaction of these processes may lead to different classes of reaction rate for chemical transformations. Accordingly, the same chemical kinetics may be classified as slow or fast depending on the relative rates of reactions and mixing, see Ranade(2002).

There are two extremes of molecular mixing which are known as microfluid and macrofluid. In microfluid, species are entirely mixed on a molecular scale while in macrofluid; there is no mixing on a molecular scale, even though, the lumps of fluid are macroscopically well mixed. Therefore, when reactants A and B are mixed on a molecular scale at a rate much faster than the reaction rate (microfluid), reaction takes

place and the effective rate will be controlled by reaction kinetics. When reactants A and B are not mixed on a molecular scale virtually no reaction can take place. So in this case they behave like in an intermediate way, exhibiting A-rich and B-rich regions with partial segregation, see Ranade(2002).

For the jet fuel autoxidation, is assumed that the distribution of dissolved O_2 (molecular oxygen) is spatially uniform throughout the bulk fuel (volume of reaction). The effect of diffusion is manifested merely on the transport of precursor species from the bulk fuel towards the wall. In general, the diffusive mass flux includes diffusion due to concentration gradients, diffusion due to thermal effects (Soret diffusion), and diffusion due to pressure and external forces. Due to the high concentration gradients, in many cases the contribution of thermal diffusion is very small compared to the concentration diffusive flux.

It is noteworthy to mention the in the course of jet fuel autoxidation and subsequent surface deposition process problem proceeds via different phases. This can be justified by the fact that the insoluble species which are originated through the jet fuel autoxidation path can form a filterable solid phase in bulk fuel. Although, for simplicity it is assumed that the contribution of all species to the formation of solid carbon occurs in a single continuous phase.

Following on the establishing objectives; the general theoretical frameworks; and the simplifications; the starting step of modelling was to develop a mathematical model i.e. proper equations and boundary equations.

Since jet fuel is considered as a Newtonian fluid, the knowledge of fluid viscosity is sufficient to develop the governing fluid dynamic equations. Navier Stokes equations represent the behaviour of an incompressible Newtonian fluid as long as the continuum assumption is valid; see Fluent User Guide (2003).

Turbulent flow is naturally unsteady and three dimensional. The flow under turbulent condition is characterised by numerous rotational structures known as turbulent eddies with a wide range of length scales. The eddy motions and the interactions between them at different length scales result in the effective contact between fluid particles which are initially separated by long distance. Hence, heat, mass, and momentum are very effectively exchanged. The rate of scalar mixing in turbulent flows is greater by orders of

magnitude than in laminar flows. Heat and mass transfer rates are also significantly higher than in turbulent flows. Turbulent flows are also characterised by fluctuating velocity filed. Since these fluctuations can be of small scale and high frequency, they are computationally too expensive to be directly simulated in practical engineering calculations. Instead, the instantaneous governing equations can be time averaged to remove small scales resulting in a modified set of equations that are computationally less expensive. However, the modified equations contain additional unknown variables and turbulence models needed to determine these variables, see Ranade (2002) and Fluent User Guide (2003).

5.3.2 Mathematical Formulation

5.3.2.1 Heat Transfer Equations

The first law of thermodynamics is used to determine the temperature distribution in axial and radial directions of tube. This includes the calculation of heat transfer through the heat conduction within the wall and heat convection and radiation between the tube wall and surrounding air and also energy generation term due to the RF heater and a change in thermal energy storage.

The energy balance for a control volume is presented as Eq 5-1.

$$\dot{E}_{in} - \dot{E}_{out} = \dot{E}_{St} \qquad \text{Eq 5-1}$$

Heating occurs uniformly within the tube volume so can be expressed in terms of volumetric heat generation rate $\dot{q}$ (W/m^3) as presented in Eq 5-2.

$$\dot{E}_{in} = \dot{q}V \qquad \text{Eq 5-2}$$

The flux of energy lost due to the convection and net radiation from the surface can be presented as Eq 5-3.

$$\dot{E}_{out} = h(\pi DL)(T_w - T_{sur}) + \varepsilon\sigma(\pi DL)(T^4 - T^4_{sur}) \qquad \text{Eq 5-3}$$

Consider a cylinder of radius r with uniformly distributed heat sources and constant thermal properties such as specific heat, density, and thermal conductivity. If the cylinder is sufficiently long enough, the appropriate differential equation may be obtained by neglecting the axial heat conduction.

$$\frac{d^2T}{dr^2} + \frac{1}{r}\frac{dT}{dr} + \frac{\dot{q}}{k} = 0 \qquad \text{Eq 5-4}$$

5.3.2.2 Continuity Equations

In general the microscopic mass balance of a species over an element of volume can be written according to the Eq 5-5.

Eq 5-5

accumulation of component k =	rate of change of component k due to convection +	rate of change of component k due + to dispersion	rate of change of component k due to reaction

A simplified way to mathematically represent the formation, destruction, and transport of a given species within the fluid is through the notation of general transport equations for the concentration of the species k as illustrated Eq 5-6.

$$\frac{\partial(k)}{\partial t} + \frac{\partial(\rho U_i k)}{\partial x_i} = \frac{\partial}{\partial x_i}(J_k \frac{\partial k}{\partial x_i}) + Sf_k + Sd_k \qquad \text{Eq 5-6}$$

Where ρ is the density of the fluid, k is the concentration of any component, U_i is the local velocity in the x_i direction , J_k is the effective diffusivity of k includes both molecular and turbulent diffusion and Sf_k and Sd_k are the source terms representing the creation and destruction of a given species k per unit volume.

The first term of the right hand side in Eq 5-6 represents the changes in species mass fraction due to the diffusive fluxes. The diffusive flux in the absence of external forces becomes as Eq 5-7.

$$J_k = -\rho D_{km} \nabla D_{kT} \frac{\nabla T}{T} \qquad \text{Eq 5-7}$$

Where D_{km} is the diffusion coefficient for the species k in the mixture and D_{kT} is the thermal mass diffusion coefficient for species k. In many cases the contribution of thermal diffusion is very small compared to the diffusive flux due to the concentration gradients. So in this case when only the diffusion due to the concentration gradient is considered and the species conservation equations become as Eq 5-8.

$$\frac{\partial}{\partial t}(\rho m_k) + \nabla.(\rho U m_k) = \nabla.(\rho D_{mk} \nabla m_k) + S_k \qquad \text{Eq 5-8}$$

The summation of species conservation equations of the form of mass fraction for all species present in the continuous phase results in the overall mass conservation equations as presented in Eq 5-9.

$$\frac{\partial}{\partial t}(\rho) + \nabla.(\rho U) = \sum_k S_k \qquad \text{Eq 5-9}$$

5.3.2.3 Turbulence Equations

The Reynolds-averaged form of the conservation equations of mass and momentum for an incompressible fluid can be written as Eq 5-10 and Eq 5-11.

$$\nabla.(\rho \overline{U}) = \sum_k \overline{S}_i \qquad \text{Eq 5-10}$$

$$\frac{\partial}{\partial t}(\rho\overline{U}) + \nabla.(\rho\overline{U}\overline{U} + \rho\overline{u}\overline{u}) = -\nabla\overline{p} - \nabla.\overline{\tau} + \rho g + \overline{F} \qquad \text{Eq 5-11}$$

Where the overbar indicates a time averaged value and u is the fluctuating velocity. The terms in this equation resemble those in the conventional equation of conservation of momentum except for an additional term appearing on the left hand side. These extra terms act as apparent stresses due to turbulent motions and are called Reynolds stresses or turbulent stresses and defined as Eq 5-12.

$$(\tau_{ij})_{turb} = \rho\overline{u}_i\overline{u}_j \qquad \text{Eq 5-12}$$

The Reynolds averaged form of conservation equation for a general variable ϕ can be written as Eq 5-13.

$$\frac{\partial}{\partial t}(\rho\overline{\phi}) + \nabla.(\rho\overline{U}\overline{\phi} + \rho\overline{u\phi'}) = \nabla.(\overline{j_\phi}) + \overline{S_k} \qquad \text{Eq 5-13}$$

In the Reynolds averaging approach, it is not necessary to resolve for all the smallest scale (spatial and temporal) phenomena since the variation of time averaged quantities occurs at much larger scales. Therefore, this approach requires much less computing resources than DNS and LES.

Time averaging of the basic governing equations of flow processes leads to the appearance of new terms in the governing equations, which can be interpreted as apparent stress gradients and heat and mass fluxes associated with the turbulent motion. In principle, governing equations for these new terms can be derived; however, these contain further unknown terms. It becomes, therefore, necessary to introduce a turbulent model which relates the new unknown terms to known terms in order to close the set of

governing equations. The process of closing the set of equations through a turbulence model introduces some approximations and assumptions.

A turbulence model is a set of equations which express relations between unknown terms appearing in Reynolds averaged governing equations with known quantities. Reynolds averaged equations consist of four equations (one continuity and three momentum conservation equations) and thirteen unknowns (three mean velocities, mean pressure, and nine Reynolds stresses). Similarly, for a general scalar variable, ϕ there is one conservation equation and four unknowns (mean value of general variable, $\overline{\phi}$ and three turbulent fluxes $\overline{u\phi'}$. The desired turbulence model has to develop a relationship between these extra unknowns' fluxes and known mean variables.

RANS based turbulence models can be grouped into two classes: one which uses the concept of turbulent or eddy viscosity and another which does not. The most widely used turbulent model for the engineering application is two equations model, namely, $k-\varepsilon$ model. For the information about this turbulent model see the Computational Fluid Dynamics text books.

5.3.2.4 Mathematical Formulation for Moving Boundary

Dynamic mesh model in Fluent can be applied to simulate flow equations as well as the chemistry of autoxidation and surface reaction where the initial boundary changes with time due to motion on the domain boundaries caused by deposition. The motion type can be illustrated as the Eq 5-28, see Fluent User Guide (2003).

The integral form of the conservation equation for a general scalar ϕ on an arbitrarily control volume V whose boundary is moving can be written as Eq 5-14

$$\frac{d}{dt}\int_V \rho\phi dV + \int_{\partial V} \rho\phi(\vec{u}-\vec{u}_g)d\vec{A} = \int_{\partial V} \Gamma\nabla\phi d\vec{A} + \int_V S_\phi dV \qquad \text{Eq 5-14}$$

Where ρ is the fluid density, $\vec{u}$ is the flow velocity vector, $\vec{u}_g$ is the grid velocity of the moving mesh, Γ is the diffusion coefficient and S_ϕ is the source term of ϕ. ∂V is used here to represent the boundary of the control volume V.

The time derivative terms can be expressed by the application of first-order backward different equation as presented in Eq 5-15.

$$\frac{d}{dt}\int_V \rho\phi dV = \frac{(\rho\phi V)^{n+1} - (\rho\phi V)^n}{\Delta t} \qquad \text{Eq 5-15}$$

Where n and n+1 denote the respective quantities at the current and next time level.

The $(n+1)^{th}$ time level volume V^{n+1} can be calculated from Eq 5-16.

$$V^{n+1} = V^n + \frac{dV}{dt}\Delta t \qquad \text{Eq 5-16}$$

Where $\frac{dV}{dt}$ is the volume time derivative of the control volume. In order to satisfy the grid conservation law, the volume time derivative of the control volume is calculated from Eq 5-17.

$$\frac{dV}{dt} = \int_{\partial V} \vec{u}_g . d\vec{A} = \sum_j^{nf} \vec{u}_{gj} . \vec{A}_j \qquad \text{Eq 5-17}$$

Where n_f denotes the number of faces on the control volume and $\vec{A}_j$ is the j face area vector.

$$\vec{u}_{gj} . \vec{A}_j = \frac{\delta V_j}{\Delta t} \qquad \text{Eq 5-18}$$

Where δV_j is the volume swept out by the control volume face j over the time step Δt.

The spring based smoothing method is used to update any cell or face zone whose boundary is moving or deforming. For non-tetrahedral cell zones (non-triangular in 2D), the spring-based method is recommended when the following conditions are encountered:

i. The boundary of the cell zone moves predominantly in one direction.
ii. The motion is predominately normal to the boundary zone.

If these conditions are not met, the resulting cells may have high skewness values.
The update of the mesh is handled automatically by Fluent at each time step based on the new positions of the boundaries. To use the dynamic mesh model, it is required to provide a starting mesh and the description of the motion of any moving zones in the model. Fluent allows describing the motion using either boundary profiles or user defined functions. It also expects that the description of the motion to be specified on either face or cell zones. If the model contains moving and non moving regions, it is required to identify these regions by grouping them into their respective face or cell zones in the starting mesh. Furthermore, regions that are deforming due to the motion on their adjacent regions must also be grouped into separate zones in the starting mesh, see Fluent User Guide (2003).
In the spring-based smoothing method, the edges between any two mesh nodes are idealised as a network of interconnected springs. The initial spacing of the edges before any boundary motion constitutes the equilibrium state of the mesh. A displacement at a given boundary node will generate a force proportional to the displacement along all the springs connected to the node. Using Hook's Law, the force on a mesh node can be expressed as: see Fluent User Guide (2003)

$$\vec{F}_i = \sum_j^{n_i} k_{ij}(\Delta\vec{x}_j - \Delta\vec{x}_i) \qquad \text{Eq 5-19}$$

Where $\Delta\vec{x}_i$ and $\Delta\vec{x}_j$ are the displacement of node i and its neighbour j, n_i is the number of neighbouring nodes connected to the node i and k_{ij} is the spring constant between node i

and its neighbour j. The spring constant for the edge connecting nodes i and j is presented in Eq 5-20.

$$k_{ij} = \frac{1}{\sqrt{|\vec{x}_i - \vec{x}_j|}} \qquad \text{Eq 5-20}$$

At equilibrium, the net force on a node due to all the springs connected to the node must be zero. This connection results in an iterative equation such that

$$\Delta\vec{x}_i^{\,m+1} = \frac{\sum_j^{ni} k_{ij}\Delta\vec{x}_j^{\,m}}{\sum_j^{ni} k_{ij}} \qquad \text{Eq 5-21}$$

Since displacements are known at the boundaries (after boundary node positions have been updated) using a Jacobi sweep on all interior nodes. At convergence, the positions are updated such that Eq 5-22.

$$\vec{x}_i^{\,n+1} = \vec{x}_i^{\,n} + \Delta\vec{x}_i^{\,m,converged} \qquad \text{Eq 5-22}$$

5.3.3 Species Boundary Condition

After selecting the relevant governing equations, it was necessary to set the required boundary conditions. The process of isolating the system under consideration from its surrounding environment is not often an easy task. Accordingly, due to the geometrical complexity of the entire fuel line from the tank to the AFTSTU heated nozzle as well as high expense of computation, application of CFD techniques for the entire fuel line is almost impracticable. Therefore, a less expensive computational technique based on the concept of perfectly stirred reactor, was primarily used to calculate species boundary condition of the jet fuel for the entrance of AFTSTU heated nozzle. This is the simplest reactor model whose performance is governed by zero dimensional approach. The major

assumption with this approach is that mixing in reactor is complete, hence, the properties of the reaction mixture are uniform in all part of the reactor vessel and are, the same as those in the exit stream.

For the simplicity, it was assumed that both low pressure and high pressure systems behave as two isothermal, constant volume reactors and there is no considerable heat lost through the fuel lines and the components. Therefore, the governing equations for the species concentrations are the rate equations presented in Eq 3-7. Correspondingly, it was assumed that the heated nozzle's upstream is composed of at least two reactors (LP system and HP) and the species concentration calculated for the low pressure will be the initial concentrations for the high pressure. Similarly, the calculated values for the high pressure system will be the species boundary conditions for the AFTSTU nozzle.

In order to perform these calculations, the values for the residence time and temperatures for each region were taken from Table 4-3, however, the analytical test results of the aviation fuel presented in Table 4-4 and Table 4-5 do not provide sufficient information about the different classes of influencing species such as polar species (AH), reactive sulphurs (SH) and hydroperoxide (ROOH) in accordance with the application of pseudo detailed mechanism of jet fuel autoxidation. Therefore, it was quite arbitrarily assumed that the fresh sample of fuel has the same composition as F3219.The calculated result of species for the AFTSTU nozzle inlet are presented in Table 5-1.

Species	Molecular Weight	Mass Fraction	Diffusion Coefficient
Initiator	169	1.99E-9	1E-8
$\dot{R}$	169	7.25E-13	1E-8
O_2	32	7.19E-5	1E-8
$R\dot{O}_2$	201	1.05E-12	1E-8
RH	170	bulk species	1E-8
RO_2H	202	1.35E-6	1E-8
Termination1	402	1.17E-12	1E-8
Termination2	370	1.07E-12	1E-8
R_2	338	1.52E-13	1E-8
$R\dot{O}$	185	1.14E-19	1E-8
$O\dot{H}$	17	2.21E-17	1E-8
ROH	186	7.98E-13	1E-8
Rprime	169	2.20E-16	1E-8
Carbonyl	16	1.45E-10	1E-8
H_2O	18	1.64E-10	1E-8
ROterm	370	1.71E-26	1E-8
$\dot{A}$	200	2.18E-9	1E-8
ProductsAH	402	1.61E-9	1E-8
SH	200	6.25E-4	1E-8
ProductSH	402	9.15E-7	1E-8
Alkane	170	1.55E-9	1E-8
AH	201	2.51E-5	1E-8
Metal	64	4.00E-10	1E-8
Soluble	402	1.58E-9	1E-8
Insoluble	402	3.15E-11	1E-10

Table 5-1: Species boundary condition for AFTS nozzle inlet with relevant molecular weight

5.3.3.1 Momentum, Thermal and Turbulence Boundary Conditions for Inlet

Jet fuel enters AFTSTU nozzle at turbulent regime. Values of density and viscosity of jet fuel are presented as in

Table 5-2. Accordingly, two user define functions (UDFs) were written for the variation of these as function of temperature compatible with the Fluent 6.3.26.

For turbulence boundary conditions, the values of 10% turbulent intensity together with the hydraulic diameter of 0.001143 m were selected.

Two types of thermal boundary conditions were set for the modelling. Firstly, a constant wall temperature for the simulation of Near Isothermal Flow Thermal Reactor (NIFTR)

was applied. Secondly a constant heat generation rate in conjunction with heat lost terms from the external surface due to convection and radiation was employed in accordance with the heated nozzle module of Aviation Fuel Thermal Stability Test Unit (AFSTU).

T [°C]	T [K]	Density [kg/m^3]	Dynamic Viscosity [kg/ms]	Kinematic Viscosity [mm^2 / s]
0	273.14	820.559	2.20E-003	2.68
10	283.14	813.033	1.78E-003	2.194
20	293.14	805.486	1.47E-003	1.821
30	303.14	797.917	1.22E-003	1.531
40	313.14	790.325	1.04E-003	1.314
50	323.14	782.706	9.19E-004	1.175
60	333.14	775.06	8.20E-004	1.058
70	343.14	767.384	7.35E-004	0.958
80	353.14	759.676	6.64E-004	0.874
90	363.14	751.934	6.02E-004	0.801
100	373.14	744.154	5.49E-004	0.738
110	383.14	736.333	5.03E-004	0.683
120	393.14	728.468	4.62E-004	0.635
130	403.14	720.555	4.27E-004	0.592
140	413.14	712.588	3.95E-004	0.555
150	423.14	704.564	3.67E-004	0.521
160	433.14	696.475	3.42E-004	0.491
170	443.14	688.316	3.20E-004	0.465
180	453.14	680.08	3.00E-004	0.441
190	463.14	671.756	2.81E-004	0.419
200	473.14	663.336	2.65E-004	0.399
210	483.14	654.807	2.50E-004	0.381
220	493.14	646.157	2.36E-004	0.365
230	503.14	637.369	2.23E-004	0.35
240	513.14	628.424	2.12E-004	0.337
250	523.14	619.3	2.01E-004	0.324
260	533.14	609.971	1.91E-004	0.313
270	543.14	600.403	1.81E-004	0.302
280	553.14	590.557	1.73E-004	0.292
290	563.14	580.384	1.64E-004	0.283

Table 5-2 :Variation of density and viscosity of jet fuel with temperature, Zedda and Raviakanti(2008), see also Moses(2007)

5.3.4 Discretization Method

After finalising the equations and boundary conditions, the next task was to choose the appropriate method to approximate the equations through discretization method.

There are many such methods; the most important are finite difference (FD), finite volume (FV) and finite element (FE) methods. All methods yield the same solution if the grid is reasonably fine. However, some methods proved to be more suitable to particular classes of problems than others. The preference is often determined by the ease of application, computational resources, and familiarity of the users.

Finite difference is the oldest method for the numerical solution of partial differential equations. In this method, the solution domain is covered by a computational grid. At each grid point, the terms containing partial derivatives of the differential equation are approximated by allocating the variable values at grid nodes. This results in one algebraic equation per grid node in which the variable value at that node and a certain number of neighbouring nodes appear as unknowns. Taylor series expansions or polynomial fitting is used to obtain approximations for the first and second order derivatives. Application of finite difference method is very simple and effective; however, this method is limited to very simple geometries.

The finite volume method uses the integral form of conservation equations as its starting point to ensure global conservation. The solution domain is again divided into number of computational cells (similar to finite difference). The differential equation is integrated over the volume of each computational cell to obtain the algebraic equations. Variable values are stored at the cell centres and interpolation is applied to express them at cell faces in terms of cell centre values. Surface and volume integrals are approximated using suitable quadrature formulae. As a consequence, one obtains an algebraic equation per computational cell in which a number of neighbouring cell centre values appears as unknowns. The finite volume method is able to accept any type of grid and is, therefore, suitable for handling complex geometry. The disadvantage of finite volume methods is that higher than second order approximations of gradient terms are difficult to implement, especially in 3 dimensional problems.

Presents the discretization methods as well as the under relaxation values used for the modelling in this thesis.

Equations	Discretization	Under Relaxation Factor
Pressure	Standard	0.3
Momentum	First Order Upwind	0.7
Turbulent Kinetic Energy	First Order Upwind	0.8
Turbulent Dissipation Rate	First Order Upwind	0.8
Turbulent Viscosity	First Order Upwind	0.9
Species	First Order Upwind	0.9

Table 5-3: Discretization Methods and under relaxation factors

Having selected the numerical methods, in the next step, it was necessary to generate an appropriate grid, i.e. discrete representations of the solution domain and discrete locations at which variables are to be calculated. Two types of grid, namely structured and unstructured grids can be used in finite volume calculations. In a structured gird, which was used in this thesis, there are families of grid lines following the constraint that grid lines of the same family do not cross each other and cross each member of the other families only once. The position of a grid point within the solution domain is, therefore, uniquely identified by a set of two (in two dimensional) or three (in three dimensional) indices. It is thus logically equivalent to Cartesian grid. The properties of a structured grid can be exploited to develop very efficient solution techniques. One major disadvantage is the difficulty in controlling the grid distribution. In a structured grid, concentration of grid points in one region for more accuracy may unnecessarily lead to small spacing in other parts of the solution domain.

The choice of method of approximation influences the accuracy and computational cost. In addition, the number of nodes involved in approximation controls the memory requirements, speed of the code and difficulty in implementing the method in computer program.

5.4 Modelling Techniques

5.4.1 Combination of CFD and Reactor Modelling

The first modelling approach used in this chapter was a combination of a two dimensional axis symmetric CFD calculation and perfect stirred reactor. Accordingly, it was assumed that AFTSTU heated nozzle is composed of a multitude of axially and radially located of the micro reactors. Each of these is characterized by a temperature and a residence time. The result of CFD calculation provides the nodal values of temperature and velocity. Then the central values were calculated from 4 nodal values of a rectangle except for the cells which are located at the boundaries. The values of the residence time were calculated from the velocity and the length of each cell. For a computation domain of 250×10(finer towards the wall) and for a constant wall temperature, the cell central values of temperature and residence time are presented in Figure 5-2 and Figure 5-3 . The 4 step global chemistry model of Katta and Roquemore was used for this calculation.

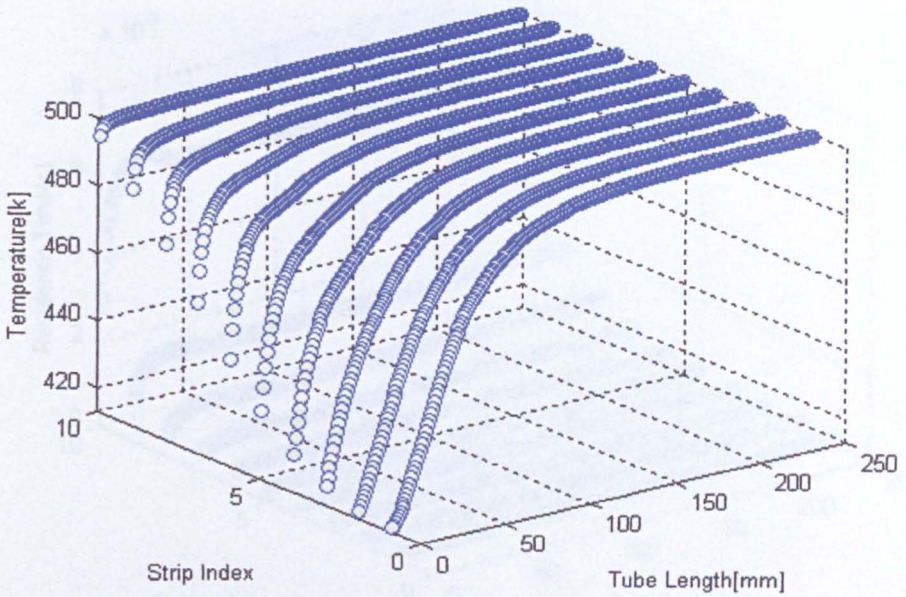

Figure 5-2 : Central values of temperature for each computational cell of geometry assimilated with AFTSTU heated nozzle module

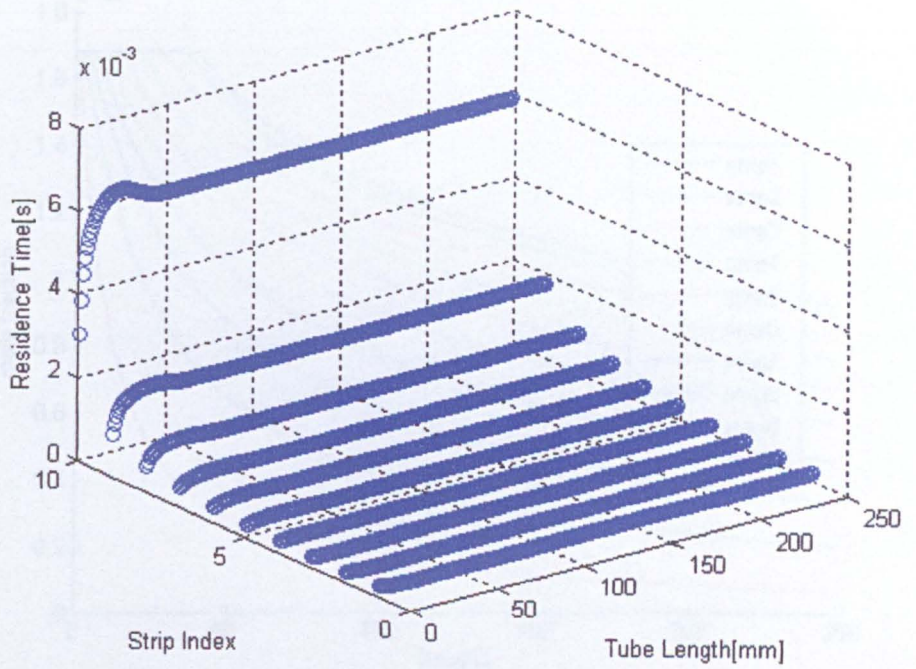

Figure 5-3: Central values of residence time for each computational cell of geometry assimilated with AFTSTU heated nozzle module

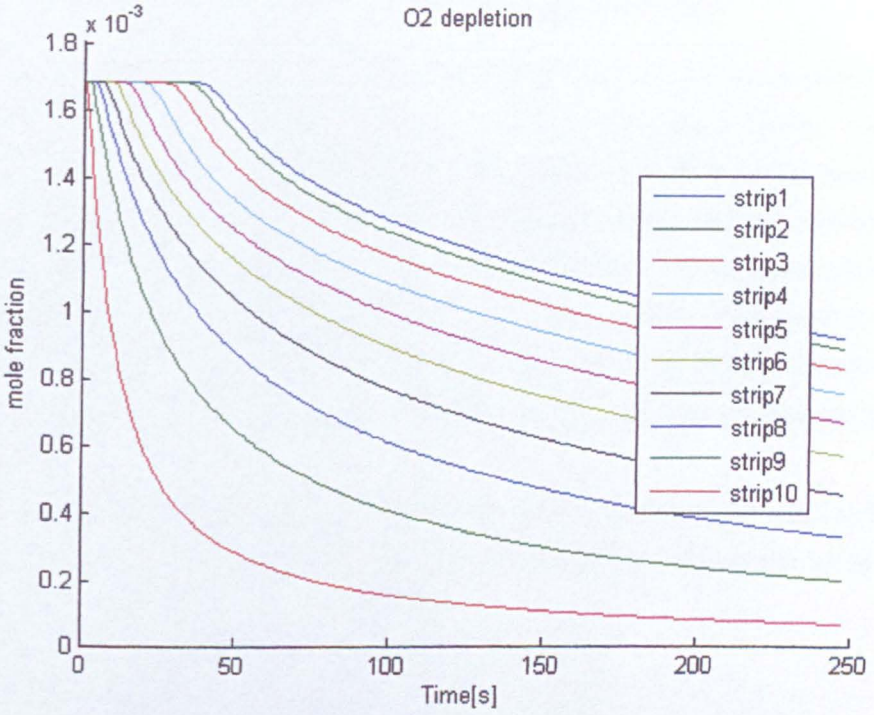

Figure 5-4: Profile of jet fuel autoxidation for each radial section of heated tube using the global mechanism of jet fuel autoxidation

The objective of this modelling was to calculate the total amount of deposit of the AFTSTU heated tube by integration of the amount of deposit over the entire volume. The results of Figure 5-2, Figure 5-3 and Figure 5-4 indicate that due to the effect of boundary layer, the amount of residence time in the wall adjacent layer is the highest and autoxidation mechanism is near completion while at the centre of the tube is incomplete. In spite of the simplicity, this model was not used for the further calculation as it was incapable of the prediction temperature rise along the tube wall. This model can be validated with the quantified deposit data.

5.4.1.1 CFD Modelling Based on the Moving Boundary

It was discussed in chapter 2 and 4 that two things must occur before a particle in a fluid with surface adhesion tendency becomes part of the fouling layer. Firstly, a combination of mechanisms such as the turbulent diffusion and Brownian motion must drive the precursor on the surface. In fact, the small size particles obey the Brownian diffusion and eddy diffusion while the large particles move according to the momentum forces due to their large mass. Second possibility is that deposit particles are initiated at the heated surface with little contribution of the particles in the bulk fuel. Thirdly, surface deposition may result from the contribution of both adhering bulk particles and deposits formed just at the wall.

An oversimplified assumption is to consider that all the precursors reach to the surface adhere there. Thus, the rate of the conversion of precursor in the deposit can be expressed via the Eq 5-23.

$$\frac{d[\text{precursor}]}{dt} = k_d C_b \qquad \text{Eq 5-23}$$

Where k_d is the deposition formation coefficient and C_b is the concentration of precursor in the bulk fuel. The value of k_d is numerically equal to the mass diffusion coefficient of the precursor.

Amongst all particles reaching to the wall some particles rebound back to the fluid. In this case deposit formation coefficient is no longer equal to the mass diffusion coefficient of the precursor; hence, a modification based on the sticking probability of the precursor particles is required to be considered for the Eq 5-23.

Sticking probability is defined as the probability of a particle that reaches on the wall remains there. If adhesion of the precursor is considered as the adsorption process then the rate of precursor sticking can be expressed according to a kinetic expression as presented in Eq 5-24.

$$\frac{d[precursor]}{dt} = f(\theta).\exp(-\frac{Ea}{RT}) \qquad \text{Eq. 5-24}$$

Katta and Roquemore (1993) and Ervin *et al* (2000) suggested that the sticking probability would vary increasingly with the shear stress at the deposit fuel interface as presented in Eq 5-25.

$$\frac{d(deposit)}{dt} = \frac{C}{\tau^{n}_{interface}}\left[\frac{\rho^{int} f_p^{int}}{MP}\right] A_{wall} \exp(\frac{-E_{wall}}{RT}) \qquad \text{Eq 5-25}$$

In Eq 5-25, C is a dimensionally correct constant of order unity, MP (kg/mol) is the molecular weight of precursor species, ρ^{int} is the density of particle at deposit fuel interface (precursor), f_p^{int} is the precursor mass fraction of at the deposit-fuel interface and τ (kg/ms^2) is shear stress.

The value of Shear stress can be calculated from surface friction factors based on the empirical relationship of Miller and Faning as presented in Eq 5-26 and Eq 5-27.

$$F = 0.25\left[\log(\frac{e/D}{3.7} + \frac{5.74}{Re^{0.9}})\right]^{-2} \qquad \text{Eq 5-26}$$

$$\tau = \frac{FV^2\rho}{2} \qquad \text{Eq 5-27}$$

In Eq 5-26 e denotes the absolute surface roughness, D represents hydraulic diameter (m) and Re is Reynolds number. In Eq 5-27 V is fluid velocity (m/s) and ρ represents fluid density (kg/m^3).

For simplicity, it was assumed that that surface tube is a smooth surface. Although, it is far from reality to ignore that as deposit forms dynamically in time the roughness of new surface composed of stainless steel and carbon deposition might be considerably altered. Eventually, from the calculated surface deposition rate, the latest radial location for the fuel-deposit interface can be calculated from Eq 5-28

$$r_{new} = r_{old}\sqrt{1-\frac{2\frac{d[deposit]}{dt}\Delta t}{\rho_{deposit} r_{old}}} \qquad \text{Eq 5-28}$$

5.4.1.2 Description of Dynamic Mesh User Define Functions

Fluent provides different macros which can be used to define UDFs that control the behaviour of a dynamic zone. For the AFTSTU cylindrical tube, it was assumed that both regions of deposit and jet fuel presented in Figure 5-5 are subject to the dynamic deformation.

DEFINE_GEOM macro was used to specify the geometry of these two deforming zones. By default, Fluent provides a mechanism for defining node motion along a planar or cylindrical surface. When Fluent updates a node on a deforming zone through spring-based smoothing or after local face remeshing, the node is repositioned by calling DEFINE_GEOM user define function.

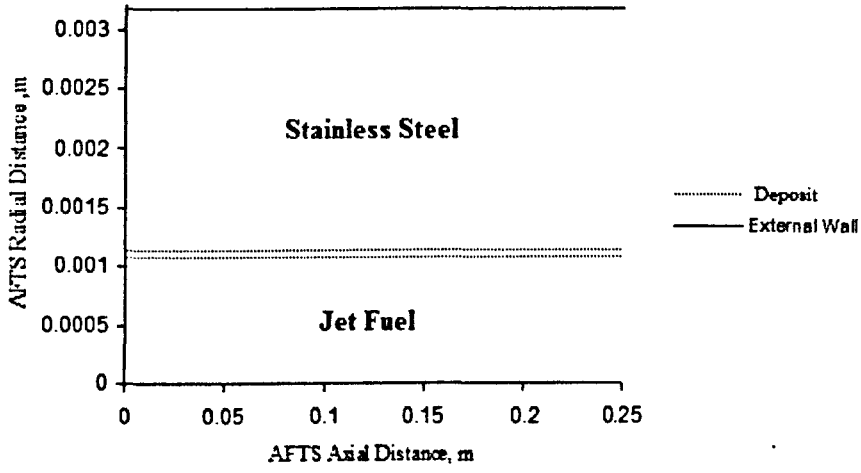

Figure 5-5: The location of AFTS nozzle external wall, fuel deposit interface and axis of symmetric.

In general a mesh is separated into control volumes or cells. Each cell is characterised by grid points (nodes), a cell centre, and the faces that borders the cell. Fluent uses internal data structures to define the domain of the mesh, to assign an order to cells, cell faces, and grid points in mesh and eventually to establish connectivity between neighbouring cells.

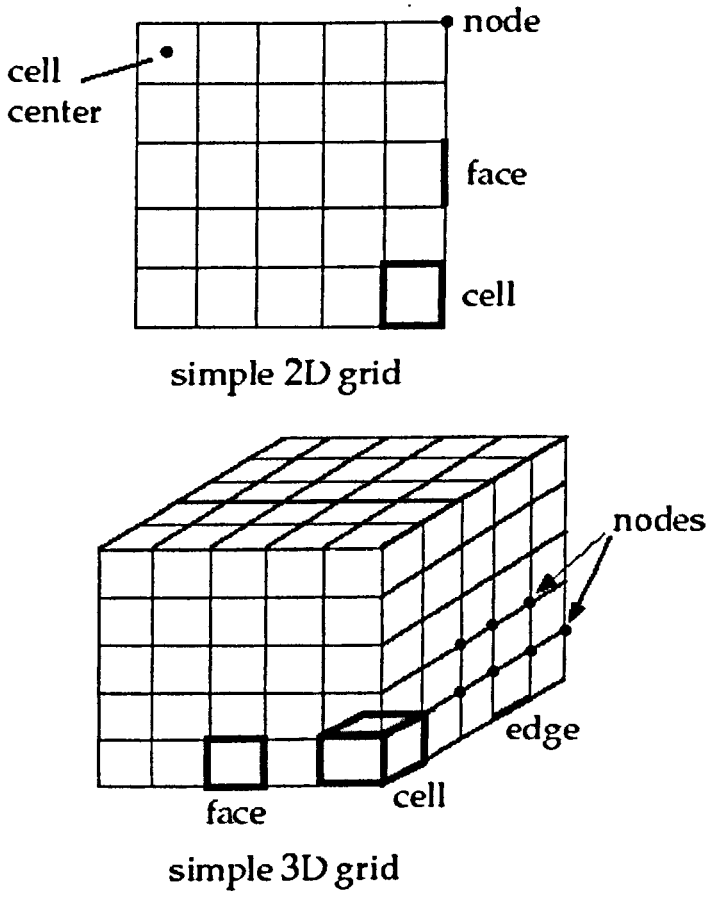

Figure 5-6: Grid components

There are four arguments to DEFINE_GEOM including name, domain, dt (dynamic thread), and position. The name of the main UDF (aftsdepositor) is a variable of the character type. Domain is a pointer to computational domain. Dynamic thread is a pointer to structure that stores the dynamic mesh attributes which is specified by the user(the lower dashed line together with the domain bordered by the dashed line which includes deposit as well as the domain bordered by the from down axis till lower dashed line from top which contains jet fuel in Figure 5-5.

Position is a real type variable and a pointer to array that stores the position in each time step. After compilation, the variables are passed by fluent solver to the UDF. The new

position is then returned to Fluent by overwriting the position array. A looping macro then was used to perform the counter over the dynamic mesh. The counter was used to return the index of each face in dynamic thread. Then a one dimensional array of species (precursor) was declared whose element is the face index in dynamic thread. For some reason in the moving boundary UDF the points are added into the array from the rightmost end of the model so the first element in the array corresponds to the maximum x coordinate. The dynamic mesh programs are presented in Appendix F.

5.5 RESULTS and DISCUSSIONS

The UDF was implemented to the CFD solver to calculate the deposit thickness for the NIFTR experimental condition. The NIFTR tube has 1.08×10^{-3} m inner diameter, 1.5875×10^{-3} m outer diameter, and 0.8 m length with a fuel flow rate of 0.25 mL/min at room temperature which assures a laminar flow regime. The near isothermal condition is provided by a constant wall temperature of 185°C. The uniform and structured rectangular cell meshing pattern was created for a 2D axisymmetric flow and chemistry calculation. The most recent version of pseudo detailed mechanism of jet fuel autoxidation of Kuprowicz *et al* together with the surface deposition sub mechanism c were used for the CFD modelling.

In order to investigate the dependence of chemical transformations on real time fuel-deposit interface temperature, a more realistic geometry compared to the conventional CFD models performed on NIFTR was created. Most of these models exclude the thickness for the wall. Correspondingly, the geometry was composed of three regions (faces in Gambit) representing bulk fuel, stainless steel and a sandwich zone allocated to the deposit (presented in Figure 5-5) for which the UDF was implemented. Although, the same UDF was enable to imitate the amount of boundary displacement caused by deposition, an extra UDF had to be written as Fluent software splits walls that border both fluid and solid zones (and also walls that border both solid zones) into two thermodynamically coupled boundaries, the first bordering the fluid and the second bordering the solid. The two boundaries are, however, thermodynamically coupled but not physically (the nodal positions aren't coupled). Therefore, the first UDF moves the

position of the boundary of the fluid zone, to maintain the integrity of the model it had to be ensured that the solid boundary wall moves the same amount as the fluid boundary.
In contrast to the experimental condition based on constant wall temperature, AFTSTU heated nozzle module runs on constant heat flux; therefore, a temperature rise at external wall occurs while the temperature at fuel deposit interface remains relatively unchanged. Hence, in the second attempt of modelling in the similar manner with the aforementioned geometry, the wall thickness model was considered. Similarly, the two UDFs were applied with the objective of imitating the experiment carried out on stage 1 of baseline test 1 of the AFTSTU heated nozzle module presented in Table 4-1.
It was discussed in the literature review, the chemistry of jet fuel autoxidation is highly sensitive to the specific species (Sulphur compounds of the form of sulfides and di sulfides, hydroperoxide, dissolved metal, antioxidant and dissolved O_2 concentration).However, the accurate measurement of those species in the jet fuel was not included for the experiments carried out in AFTSTU heated nozzle module. Therefore, one of the fuel samples in the work published by Kuprowicz *et al* named as F3219, was selected completely arbitrarily.

5.5.1 Validation of Dynamic Mesh Model with NIFTR Experiment

Firstly, the zero dimensional calculation was performed to investigate the autoxidative behaviour of the selected jet fuel samples. Figure 5-7 indicates that this fuel exhibits the behaviour of relatively a slow oxidizing fuel; hence, approximately duration of 9 minutes is required for the total amount of dissolved O_2 to be completely consumed. By a closer look at the graph, it can be observed that in spite of low reaction rate for the oxygen depletion at the first minute of experiment, the rate of process is accelerated for the longer period of test.

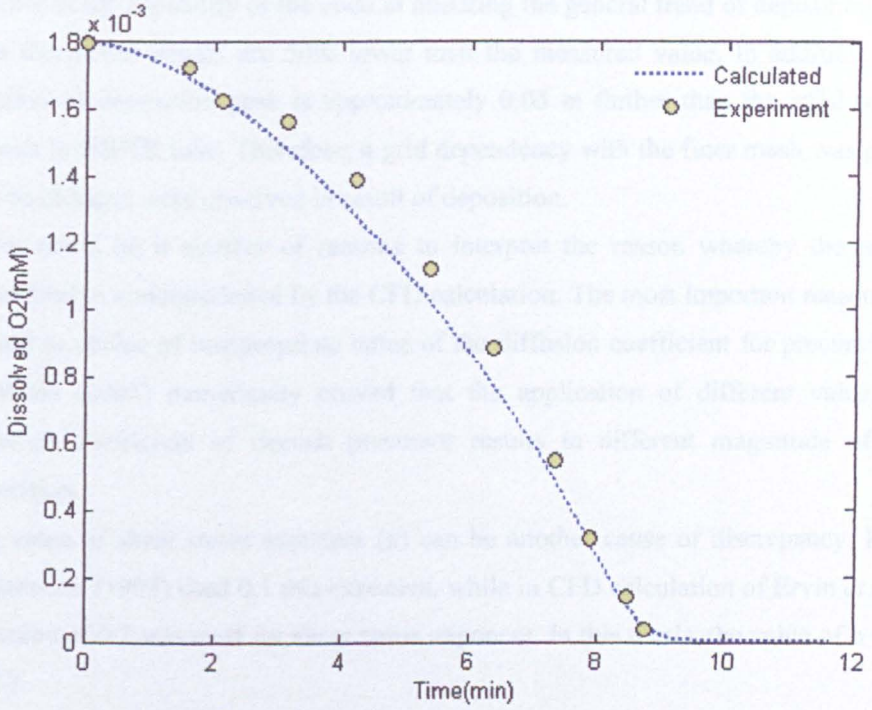

Figure 5-7: A zero dimensional validation of dissolved O_2 consumption for F3219 at 185°C with the experiment carried out by Kuprowicz *et al*(2007)

In the next step, a steady state CFD calculation was carried out to imitate the deposit the total amount of deposit formed in the NIFTR tube as presented in Figure 5-8. The both experimental and simulation results indicate that the total amount of deposit increases with respect to the axial distance along the heated tube. The location of peak of deposition in both experimental and model proved that the surface deposition occur in the position corresponding to the highest autoxidation rate. Generally this location depends on the type of jet fuel sample in a way that fuels with different chemical compositions exhibit different autoxidation rate as well as surface deposition propensity. Accordingly, the peak of deposition for the fuel sample used in this simulation is approximately 0.5m downstream of fuel inlet.

In spite of the capability of the code in imitating the general trend of deposition, it can be seen the model results are 50% lower than the measured value. In addition, the axial location of deposition peak is approximately 0.05 m farther than the axial location of deposit in NIFTR tube. Therefore, a grid dependency with the finer mesh was performed and no changes were observed in result of deposition.

There could be a number of reasons to interpret the reason whereby the amount of deposition in underpredicted by the CFD calculation. The most important reason could be related to choice of inappropriate value of the diffusion coefficient for precursor species as Wade (2005) numerically proved that the application of different values for the diffusion coefficient of deposit precursor results in different magnitude of peak of deposition.

The value of shear stress exponent (n) can be another cause of discrepancy. Katta and Roquemore (1993) used 0.1 this exponent, while in CFD calculation of Ervin *et al* (2000) the value of 0.7 was used for shear stress exponent. In this thesis, the value of n was used as 0.7.

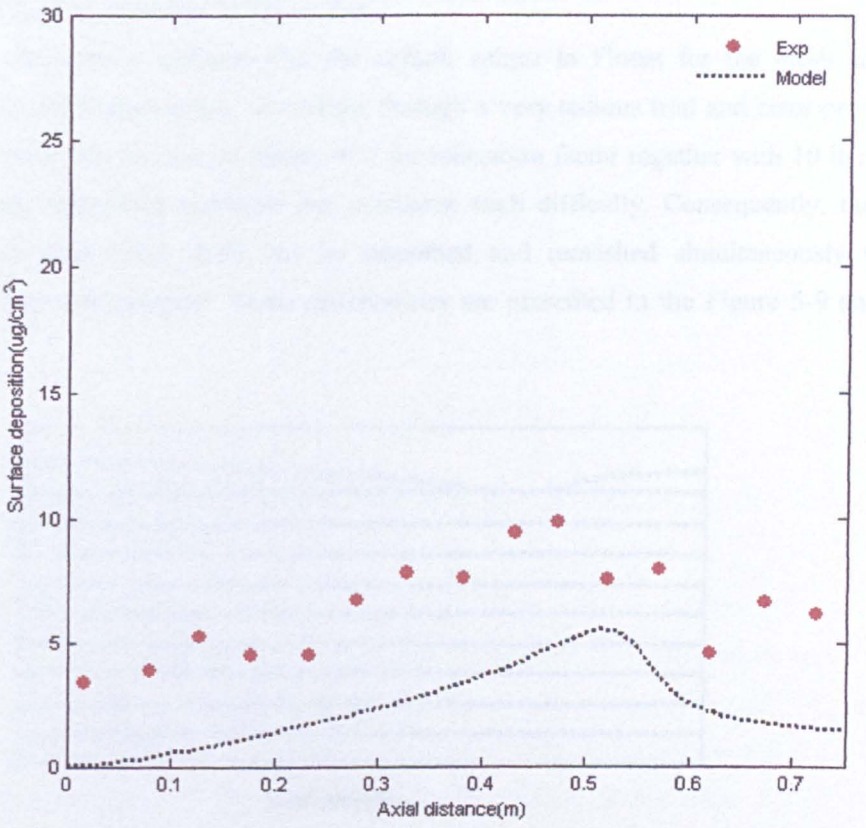

Figure 5-8: The amount of deposition for steady state calculation in NIFTR

In the next step, the UDFs were implemented into the solver and a transient calculation was carried out for the duration of 72 hours. During a number of test runs it was proved that the amount of boundary displacement is independent of the values of the time step however, the choice of larger values for the time step may result in the creation of negative cell volume causing calculation to crash.

In the first attempt of modelling, it was observed that regardless of the value of the time step, after a certain number of iterations equal to the physical time of 8.5 h the calculation crashes due to the negative volume cell .The negative volume occurs when the moving

boundary (fuel-deposit interface) intersects with the first grid line of the adjacent zone (bulk fuel) as presented in Figure 5-9.

This observation indicates that the default values in Fluent for the mesh smoothing process are inappropriate. Therefore, through a very tedious trial and error procedure, it was found that the use of values of 1 for relaxation factor together with 10 iterations in Laplace smoothing approach can overcome such difficulty. Consequently, the default interior zone (bulk fuel) can be smoothed and remeshed simultaneously with the boundary displacement. These observations are presented in the Figure 5-9 and Figure 5-10 .

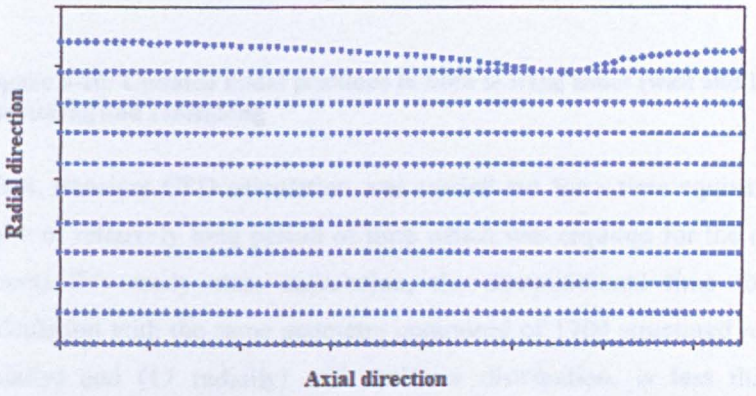

Figure 5-9: The occurrence of negative volume due to the intersection of moving wall and the fist grid line of bulk fuel

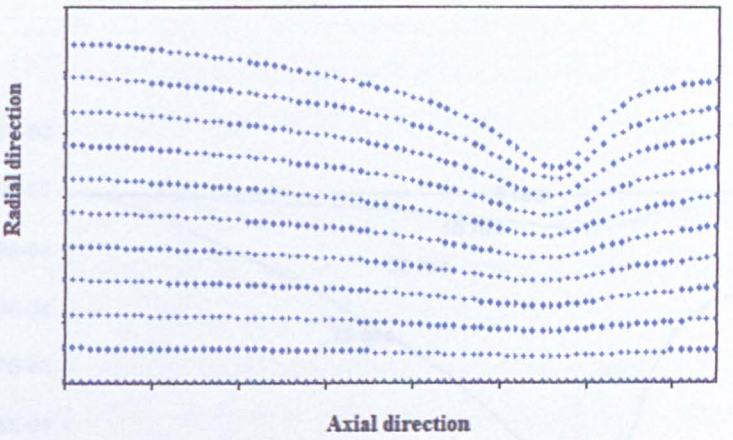

Figure 5-10: Updated nodal positions in both moving zones (wall and bulk fuel) after smoothing and remeshing

Then, transient CFD calculation was carried out for a time equivalent to the 72 hrs. In spite of relatively long period of time which was required for the convergence (about 8 hours) for steady state calculation, the computational time for moving boundary calculation with the same geometry composed of 1700 structured rectangular mesh (100 axially) and (17 radially) with uniform distribution, is less than 1 hour on High Performance Computing Service (HPC) in the Sheffield node of the White Rose Computing Grid, known as Iceberg. This includes a head node connected to a farm of execution nodes, accessible to networked computers at Sheffield. The original system was supplied by Sun Microsystems in 2005. Since then it has undergone steadily evolution and expansion to meet the needs of the research community. The latest additions to the cluster (in early 2009) include total of 23′ 8-processor nodes. Disk storage system has also been recently updated to enhance the amount of storage available to users. The current specifications are of the HPC is:

i. 6 Sun x2200 nodes, each with 4 cores and 16 GB of RAM;
ii. 23 "Hawley" nodes, each with 8 cores and 32 GB of RAM each; this makes total number of cores to be equal to 568;
iii. Scratch space on each node is 400 Gbytes;
iv. All nodes have AMD processors

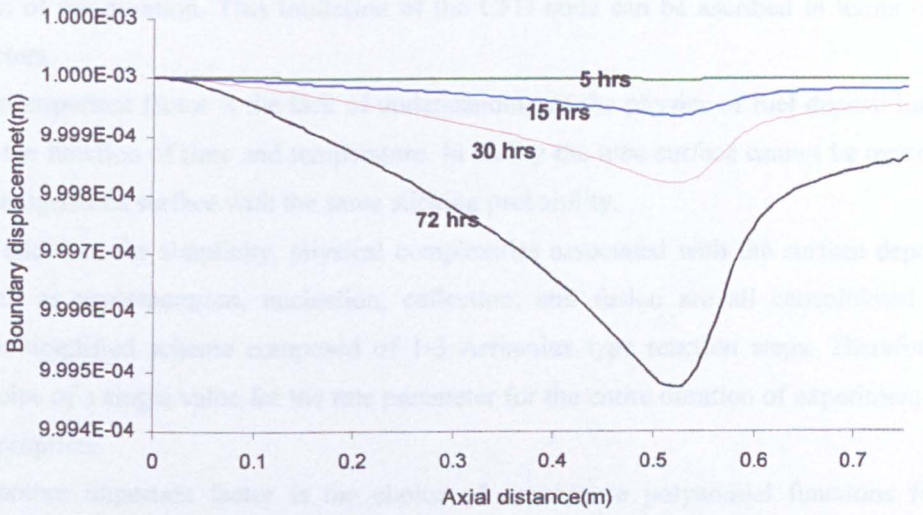

Figure 5-11: The amount of wall boundary displacement caused by deposition in NIFTR tube for different time

The modelling results presented in Figure 5-11 clearly depict that the highest amount of displacement occurs in the location corresponding to the maximum value of autoxidation rate in a steady state calculation. Explicitly, the boundary displacement starts form a zero value at the tube inlet and increases moderately during the first 0.05 m after fuel inlet along heated tube then reaches to its maximum value followed by a relatively dramatic decrease till approximately 0.6 m downstream the fuel inlet followed by a moderate drop until tube exit.

A closer look at the position of fuel-deposit interface for the different periods of time (5hrs, 15 hrs, 30 hrs and 72 hrs) indicate that the formation of deposit becomes significant after 15 hrs. Comparing the magnitude of the displacements values for 5 hrs (0.003 μm), 15 hrs (0.065 μm) and 30 hrs (1.8 μm) prove that there is an invariant zone of the deposition for the first 15 hrs of test run. The invariant zone is justified by the existence of a period known as "induction period" or "deposit hold off" which manifests itself in most of the experiments carried out on the heated tubes for the investigation jet fuel

thermal stability. Although the growth of deposit within the entire process of jet fuel thermal exposure is believed to be non linear and very smooth, the simulated results presented in Figure 5-12 depict that the profile of deposit growth becomes linear for the rest of the duration. This limitation of the CFD code can be ascribed in terms number factors.

An important factor is the lack of understanding of the physics of fuel deposit interface as the function of time and temperature. In reality the tube surface cannot be treated as a homogeneous surface with the same sticking probability.

In addition, for simplicity, physical complexities associated with the surface deposition such as agglomeration, nucleation, collection, and fusion are all consolidated in an oversimplified scheme composed of 1-3 Arrhenius type reaction steps. Therefore, the choice of a single value for the rate parameter for the entire duration of experiment is not appropriate.

Another important factor is the choice of appropriate polynomial functions for the thermal properties such as thermal conductivity, density, and heat capacity of deposit with respect to the time and temperature. Due to the lack of these functions, in this research they were considered as constant values. Accordingly with the application of thermal properties as constant values for both deposit and stainless steel and also with the use of dynamic viscosity and density as the polynomial functions for jet fuel, the predicted temperature of the jet fuel and fuel-deposit interface showed no changes throughout the calculation. However, due to the thermal insulative characteristics of deposit, when it is subject to the constant temperature at outer wall, the expectation was to observe a drop of temperature at fuel-deposit interface as deposit forms. This is indicated in Figure 5-13.

Property	Stainless Steel	deposit
Thermal conductivity(W/m.K)	16	0.1-0.16
Density(kg/m^3)	8030	1000
Heat Capacity(j/kg.K)	500	800
Dynamic Viscosity(kg/m.s)	-	-

Table 5-4: the values of thermal properties of stainless steel, deposit

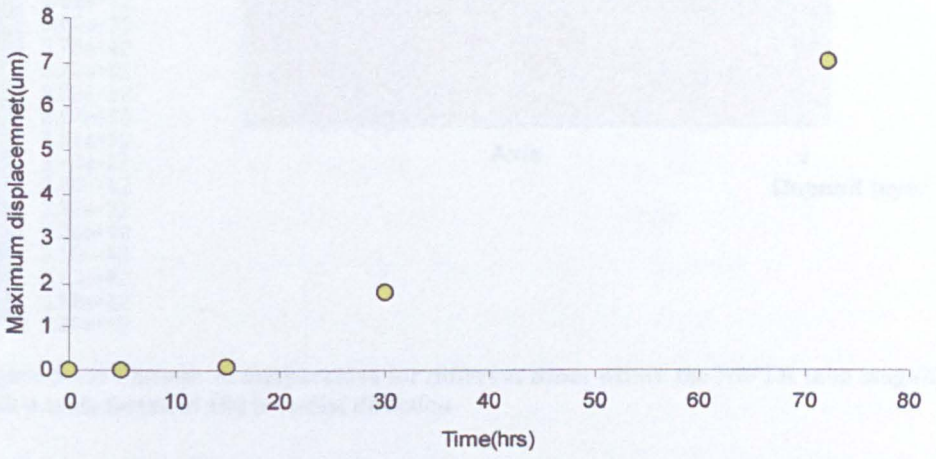

Figure 5-12 : Simulated maximum boundary displacement over different period of time

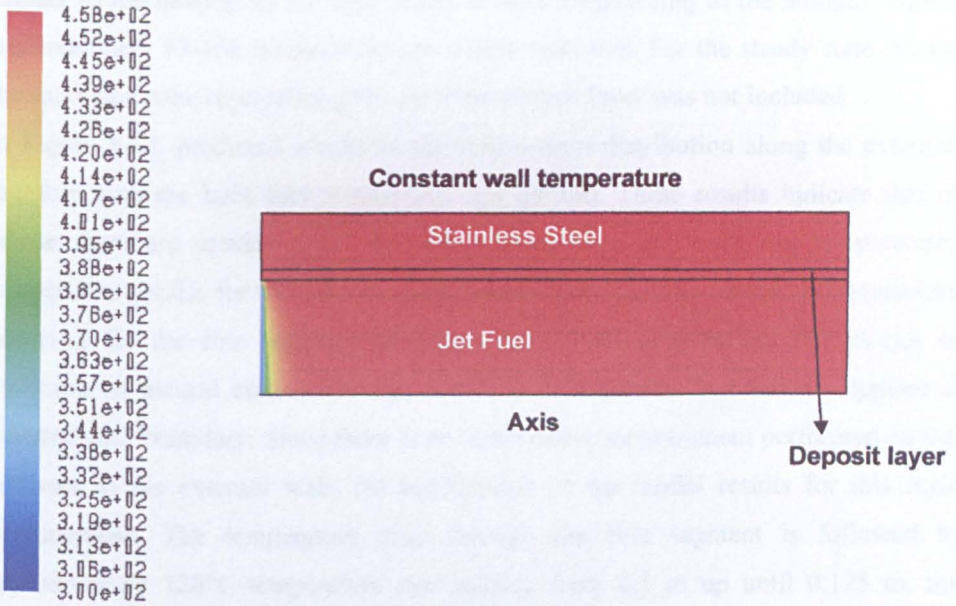

Figure 5-13: Contour of temperature for different zones within the NIFTR tube magnified with a scale factor 0f 150 in radial direction

5.5.2 Validation of Dynamic Mesh Model with AFTSTU Heated Nozzle

A steady state calculation was performed to imitate the temperature profile across the external wall and for the bulk fuel. The thermal and momentum boundary conditions were set up on the basis of the test conditions of the AFTSTU heated nozzle module for the baseline1 test stage1 corresponding to the lowest power supplied by the RF heater unit presented in the Table 4-1. Accordingly the uniform inlet velocity of the 1.557 m/s with a fixed temperature of 423k was considered for the inlet velocity. With respect to the value of viscosity of jet fuel at fuel inlet temperature, the calculation of Reynolds number indicate that the fluid flow falls in turbulent regime .Therefore, k-ε turbulence model was used to simulate the impact of turbulence on the flow filed. Correspondingly the value of 10% was used for the turbulent intensity and for the hydraulic diameter the value of 0.001408 m was considered. The set up of the wall boundary condition was in a way to establish an energy generation rate through the second segment of the stainless where is

subject to the heating by RF unit heater to be corresponding to the amount required for approximately 13-15k temperature rise within bulk fuel. For the steady state calculation, the sandwich zone representing the growing deposit layer was not included.

In Figure 5-14, predicted results of the temperature distribution along the external wall together with the bulk fuel temperature are plotted. These results indicate that on the whole, there are upward trend for both external wall and bulk fuel temperature. The temperature profile for the external wall depicts that a slightly decrease of temperature is observed for the first segment of heated tube. This temperature drop is due to the inclusion of natural convection and radiative heat transfer sub models applied at the external wall boundary. Since there is no temperature measurement performed on the first segment of the external wall, the justification of the model results for this region is inappropriate. The temperature drop through the first segment is followed by an approximately 120°C temperature rise starting from 0.1 m up until 0.125 m. Such a dramatic increase is due to the high amount of heat generated via the second segment of the tube representing the RF heater. From the axial distance of 0.125m until 0.225m a moderate temperature rise of about 30 k is observed which is followed by a very sharp temperature drop of 100k within 0.05 m for the third segment of the external wall. Such temperature drop is due to the natural convection and radiative heat transfer through the external wall boundary.

In the CFD model, it was wrongly assumed that there is axial heat convection through the tube exit, however, in reality, AFTSTU heated nozzle is attached to the rest of the fuel line; therefore, conductive heat transfer for this region seems to be more appropriate. To sum up, the simulated results of the external wall proved relatively a good consistency with the experimental points throughout the second segment.

The simulated temperature profile indicate an invariant temperature zone from the nozzle inlet until approximately 0.11 m downstream of the fuel inlet followed by nearly a linear temperature rise up to the nozzle exit. A total temperature rise of 13-15k is observed within the bulk fuel matching up with the experiment. Figure 5-15 represents the contour of temperature for various segments throughout the AFTSTU nozzle. Figure 5-16 represents a cross sectional temperature profile for an axial location at 0.0005m downstream of the fuel inlet.

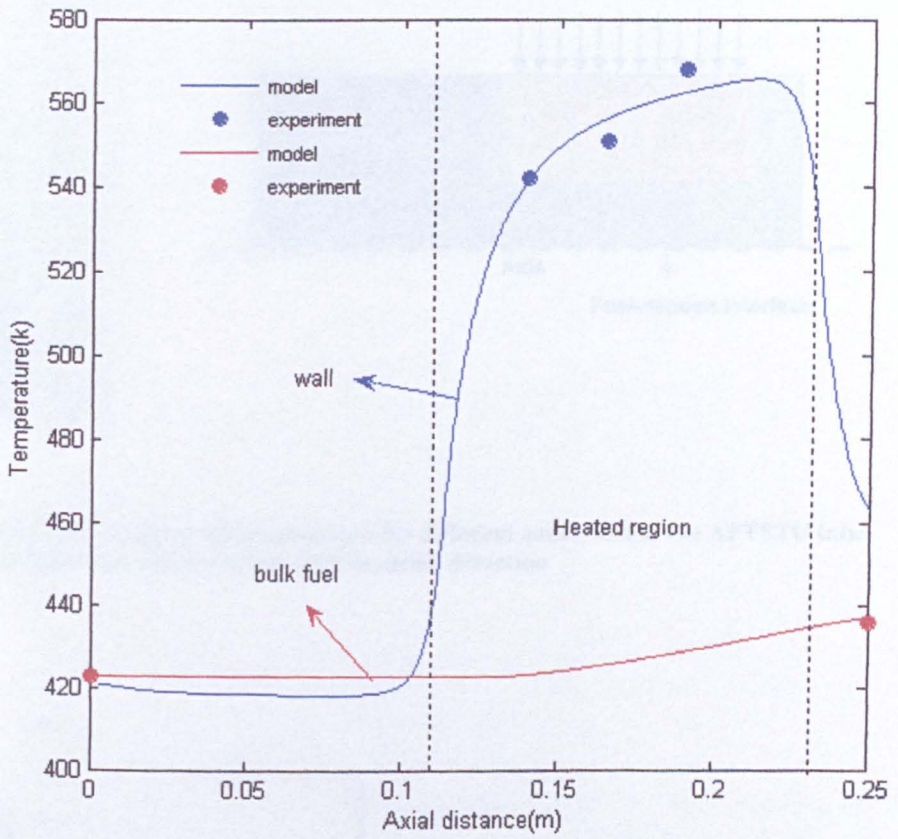

Figure 5-14: Temperature profile across the wall and the bulk fuel in heated nozzle module of AFTSTU

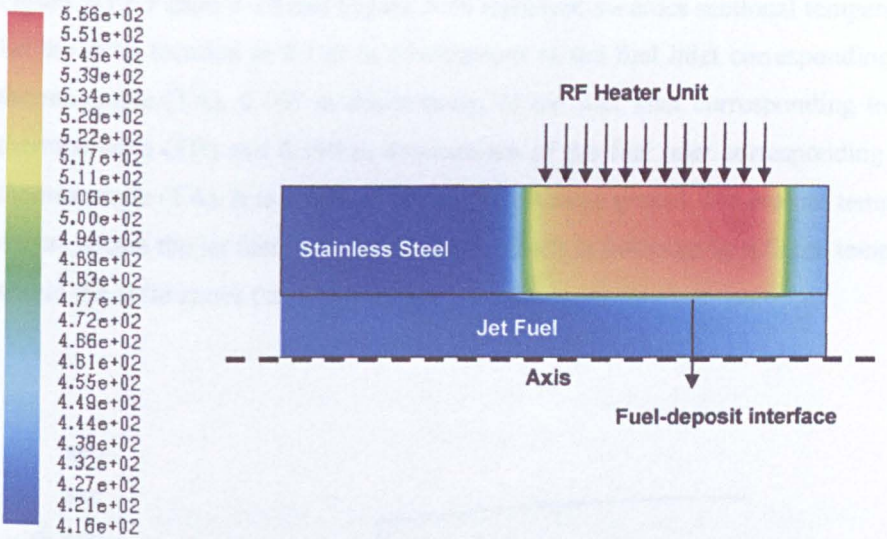

Figure 5-15: Contour of temperature for different zones within the AFTSTU tube, magnified with a scale factor of 25 in radial direction

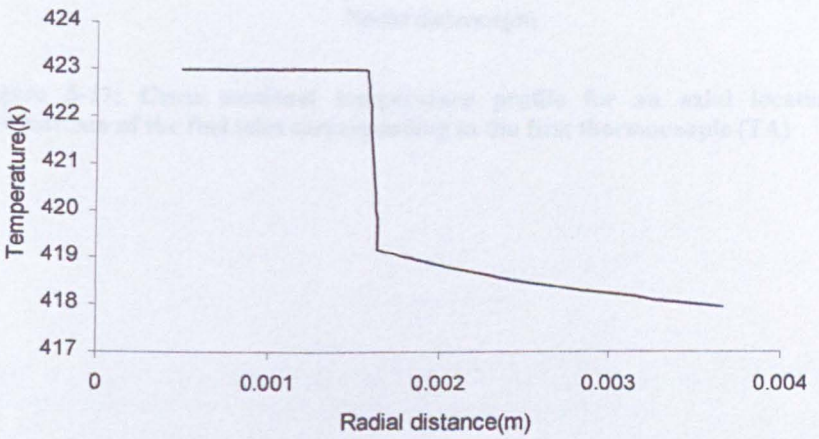

Figure 5-16 : Cross sectional temperature profile for an axial location at 0.0005m downstream of the fuel inlet

Figure 5-17, Figure 5-18 and Figure 5-19 represent the cross sectional temperature profile for the axial location at 0.140 m downstream of the fuel inlet corresponding to the first thermocouple (TA), 0.165 m downstream of the fuel inlet corresponding to the second thermocouple (TB) and 0.190 m downstream of the fuel inlet corresponding to the third thermocouple (TA). It is observed that in the all three graphs, a curvature temperature rise occurs within the jet fuel in radial direction which is followed by a linear temperature rise within the solid zones (stainless steel).

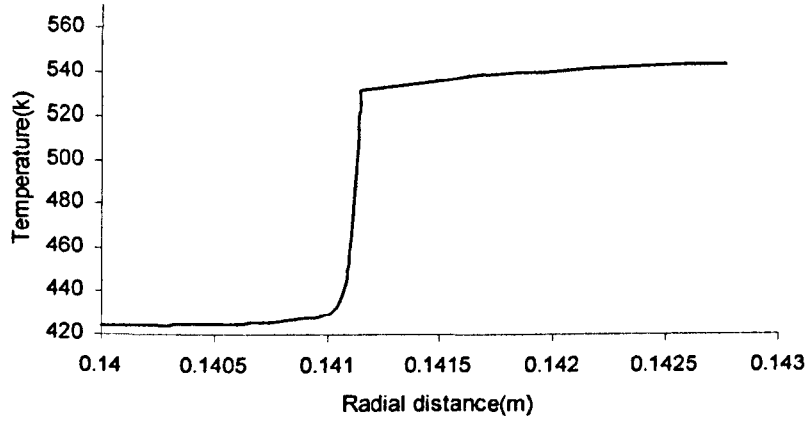

Figure 5-17: Cross sectional temperature profile for an axial location at 0.140 m downstream of the fuel inlet corresponding to the first thermocouple (TA)

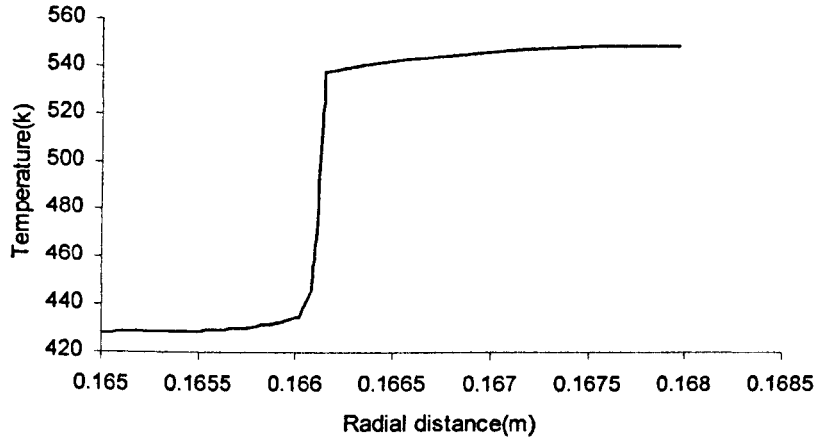

Figure 5-18: Cross sectional temperature profile for an axial location at 0.165 m downstream of the fuel inlet corresponding to the second thermocouple (TB)

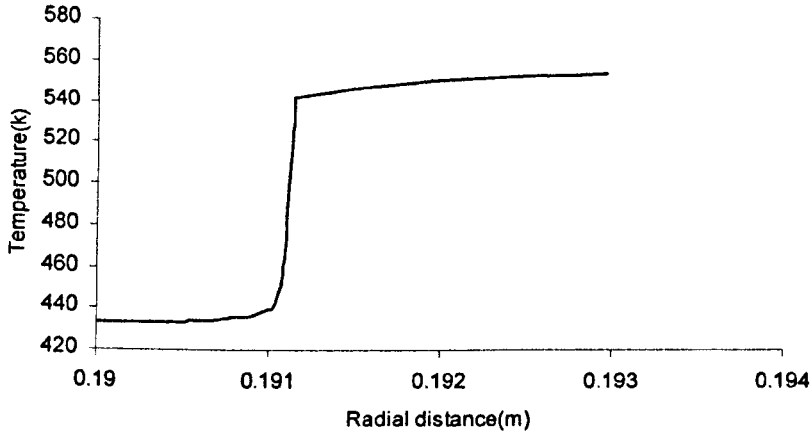

Figure 5-19: Cross sectional temperature profile for an axial location at 0.190m downstream of the fuel inlet corresponding to the third thermocouple (TC)

Figure 5-20 represents the prediction of the dissolved oxygen depletion in thermally stressed jet fuel within the heated tube. With respect to the length of fuel passage through the AFTSTU heated nozzle and the velocity of fuel, the residence time for a fluid element within the tube is about 0.16s. Under this circumstance, the total amount of oxygen

depletion is approximately 0.02 of initial value. Qualitatively, the rate of autoxidation is very low, almost negligible, within the first segment of AFTSTU heated nozzle followed by a sharp increase of rate throughout the second segment. The irregular behaviour observed within the third segment is more likely to be a computational error. Another possibility is that the change of temperature regime from the second segment to the third causes the reaction step responsible for the thermal decomposition peroxide radical to be slightly more significant as presented below.

$RO_2^{\bullet} \rightarrow R^{\bullet} + O_2$ 1×10^{16} 19

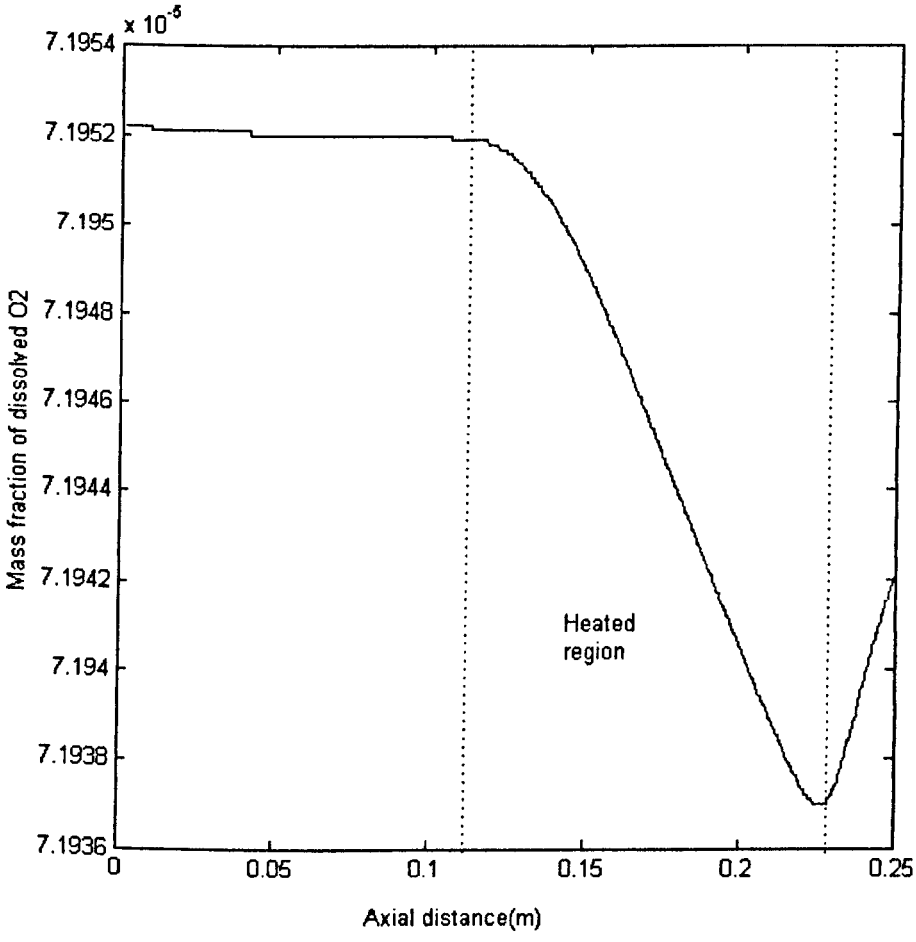

Figure 5-20: The profile of oxygen consumption in AFSTTU heated nozzle at the fuel-deposit interface

Figure 5-21 represents the prediction of the insoluble species (deposit precursor) for an axial location of 0.190m downstream of the fuel inlet corresponding to the location of the third thermocouple (TC). It is observed that as a consequence of mass diffusion the amount of deposit precursor increases from the axis towards the fuel-deposit interface where the surface reaction occurs. The values that have been employed for the impact of sticking probability on surface reaction were as 0.015E-3 m for the absolute surface roughness of stainless steel, 2.11E-3 m for hydraulic diameter, 16600 for the Reynolds number. The values for the mass diffusion coefficients of species were taken form Wade (2005).

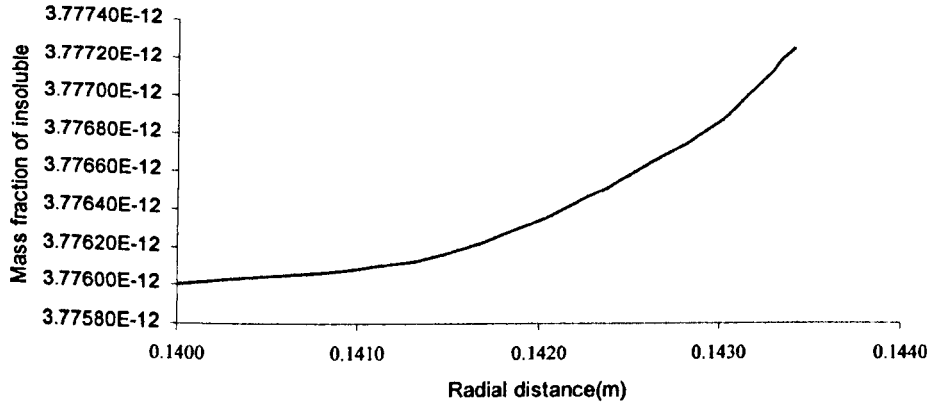

Figure 5-21: Cross sectional profile of mass fraction of insoluble species(deposit precursor) for an axial location of 0.190m downstream of the fuel inlet corresponding to the third thermocouple(TC)

In the next step, the unsteady state calculation with dynamic mesh was carried out. The same observation with regard of negative volume was occurred for after a computational time equal to 10 h. The values of 1 for the relaxation factor together with 25-50 numbers of iterations in Laplace smoothing approach can overcome such difficulty. With the application of same computational power explained for the NIFTR simulation, for a total number of 25500 cells, 1275 axially located with the same interval count, 10 cells for the fluid zone with the interval count of 0.85(denser towards the fuel-deposit interface), 2

cells for deposit layer with the 1 interval count value and 8 cells equally distributed along the stainless steel, a time space of 3 hours was required for the steady state calculation to converge. Also, 18 hours time for the unsteady state calculation was required.

Figure 5-22 represents the simulated results of the total amount of displacement for four different thermal stressing times. It is observed that regardless of the duration of thermal exposure, the amount of fuel-deposit boundary displacement is insignificant for the first segment of the tube while, for the second segment, the boundary displacement becomes meaningful. It is observed that the rate of deposition is higher from the beginning and becomes slightly lower in the course of process. The maximum amount of displacement occurred at the point where the rate of autoxidation was the highest followed by a dramatic decrease in the third segment. These results indicate that the duration of thermal exposure has a significant impact upon the amount of displacement. By a closer look at Figure 5-22 it can be observed that the amount of displacement becomes significant after 20h of thermal exposure time. The results of displacement for the first 15 hours are not plotted in the figure as they appeared in the order of 1E-12 and effectively overlapped with the first position of fuel-deposit interface at t=0.

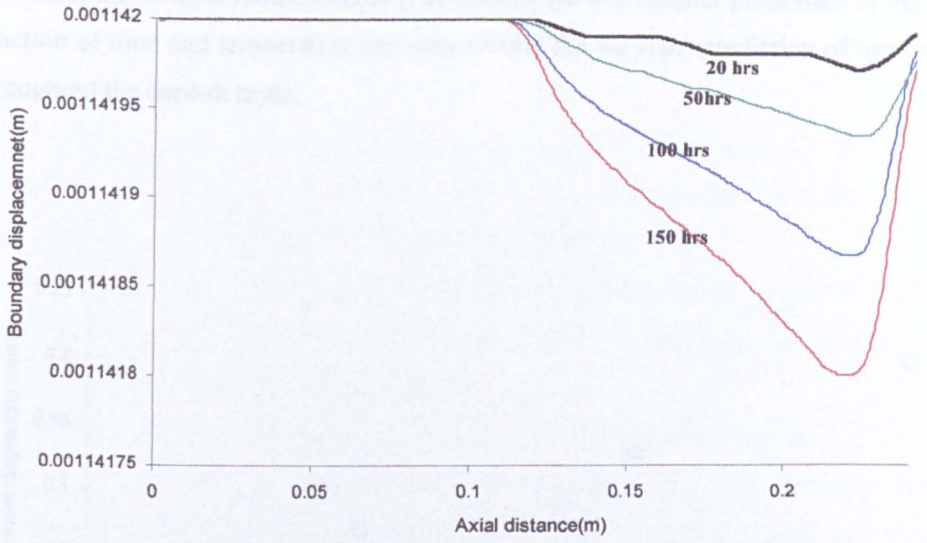

Figure 5-22: Boundary displacement due to deposition in heated nozzle of AFTSTU

Figure 5-23 depicts the simulated amount of deposit thickness for different thermal exposure time. These are enable to qualitatively represent the induction period occurred during the first stage of deposition. The growth of deposit in heated tube exhibits a sharp rise between 15 hrs and 20 h; while, the experimental results of temperature rise in Figure 4-11 indicate a smooth increase of temperature for the entire period of thermal stressing. Such unrealistic jump was due to the lack of accuracy of displacement calculation for the shorter thermal exposure period. It has to be mentioned that this also happened between 15-20 h thermal exposure time in the results of deposit amount in Katta and Roquemore. Following on the induction period, the predicted results for the higher duration of thermal exposure showed a linear behaviour. This might be related to the lack of appropriateness of the surface deposition sub mechanism applied. It was previously mentioned that there are multitude of surface and bulk interactions leading to the formation of deposit. Perhaps, the application of three step mechanism cannot realistically describe the surface phenomena.

Secondly, the reliable mathematical polynomials for the thermal properties of deposit as function of time and temperature are very crucial for the right prediction of heat transfer throughout the deposit layer.

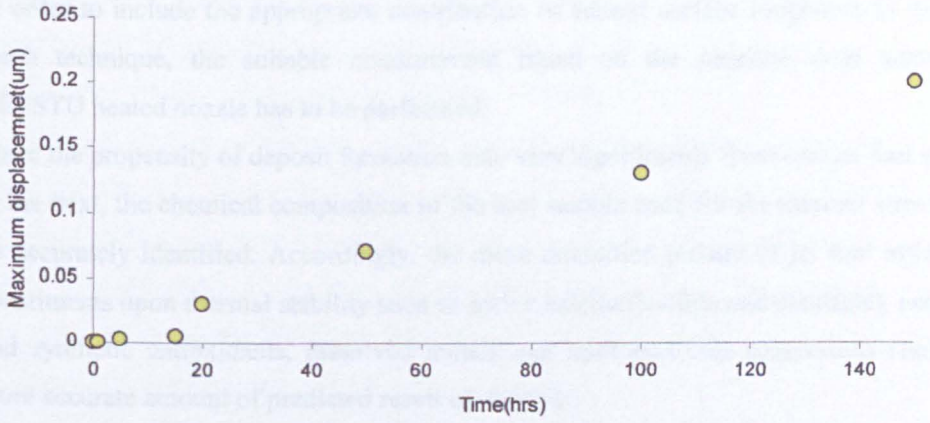

Figure 5-23: The amount of deposit thickness in heated nozzle of AFTSTU

5.6 CONCLUSION

The CFD model based on the dynamic mesh approach proved to be capable of predicting of the deposit growth in a real time calculation for a two dimensional cylindrical passage. This model can be applied to the different experimental conditions for which the fuel passage is considered to be cylindrical.

There are a number of limitations in terms of the application of this model for the modified geometry such as elbow shape or contraction/expansion nozzle as in this technique the boundary movement was considered to be only in radial direction. Hence, for the application presented approach, the formulation for the new boundary after each time step must be modified. One suggestion is to consider that the displacement occurs in the direction normal to the boundary. However, a fluid flow calculation in association with the chemistry must be carried out to identify the regions where the deposition rate is the highest.

The actual code has not been validated so far with the quantified amount of deposited carbon on inner surface of AFTSTU heated nozzle as such facility has not been available during this research.

More focus ought to be on finding the reliable functions for the thermal properties of the deposit. Accordingly, a morphological analysis ought to be carried out in order to identify the 3D profile as well as the elemental analysis of the deposit.

In order to include the appropriate contribution of variant surface roughness in dynamic mesh technique, the suitable measurement based on the pressure drop across the AFTSTU heated nozzle has to be performed.

Since the propensity of deposit formation may vary significantly from one jet fuel sample to the next, the chemical composition of the fuel sample used for the thermal stress must be accurately identified. Accordingly, the more quantified picture of jet fuel influential constituents upon thermal stability such as active sulphur(Sulfide and disulfide), naturally and synthetic antioxidants, dissolved metals and hydroperoxide compounds results in more accurate amount of predicted result of deposit.

Since the validation of pseudo-detailed mechanism has been mostly performed in the laminar flow regime, the reaction rate parameters have to be optimised by the application of technique developed by Wade (2005).

The simplistic reactor/CFD approach which was developed in this thesis has also to be validated with the results of carbon burn off. The ease of use and low expense of computation makes this approach to be very practical for the preliminary analysis.

Another possible mathematical formulation which is slightly closer to the physics of deposition is proposed to include a suggestive factor called as "surface coverage factor" which accounts for the change of the area covered by the deposit throughout the time dependent modelling.

CHAPTER 6

DISCUSION AND SUGGESTION FOR FUTURE WORK

6.1 Thesis Recapitulation

A literature survey has been provided in Chapter 2 addressing the physico-chemical aspects of jet fuel autoxidation process along with the surface deposition phenomena. The significance of these processes in aviation has been discussed. The impact of various constituents of fuel on thermal degradation process has also been highlighted. Various chemical schemes for the description of processes have also been provided. Moreover, different techniques, apparatus, and rigs for the experimental investigation of process have been addressed. At the final section of the Chapter 2, several computational fluid dynamic techniques for simulation of jet fuel thermal degradation have been reviewed.

In Chapter 3, a mathematical formulation for calculation of the rate of the equations has been presented. Based on the mathematical model, a MATLAB computer code was developed to integrate the non linear system of the equations representing the jet fuel autoxidation mechanism, namely pseudo detailed mechanism. The model results showed reasonably good agreement with the experimental data based on the results of the NIFTR which are publicly available; see Jones and Balster (1993). Furthermore, a formulation for the sensitivity analysis has been presented and applied to the pseudo detailed mechanism in order to compute the dependence of the oxygen depletion and hydroperoxide species formation on the rate of the reactions. The calculated results indicated that the rate of three reaction steps are insignificant to these two species, hence, the chemical scheme was further reduced.

The description of AFTSTU, experimentation method, and the results has been addressed in Chapter 4. The experimental data have been analysed and based on the previous physical models and theories of jet fuel thermal stability an explanation has been provided to address the typical behaviour of surface deposition along the AFTSTU heated nozzle.

In Chapter 5, two modelling approaches have been addressed. The first model is based on the combination of the reactor modelling and CFD. A MATLAB computer code was generated to read the local values of velocities and temperature from Fluent solver. By the use of the global chemistry scheme for fuel thermal degradation, it was attempted to calculate the total amount of deposit over the entire volume of the tube. Because this model is incapable of prediction of temperature distribution across the wall, it was not included for the further calculations in this thesis.

In the other modelling approach, based on the dynamic mesh technique a CFD simulation was performed. With the application of this technique, it was assumed that the fuel-deposit interface boundary is subject to a real time displacement caused by the growth of the deposit. A mathematical formulation has been presented to address the sticking probability of the precursor species on the surface. All these issues were considered in two user define functions. These functions were compiled and implemented into Fluent to imitate the surface deposition in both NIFTR and AFTSTU tubes.

Experimental results of AFTSTU heated nozzle module indicate that the temperature along the external wall increases dynamically throughout the thermal exposure time for all thermocouples. The increase of temperature at the external wall can be explained in terms of the thermally insulative characteristics of the deposit layer while the constant heat flux is generated across the tube wall. The recorded data by the farthest thermocouple show that three stage behaviour is clearly manifested for this point when the highest thermal load is supplied. It is, however, believed that if the duration of exposure is increased enough, is more likely to observe such three stage behaviour for all of the thermocouples.

Interpretation of the initial stage, namely induction period is complicated. The thermocouple at the tube exit proved that the fuel temperature at this point remains unchanged during the entire experiment. In addition, the chemistry of jet fuel for each stage of the tests, at any instant, should be the same as jet fuel is not subject to the recirculation. However, there was no facility to measure the temperature of the fuel-interface during the test. Katta and Roquemore (1993) reported that the temperature at the interface remains undisturbed for the entire duration of the test. In this way, if both chemistry and temperature in the deposit adjacent layer are constant, the reason for the

induction period may be related to the unknown interaction of precursor particle and wall surface. Hazlett (1990) reported that a number of phenomena contribute to the surface deposition. It is assumed that the ensemble of surface deposition processes is a non linear process. Induction period may be a sticking retardation phase as a consequence of agglomeration, collection, and fusion. Throughout the agglomeration step, the insoluble products which are generated during the autoxidation are transformed to the micro spherical species ranging from 500 to 3000 Å in size. The micro spherical particles then settle or collect on surfaces after impingement from the moving fluid. Loss of volatile fuel can leave non-volatile particles on surfaces. Following on collection, particles undergo coalescence and plastic flow to form varnish like substrate on which additional particles collect. Further oxidation may take place to form 'coke' like deposits. Probably, during the temperature rise stage, the surface interaction with the precursor will be higher. The third stage, namely level off, might be related to the partially and then fully coverage of the stainless steel surface resulting to a decrease in surface deposition.

For the baseline test 2, the fuel temperature was increased by the application of High Pressure (HP) heater. In this case, the higher amount of precursor which is favoured by higher temperature results in the more pronounced temperature. In particular, the higher temperature at the fuel inlet increases the rate autoxidation in heated tube. Under this situation, the formation of precursor species is higher and hence more deposition takes place.

6.2 Theoretical Investigation of Carbon Deposition in AFTSTU Heated Nozzle Module

Application of pseudo detailed mechanism of jet fuel thermal oxidative stability in a zero dimensional modelling, which has been carried out in this thesis, indicates that the initial step of the mechanism, that is, (I→R˙) is extremely slow reaction and it supplies a very low concentration of alkyl radicals (R˙) that are not enough to interfere with the overall oxidation process. Hence, this step can be effectively removed from the mechanism as thermal decomposition of very low levels (micro molar) of hydroperoxides found in jet fuels are sufficient to initiate the chain without including the "fake" initiation step. The

results of sensitivity analysis depicts that the alkyl radical is significantly sensitive to the reaction step 9 and 18 of the pseudo detailed mechanism as presented in Table 2-3.

In this mechanism, the equal number of moles for both alkoxy radical ($RO^{\bullet}$) and hydroxyl radical ($OH^{\bullet}$) is expected to be generated through the hydroperoxide decomposition steps. However, further participation of alkoxy radical ($RO^{\bullet}$) in more reactions (10, 11, 13) compare to the contribution of hydroxyl radical (only reaction 12) is the reason for the concentration of hydroxyl radical being significantly higher throughout the autoxidation process. There is a schematic similarity between the two of the propagation step reactions, namely, reaction steps 10($RO^{\bullet}+RH \rightarrow ROH+ R^{\bullet}$) and reaction 12($OH^{\bullet}+RH \rightarrow H_2O+ R^{\bullet}$) in terms of alkyl radical ($R^{\bullet}$) formation, however, as the molar concentration of bulk fuel (RH) is approximately constant during the process, the rate for the reaction step 12 is noticeably higher than reaction step10 due to the higher concentration of hydroxyl radical ($OH^{\bullet}$).

By setting the pre exponential factor of the reaction 10 equal to zero no changes were observed in the profile of species of interest, namely dissolved O_2 and hydroperoxide species. Although the reaction 12 is an important step to carry on the chain, the complete elimination of alkoxy radical ($RO^{\bullet}$) results that the species of interest to be under predicted. Further contribution of alkoxy radical ($RO^{\bullet}$) to the mechanism is described in the pseudo-detailed mechanism thorough the steps (10, 11, 13 and 14). However, by elimination of reaction steps (10 and 13) or (11 and 14) no changes were observed in the concentration species of interest.

Although this model is commonly applicable for any two dimensional cylindrical passages with moving boundaries, this is not ready to accurately reproduce the temperature distribution across the external wall. There are also a number of limitations in terms of the application of this model in modified geometry such as elbow shape or contraction/expansion nozzle. In the presented model the boundary movement was assumed to be only in radial direction. Hence, in order to apply it to the non cylindrical passages further assumptions ought to be considered. One assumption is to consider that boundary displacement occurs in the direction normal to the flow direction. In addition, a fluid flow calculation in association with the chemistry must be carried out to identify the regions where the deposition rate is the highest.

A major drawback of the CFD modeling based on the moving boundary technique performed in this thesis was the application of inappropriate thermal property values for deposit layer as function of temperature. To date there is no available functions for thermal conductivity, heat capacity and density of growing deposit. Therefore, a sensitivity analysis must perform to investigate the impact of these properties on the predictive power of the model.

An arbitrarily function for thermal conductivity of the deposit was assumed and implemented in to the CFD model. Although, the simulated results showed that the code is capable of predicting the temperature rise for the external wall in a non linear manner, the calculation was crashed due to the occurrence of negative cell volume. Therefore, the suggested function was not included in this thesis, however, will be published separately once the problem with negative volume is fixed and the problem is optimized.

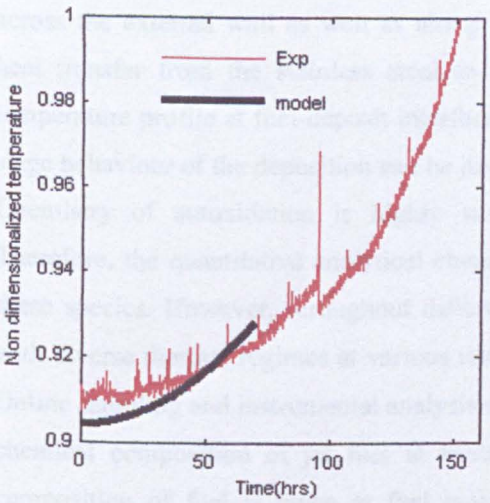

The actual code has not been validated so far by the quantified amount of deposited carbon on inner surface of AFTSTU heated nozzle as such facility was not available during this research.

6.3 Suggestion for the Future Works

Reliable polynomials for deposit thermal properties must be provided to represent their change with temperature and time. For doing this, analysis with Scanning Electron Microscope (SEM) is recommended to be applied. By the application of SEM, firstly three dimensional topography of the deposit for some regions of the heated tube can be provided. Secondly, the application of Energy-dispersive X-ray spectroscopy (EDS) which is an analytical technique used for the elemental analysis or chemical characterisation of the sample can more precisely determine gain information about the constituents of deposit. In this research, it was assumed that the deposit is fully made from carbon.

Once the reliable thermal properties of the deposit are available, the CFD model needs to be slightly modified to be capable of imitating more accurate temperature distribution across the external wall as well as along the fuel-deposit layer. Accurate prediction of heat transfer from the stainless steel to the deposit and to the fluid gives the right temperature profile at fuel-deposit interface. Once this is provided, then the typical three stage behaviour of the deposition can be justified.

Chemistry of autoxidation is highly sensitive to some of the fuel's constituents. Therefore, the quantitative analytical chemistry tests ought to be performed to measure these species. However, throughout different compartments of AFTSTU, jet fuel faces with diverse thermal regimes at various residence times, hence, changes its composition. Online sampling and instrumental analysis a test are certain solutions for quantification of chemical composition of jet fuel at heated tube entrance. Alternatively, if chemical composition of fuel is given at fuel tank, a reactor calculation can approximate the constituents of the jet fuel at tube entrance.

Once more accurate heat transfer prediction can be obtained, based on the assumption that deposit is fully made from the carbon; Carbon Burn off (CBO) ought to be used to quantify the total amount of deposit for each heated tube. As the experiment performed in this thesis includes two baseline tests, each consists of four stages; surface deposition can be presented against power supplied.

A more comprehensive sub mechanism for the surface deposition needs to be provided. Therefore, in order to include a more realistic physic of sticking probability for the longer

duration of thermal exposure, another possible mathematical formulation which accounts for a suggestive factor named as surface coverage ought to be implemented into the dynamic mesh udf.

To sum up , in order to be able to reproduce the level off period during the deposition, that is the decrease of deposition rate for the third stage of deposition as was shown in experimental results, the surface coverage factor φ is proposed to considers that the formation of deposit varies between two limits when the surface metal is clean (φ=0) and the situation when is fully covered (φ=1).Consequently, deposit formation in the time interval between these two limits can be described by any combination of the first and the second terms in the following equations.

$$\frac{d[\text{prcursor}]}{dt} = (1-\phi)\exp(\frac{-Ea_1}{RT}) + \phi.\exp(\frac{-Ea_2}{RT}) \qquad \text{Eq.0-1}$$

Therefore inclusion of surface coverage factor φ in above results in following equation.

$$\frac{d(\text{deposit})}{dt} = \frac{C}{\tau^{n}_{\text{interface}}}\left[\frac{\rho^{\text{int}} f_p^{\text{int}}}{MP}\right]\left[(1-\phi)\exp\left(\frac{-Ea_{\text{wallA}}}{RT}\right) + (\phi\exp\left(\frac{-Ea_{\text{wallB}}}{RT}\right)\right] \qquad \text{Eq 0-2}$$

REFRENCES

Albright.L.F & Marek.J.C (1988) Coke Formation during Pyrolysis: Roles of Residence Time, Reactor Geometry, and Time of Operation. *Ind. Eng. Chem. Chem.Res,* 27.755-762

Altin.O & Eser.S (2000) Characterization of Carbon Deposits from Jet Fuel on Inconel 600 and Inconel X Surfaces. *Ind. Eng. Chem. Res,* 39, 642-645

Altin.O & Eser.S (2001) Analysis of Solid Deposits from Thermal Stressing of a JP-8 Fuel on Different Tube Surfaces in a Flow Reactor. *Ind. Eng. Chem. Chem.Res,* 40, 596-603

Balster.L.M, Balster.W.J & Jones.E.G (1996) Thermal Stability of Jet Fuel/Paraffin Blends. *Energy & Fuels,* 12, 1176-1180

Benson.S.W (1968) *Thermo chemical Kinetics, Methods for Estimation of Thermo chemical Data and Rate Parameters*

Benson.S.W & Shaw.R (1970) *Organic Peroxide*, Whiley-Interscience; New York.

Biddle.T.B (1993) Development of an Advanced JP-8 Fuel. United Technologies Corporation, Pratt & Whitney

Blakey.S.G &Wilson.C.W (2008) AFTS test report: Baseline tests The University of Sheffield, Department of Mechanical Engineering

Bolshakov.G.F (1974) The Physico-Chemical Principles of the Formation of Deposits in Jet Fuels. Defense Technical Information Center

Bott.T.R (1995) *Fouling of Heat Exchangers. Elsevier Sc.Netherland*

Chin.J.S & Lefebvre.A.H (1993) Influence of Flow Conditions on Deposits From Heated Hydrocarbon Fuels. *Journal of Engineering for Gas Turbines and Power,* 115, 433-438

CRC (1983) Low Temperature Behavior of Fuels in Simulated Aircraft Tanks.

CRC (1984) *Handbook of aviation fuel properties,* Atlanta, GA

Dagget.D.L, Veninger.A, Lewis.C, Bullock.S & Kamin.R (1995) The Development of an Aviation Fuel Thermal Stability Test Unit. *Journal of Engineering for Gas Turbines and Power,* 117,468-473

Denison.G & Condit.P (1945) Oxidation of Lubricating Oils, Mechanism of Sulphur Inhibition. *Ind.Eng.Chem.Res,* 37, 650-661

Denison.G & Condit.P (1949) Oxidation of Lubricating Oils, Dialkyl Selenides as Inhibitors. *Ind.Eng.Chem.Res,* 41, 945-949

Edwards.T & Zabarnick.S (1993) Supercritical Fuel Deposition Mechanism. *Ind. Eng. Chem. Res,* 32,3117-3122

Elliot.L, Ingham.D.B, Kyne.A.G, Mera.N.S, Pourkashanian.M & Wilson.C.W (2003) Optimisation of Reaction Mechanisms for Aviation Fuels using a Multi-Objective Genetic Algorithm *Genetic and Evolutionary Computation Conference.* Berlin, Springer Verlag.

Emanuel.N.M, Denisov.E.T & Marizus.Z.K (1967) *Liquid Phase Oxidation of Hydrocarbons.*

Epstein, N (1986) *Heat Exchanger Sourcebook,* Ed. hemisphere, Washington DC

Ervin.J.S, Ward.T.A, Williams.T.F & Bento.J (2003) Surface Deposition Within Treated and Untreated Stainless Steel Tubes Resulting from Thermal Oxidative and Pyrolytic Degradation of Jet Fuel. *Energy & Fuels,* 17, 577-586.

Ervin.J.S, Williams.T.F & Katta.V.R (1996) Global Kinetic Modeling of Aviation Fuel Fouling in Cooled Regions in Flowing System. *Ind. Eng. Chem. Res,* 35, 8.4028-4037

Ervin.J.S & Zabarnick.S (1998) Computational Fluid Dynamics Simulations of Jet FuelOxidation Incorporating Pesudo-Detailed Chemical Kinetics. *Energy & Fuels,* 12, 334-352

Ervin.J.S, Zabarnick.S & Williams.T.F (2000) One Dimensional Simulations of Jet Fuel Thermal Oxidative Degradation and Deposit Formation within Cylindrical Passages. *Journal of Energy Res.Technology,* 122, 229-238

Fathoni.A.Z & Batts.B.D (1991) A Literature Review of Fuel Stability Studies with a Particular Emphasis on Shale Oil. *Energy & Fuels,* 6, 681-693

Fink.D.F & Nixon.A.C (1954) Stability of Aircraft Turbine Fuels. *Ind.Eng.Chem.Res,* 46, 2166-2173

Fish.A (1970) *Organic Peroxide, Vol.1,* Whiley-Interscience, New York.

Fodor.G.E, Naegeli.D.W & Kohl.K.B (1998) Peroxide Formation in Jet Fuels. *Energy & Fuels,* 2, 729-734

Goel.P & Boehman.A.L (2000) Numerical simulation of jet fuel degradation flow reactors. *Energy & Fuels,* 14, 953-962

Hardy.D.R, Beal.E.J & Burnet.J.C (1992) *5th International Conference on Stability Handling Liquid Fuels, 1992.* Washington DC

Hazlett.R.N (1991) *Thermal Oxidation Stability of Aviation Turbine Fuels,* ASTM

Hazlett.R.N, Hall.J.M & Matson.M (1977) Reactions of Aerated N-Dodecane Liquid Flowing over Heated metal tubes. *Ind. Eng. Chem. Process Des.Dev,* 16, 171-177

Hazlett.R.N, Schreifelst.J.A, Stalick.W.M, Morris.R.E & Mushrush.G.M (1991) Distillate Fuel Insolubles: Formation Conditions and Characterization. *Energy & Fuels,* 5, 546-574

Heneghan.S.P & Zabarnick.S (1994) Oxidation of jet fuels and the formation of deposit. *Fuel,* 73, 35-43

Heneghan.S.P, Zabarnick.S, Ballal.D.R & Harrison.W (1996) Development of a Thermally Stable Jet Fuel. *Journal of Energy Res.Technology118,170-179*

Hobday.A & Lewis.C (1995) Aviation Fuel Thermal Stability Test Unit Documentation. Rolls Royce,Derby

Hogin.D.R & Clinkenbeard.W.L (1960) *Petroleum Products Handbook,* New York, McGraw-Hill

Huang.He, Spadaccini.L.J & Sobel.D.R (2002) Fuel-Cooled Thermal Managmenet For Advanced Aero Engines. *ASME Turbo Expo.* The Netherlands

Irvine , S. A., Schoettmer, A. K., Bates , R. W. & Meyer, M. L. (2004) History of Sulfur Content Effects on the Thermal Stability of RP-1 Under Heated Conditions. *40th AIAA/ASME/SAE/ASEE, Joint Propulsion Conference and Exhibit.* Fort Lauderdale, FL

Ivanov, A. A. & Kafengauz, N. L. (1968) Thermal Conductivies of Carbon Deposits Formed on the Walls of Heat Exchanger. *Translated from Khimia i Tekhnologiya Topliv i Masel* 11, 11-13

Jones.E.G & Balster.W.J (1993) Phenomenological Study of the Formation of Insolubles in Jet-A Fuel. *Energy & Fuels,* 7, 968-977

Jones.E.G, Balster.W.J & Balster.L.M (1997) Impact of Additives on the Autoxidation of a Thermally Stable Aviation Fuel. *Energy & Fuels,* 11, 610-614

Jones.E.G, Balster.W.J & Post.M.E (1995) Degradation of a Jet Fuel in a Single-Pass Heat Exchanger. *Journal of Engineering for Gas Turbines and Power,* 117, 125-133

Jones.E.G, Blaster.L.J & Blaster.W.J (1996) Autoxidation of Aviation Fuels in heated tubes:Surface effect. *Energy and Fuels,* 10, 831-836

Jones.E.G., Balster.L.M. & Balster.W.J (1998) Autoxidation of Neat and Blended Aviation Fuels. *Energy & Fuels,* 12, 990-995

Katta.V.R, Jones.E.G & Roquemore.W.M (1998) Modeling of Deposition Process in Liquid Fuels. *Combustion Science Technology,* 139, 75-111

Katta.V.R & Roquemore.W.M (1993) Numerical Method for Simulating Fluid-Dynamic and Heat Transfer Changes in Jet-Engine Injector Feed Arm Due to Fouling. *Journal of Themophysics and Heat Transfer,* 7, 651-660

Kendall.D.R & Mills.J.S (1986) Thermal Stability of Aviation Kerosines:Techniques To Characterize Their Oxidation Properties. *Ind. Eng. Chem. Prod.Res.Dev,* 25, 360-366.

Kennealy.J.P & Moore.W.M (1977) A Numerical Method for Chemical Kinetics Modeling Based Taylor Series Expansion. *The Journal of Physical Chemistry,* 81,2413-2419

Krazinski.J.L, Vanka.S.P, Pearce.J.A & Roquemore.W.M (1992) A Computational Fluid Dynamics and Chemistry Model for Jet Fuel Thermal Stability. *Journal of Engineering for Gas Turbines and Power,* 114, 104-110

Kuprowicz.N.J, Ervin.J.S & Zabarnick.S (2004) Modeling the liquid-phase oxidation of hydrocarbons over a range of temperatures and dissolved oxygen concentrations with pseudo detailed chemical kinetics. *Fuel,* 83, 1795-1801

Kuprowicz.N.J, Zabarnick.S, West.Z.J & Ervin.J.S (2007) Use of Measured Species Class Concentrations with Chemical Kinetic Modeling for the Prediction of Autoxidation and Deposition of Jet Fuels. *Energy & Fuels,* 21, 530-544

Laidler.K.J (1987) *Chemical Kinetics,* McGraw-Hill Book Company

Leis.J & Kramer.M (1988) The Simultaneous Solution and Sensitivity Analysis of Systems Described By Ordinary Differential Equations. *ACM Transactions on Mathematical Software,* 14, 45-60

Marteney.P.J & Spadaccini.L.J (1986) Thermal Decomposition of Aircraft Fuel. *Journal of Energy Res.Technology,* 108, 648-653

MATLAB Help (2005)

Maurice.L.Q, Lander.H, Edwards.T & Harrison.W.E (2000) Advanced Aviation Fuels: A Look Ahead Via a Historical Perspective. *Fuel, ,* 80, 747-756

Mayo.F.R & Lan.B.Y (1986) Gum and Deposit Formation from Jet Turbine and Diesel Fuels at 130 C. *Ind. Eng. Chem. Chem.Res,* 25, 333-348

Mayo.F.R & Lan.B.Y (1987) Gum and Deposit Formation from Jet Turbine and Diesel Fuels at 100 C. *Ind. Eng. Chem. Chem.Res,* 26, 215-220

Mccarty.J.G & Wise.H (1979) Hydrogenation of Surface Carbon on Alumina Supported Nickel. *Journal of Catalysis,* 57, 406-413

Mellor.A.M (1990) *Design of Modern Gas Turbine Combustors,* Academic Press

Mill.T & Hendry.D.G (1980) Kinetics and Mechanisms of Free Radical Oxidation of Alkanes and Olefines in the Liquid Phase. *Kinetics and Mechanisms of Free Radical Oxidation of Alkanes and Olefines in the Liquid Phase* Amesterdam, Bamford, C.H., and Tipper, C.F.H, eds., Elsevier Scientific Publishing Company.

Morris.R.W.Jr, Minus.D, Zabarnick.S, Balster.L.M, Binns.K.E, Dieterle.G & Biddle.T.B (2002) Protocol of Test Methods for Evaluating High Heat Sink Fuel Thermal Stability Additives For Aviation Jet Fuel JP-8+100. AFLR-PR-WP-TR-2002-2037

Moses.C.A (2007) Development of the Protocol for Acceptance of Synthetic Fuels Under Commercial Specification. San Antonio,Texas, Fuels and Lubricants Technology Departmnet Southwest Research Institute(SWRI)

Mushrush.G.W & Hazlett.R.N (1984) Pyrolysis of Organic Compounds Containing Long Unbranched Alkyl Groups. *Ind. Eng. Chem. Fundam,* 23, 288-294

Mushrush.G.W, Hazlett.R.N & Eaton.H.G (1985) Liquid Phase Oxidation of Undecanal by tert-Butyl Hydroperoxide in Dodecane. *Ind. Eng. Chem. Chem.Res,* 24, 290-293

Mushrush.G.W, Hazlett.R.N, Pellenbarg.R.E & Hardy.D.R (1991) Role of Sulfur Compounds in Fuel Instability : A Model Study of the Formation of Sulfunic Acids From Hexyl Sulfide and Hexyl Disulfide. *Energy & Fuels,* 5, 258-262.

Naegli.D.W (1997) Thermal Stability of Jet Fuels: Kinetics of Forming Deposit Precursor. San Antonio, Texas, U.S.Army TARDEC Fuels and Lubricants Research Facility , Southwest Research Institute

Pande.S.G & Hardy.D.R (1997) Compariosn of the Effects of Storage Conditions,Type of Soluble Copper, and MDA on JP-5 Fuel Thermal Stability. *6th International Conference on Stability and Handling of Liquid Fuels.* Vancouver,B.C., Canada.

Pande.S.G, Hardy.D.R, Kamin.R.A, Nowack.C.J, Collbert.J.E, Morris.R.E & Salvucci.L (2001) Quest for a Reliable Method for Determining Aviation Fuel Thermal Stability: Comparison of Turbulent and Laminar Flow Test Devices. *Energy & Fuels,* 15, 224-235

Penn State University (1993) Compositional Factors Affecting Thermal Degradation of Jet Fuels. *Fuel Science Program, Department of Materials Science & Engineering, the Pennsylvania State University.* Aero Propulsion and Power Directorate, Wright Laboratory

Pearce.P (2001) Sulfur in US Military Jet Fuels. US AIR FORCE RESEARCH LABORATORY

Pickard.J.M & Jones.E.G (1997) Catalysis of Jet-A Fuel Autoxidation by Fe_2O_3. *Energy & Fuels,* 11, 1232-1236

Pickard.J.M & Jones.E.G (1998) Liquid-Phase Oxidation Kinetics: Paraffin Blends. *Energy & Fuels,* 12, 1241-1244

Press.W, Teukolsky.S, Vetterling.W and Flannery.B (1992) *Numerical Recepies in Fotran 77.*

Rabitz.H, Kramer.M & Dacol.D (1983) Sensitivity Analysis in Chemical Kinetics. *Ann.Rev.Phys.Chem,* 34, 419-461

Ranade.V.V (2002) *Computational Flow Modeling for Chemical Reactor Engineering,* Academic Press

Reddy.K.T, C. N. P., Cohen.R.S (1988) Modified Reaction Mechanism of Aerated n-dodecane Liquid Flowing Over Heated Metal Tubes. *Energy & Fuels,* 2, 205-213

Rolls Royce, Derby (2000) *Gas Turbine Combustor*

Rowson.P (2001) Evaluation of the JP-8+100 Jet Fuel Thermal Stability Additive, DSTO-TR-1135-1165

Rubey.W.A, Striebich.R.C, Tissandier.M.D, Tirey.D.A & Anderson.S.D (1995) Gas Chromatographic Measurement of Trace Oxygen and Other Dissolved Gases in Thermally Stressed Jet Fuel. *Journal of Chromatography Science,* 33, 434-437

Schreifels.J.A, Morris.R.E, Turner.N.H, Mowery.R.L & Hues.S.M (1991) Adsorption of a Metal Deactivator Additive onto Metal Surfaces. *Energy & Fuels,* 5, 263-268

Schwartz.F.G & Eccleston.B.H (1962) Survey of Research on Thermal Stability of Petroleum Jet Fuels. *Information Circular IC 8140, Bureau of Mines,*

Siouris.S (2009) Simulations of Lubricant Degradation, Deposition , and Elastomer Relaxation for Aviation gas Turbine Lubrication Systems. *Mechanical Engineering.* Sheffield, University of Sheffield

Spadaccini.L.J, Sobel.D.R & Huang.H (2001) Deposit Formation and Mitigation in aircraft Fuels. *Journal of Engineering for Gas Turbines and Power,* 123, 741-746

Swiheart.M (2006) Chemical Kinetic and Reactor Design Lecture Notes, Buffalo State University

Taylor.S (2005) Jet Fuel Thermal Stability: Measurement Technologies. *AERONET III Workshop on Thermal Stability,* The University of Sheffield

Taylor.S.E & Wallace.T.J (1968) Kinetics of Deposit Formation from Hydrocarbons. Effects of Trace Sulphur Compounds. *Industrial and Engineering Chemistry ,Product and Research Development,* 7, 495-515

Taylor.W.F & Frankenfeld.J.W (1988) Chemistry and Mechanism of Distillate Fuel Stability. *Proceeding 2nd International Conference on Long Term Storage Stabilities ofLiquid Fuels.* San Antonio, Texas

Thomas.J.R & Harle.O.L (1959) Substrate Effects on the Decomposition of Alkyl Hydroperoxides and Their Influence upon Autoxidation , *The Journal of Physical Chemistry,* 7, 84-96

Thompson.R.B, Druge.L.W & Chenicek.J.A (1949) *Ind. Eng. Chem. Chem.Res,* 41

Turanyi.T (1990) Sensitivity Analysis of Complex Kinetic Systems. Tools and Applications. *Journal of Mathematical Chemistry,* 5, 203-248

Wade.A.S (2005) A Theoretical Investigation into Thermal Oxidation and Deposition processes in Aviation Fuels Using Genetic Algorithms. *Energy and Resources Research Institute.* Leeds, University of Leeds

Wade.A.S, Kyne.A.G, Mera.N.S & Pourkashanian.M (2004) Optimisation of the Arrhenius Parameters in a Semi-Detailed Mechanism for Jet Fuel Thermal Degradation Using Genetic Algorithm, ASME Turbo Conference, 324-330

Walling.C (1957) *Free Radicals in Solution*, Whiley-Interscience

Walte.T.R (1957) General Theory of Bimolecular Reaction Rates in Solids and Liquids. *Journal of Chemical Physics,* 28, 103-107

Watkins.J.M.$_{Jr.}$, Mushrush.G.W, R.N.Hazlett.R.N & Beal.E.J (1989) Hydroperoxide Formation and Reactivity in Jet Fuels. *Energy & Fuels,* 3, 231-236

White.P (2000) Aviation Fuel Thermal Stability Test Unit Software Upgrade Final Report. *Electrical& Electronic Engineering Dissertation.* Derby, University of Derby

Young.T.R & Boris.J.P (1977) A Numerical Technique for Solving Stiff Ordinary Differential Equations Associated with the Chemical Kinetics of Reactive Flow Problems. *The Journal of Physical Chemistry,* 81

Zabarnick.S (1998) Pseudo-detailed Chemical Kinetic Modeling of Antioxidant Chemistry for Jet Fuel Applications. *Energy & Fuels,* 12, 547-553

Zabarnick.S (2005) Private Communication.

Zabarnick, S. & Phelps, D. K. (2006) Density Functional Theory Calculations of Energetics and Kinetics of Jet Fuel Autoxidation Reactions. *Energy & Fuels,* 20, 488-497

Zabarnick.S (1993) Chemical Kinetic Modeling of Jet Fuel Autoxidation Chemistry. *Ind.Eng.Chem.Res,* 32, 1012-1017

Zabarnick.S & Mick.M.S (1999) Inhibition of Jet Fuel Oxidation by Addition of Hydroperoxide-Decomposing Species. *Ind. Eng. Chem. Chem.Res,* 38, 3357-3563

Zedda.M & Ravikanti.M (2008) Variation of Jet Fuel Parameters as Function of Temperature. Derby, Rolls Royce Derby

APENDIX A

Description of the Integrator Code

AFTS integrator is a rather straight forward code which integrates the non linear system of ordinary differential equations representing the chemical kinetic scheme. The code is able to integrate the system for both directions (forward and backward) however, as Jet Fuel Autoxidation reactions is unlikely to reach to the equilibrium state only the forward reactions are considered. Once the reliable thermodynamic data base for the species is available the backward reactions can be included, however, the associated function with AFTS.m (dCdt) ought to be slightly modified.

The solution of energy balance is not considered in the integration as it was assumed that the energetic of the process is not significant. For the mole balance calculation, in order to overcome the stiffness associated with integration which is caused by different time scales of existing reaction steps, the predictor corrector method, namely Gear's method was.(See chapter 3)

Theory

The matrix notation of the reaction rates has been comprehensively discussed in chapter 3. Here the equation is re written.

$$\sum_{j=1}^{N} \alpha_{ij} A_j = 0$$

$$i = 1..M$$

Where:

N is the number of species and M is the number of reactions and α_{ij} is the stoichiometric coefficient of species j in reaction i

By convention $\alpha_{ij} < 0$ for reactants and $\alpha_{ij} > 0$ for the products

The integrable form of ordinary differential equations can be written as in:

$$\frac{d\underline{C}}{dt} = \underline{f} = \underline{\alpha}^T \underline{r}$$

Where $\underline{\alpha}^T$ is the transpose of stoichiometric coefficients and $\underline{r}$ is the matrix of reaction rates. According to the above equation, the integrable form a chemical kinetic scheme, for instance, the scheme representing liquid phase autoxidation of jet fuel can be written as following:

Number of reactions

$$\frac{d}{dt}\begin{bmatrix}
I \\ R^{\bullet} \\ O_2 \\ RO_2^{\bullet} \\ RH \\ RO_2H \\ \text{Termination} \\ R_2 \\ RO^{\bullet} \\ OH^{\bullet} \\ ROH \\ \text{Rprime} \\ \text{Carbonyl} \\ H_2O \\ \text{ROterm} \\ \text{alkane} \\ AH \\ A^{\bullet} \\ AO_2^{\bullet} \\ AO_2H \\ \text{ProductAH} \\ SH \\ \text{ProductSH}
\end{bmatrix} =
\begin{bmatrix}
-1 & 0 & 0 & 0 & 0 & 0 & 0 & 0 & 0 & 0 & 0 & 0 & 0 & 0 & 0 & 0 & 0 & 0 \\
1 & -1 & 1 & 0 & 0 & 1 & 0 & 0 & 0 & -2 & 0 & 1 & 0 & 1 & 0 & 1 & 0 & 1 & -1 \\
0 & -1 & 0 & 0 & 0 & 0 & -1 & 0 & 0 & 0 & 0 & 0 & 0 & 0 & 0 & 0 & 0 & 1 & 0 \\
0 & 1 & -1 & -2 & -1 & 0 & 0 & 0 & 0 & 0 & 0 & 0 & 0 & 0 & 0 & 0 & 0 & -1 & -1 \\
0 & 0 & -1 & 0 & 0 & -1 & 0 & 0 & 0 & 0 & 0 & -1 & 0 & -1 & 0 & -1 & 0 & 0 & 0 \\
0 & 0 & 1 & 0 & 1 & 0 & 0 & 0 & 0 & 0 & -1 & 0 & 0 & 0 & 0 & 0 & -1 & 0 & 0 \\
0 & 0 & 0 & 1 & 0 & 0 & 0 & 0 & 0 & 0 & 0 & 0 & 0 & 0 & 0 & 0 & 0 & 0 & 1 \\
0 & 0 & 0 & 0 & 0 & 0 & 0 & 0 & 0 & 1 & 0 & 0 & 0 & 0 & 0 & 0 & 0 & 0 & 0 \\
0 & 0 & 0 & 0 & 0 & 0 & 0 & 0 & 0 & 0 & 1 & -1 & -1 & 0 & -2 & 0 & 0 & 0 & 0 \\
0 & 0 & 0 & 0 & 0 & 0 & 0 & 0 & 0 & 0 & 1 & 0 & 0 & -1 & 0 & 0 & 0 & 0 & 0 \\
0 & 0 & 0 & 0 & 0 & 0 & 0 & 0 & 0 & 0 & 0 & 1 & 0 & 0 & 0 & 0 & 0 & 0 & 0 \\
0 & 0 & 0 & 0 & 0 & 0 & 0 & 0 & 0 & 0 & 0 & 0 & 1 & 0 & 0 & -1 & 0 & 0 & 0 \\
0 & 0 & 0 & 0 & 0 & 0 & 0 & 0 & 0 & 0 & 0 & 0 & 1 & 0 & 0 & 0 & 0 & 0 & 0 \\
0 & 0 & 0 & 0 & 0 & 0 & 0 & 0 & 0 & 0 & 0 & 0 & 0 & 1 & 0 & 0 & 0 & 0 & 0 \\
0 & 0 & 0 & 0 & 0 & 0 & 0 & 0 & 0 & 0 & 0 & 0 & 0 & 0 & 1 & 0 & 0 & 0 & 0 \\
0 & 0 & 0 & 0 & -1 & 0 & 0 & -1 & 0 & 0 & 0 & 0 & 0 & 0 & 0 & 0 & 0 & 0 & 0 \\
0 & 0 & 0 & 0 & 1 & 0 & -1 & 1 & 0 & 0 & 0 & 0 & 0 & 0 & 0 & 0 & 0 & 0 & 0 \\
0 & 0 & 0 & 0 & 0 & -1 & 1 & -1 & -2 & 0 & 0 & 0 & 0 & 0 & 0 & 0 & 0 & 0 & 0 \\
0 & 0 & 0 & 0 & 0 & 1 & 0 & 1 & 0 & 0 & 0 & 0 & 0 & 0 & 0 & 0 & 0 & 0 & 0 \\
0 & 0 & 0 & 0 & 0 & 0 & 0 & 0 & 1 & 0 & 0 & 0 & 0 & 0 & 0 & 0 & 0 & 0 & 0 \\
0 & 0 & 0 & 0 & 0 & 0 & 0 & 0 & 0 & 0 & 0 & 0 & 0 & 0 & 0 & 0 & -1 & 0 & 0 \\
0 & 0 & 0 & 0 & 0 & 0 & 0 & 0 & 0 & 0 & 0 & 0 & 0 & 0 & 0 & 1 & 0 & 0
\end{bmatrix}
\begin{bmatrix}
R_1 \\ R_2 \\ R_3 \\ R_4 \\ R_5 \\ R_6 \\ R_7 \\ R_8 \\ R_9 \\ R_{10} \\ R_{11} \\ R_{12} \\ R_{13} \\ R_{14} \\ R_{15} \\ R_{16} \\ R_{17} \\ R_{18} \\ R_{19}
\end{bmatrix}$$

Number of species

Traspose of alpha

It ought to be mentioned that the stoichiometric matrix α_{ij} is constructed by the code automatically based on the mechanism which has to be provided by the user.

There are also two text files, which have to be located in the same directory as the integrator code and the functions are.

The text files are named as AFTS.txt and mechanism.txt respectively.

AFTS.txt contains 7 columns. The first column is the species index (i=1...N), the second, third and forth are the coefficients for the calculation of specific heat (Cp) as the polynomial functions. The fifth is the enthalpy of formation, sixth entropy and the last column is the species name. This file is considered as the thermodynamic data base for the species. The reason why the coefficients and the columns of the enthalpy and entropy are put in the table is mainly due the future calculation of the backward reactions. In fact, a data base for these values has been provided by the author of this thesis on the basis of Benson methods (group additivity), however; these values are not reliable enough and should be recalculated and validated with some similar and well known species whose properties are already available. Anyway, theses columns 2-6 are not of used by the integrator code at this stage.

However, if one desires to eliminate for the text file, the following modification in AFTS.m code must be considered.

```
[no a b c H S  spec]=textread('AFTS.txt','%f %f %f %f %f %f %s',-1);
into:
               [no  spec]=textread('AFTS.txt','%f %s',-1);
```

mechanism.txt

From the AFTS.txt we know that every single species has an index number. So in the mechanism.txt, species appear with the index rather than with the formula, name or etc. Conventionally as $\alpha_{ij}<0$ for reactants and $\alpha_{ij}>0$ for the products the sign for the reactant species in every elementary step is negative and positive signs are assigned to the products. The **mechanism.txt** file has 8 columns. The first one obviously is the reaction index. The second and the third columns are for the reactant species and the fourth, fifth and sixth are for the product species. The seventh is assigned for the pre exponential factors and the last column is for the activation energy respectively.

```
[ar br cr dr er fr A_a E_a]=textread('mechanism.txt','%f %f %f %f %f %f %f %f',-1);
```

This portion of code receives the necessary textual information for the construction of stoichiometric matrix from the mechanism.txt and will treat them as the integers. The reason why two positions (br and cr) are specified for the reactants is because the most of the reactions in the case of autoxidation mechanism are bi molecular except for the reaction steps (1, 11, and 18) which are the "fake" initiation step and the mono molecular decomposition.

For product species there are three positions specified (dr, er, fr), however, according to the most of the autoxidation scheme, usually only one or two species are required. Therefore, the last position in mechanism.txt is considered as null.

So in order to correctly set the text file for mechanism.txt the user has to do following:

For instance for a reaction step like reaction step 1:

-Decide which species are involved in the reaction step ($I, R^{\bullet}$) and what the indices are assigned to the species in the **AFTS.txt.**

So in our example the assigned index for I in the **AFTS.txt** is (1) and for $R^{\bullet}$ is (2).

-If the species is reactant, it is required to assign a minus (-) prior to it (By Convention).

If there is no any other species involved in the reaction step for the other positions we simply type (0) followed by the prexponential factor and activation energy.

Hence, the reaction step (1) in the pseudo detailed mechanism for the application in the **mechanism.txt** must be written as:

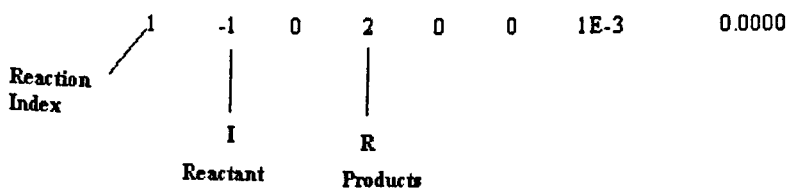

After the two text files are constructed, then the numerical input have to be entered for the code as followings:

Temperature (in Kelvin), R (Universal Constant of Gases in $kcal \cdot k^{-1} \cdot mol^{-1}$), texp (residence time), number of species as well as number of reaction steps must be specified. Finally the initial concentration (at t=0) of species must be specified.

APPENDIX B

Technical Drawing of AFTSTU Heated Nozzle

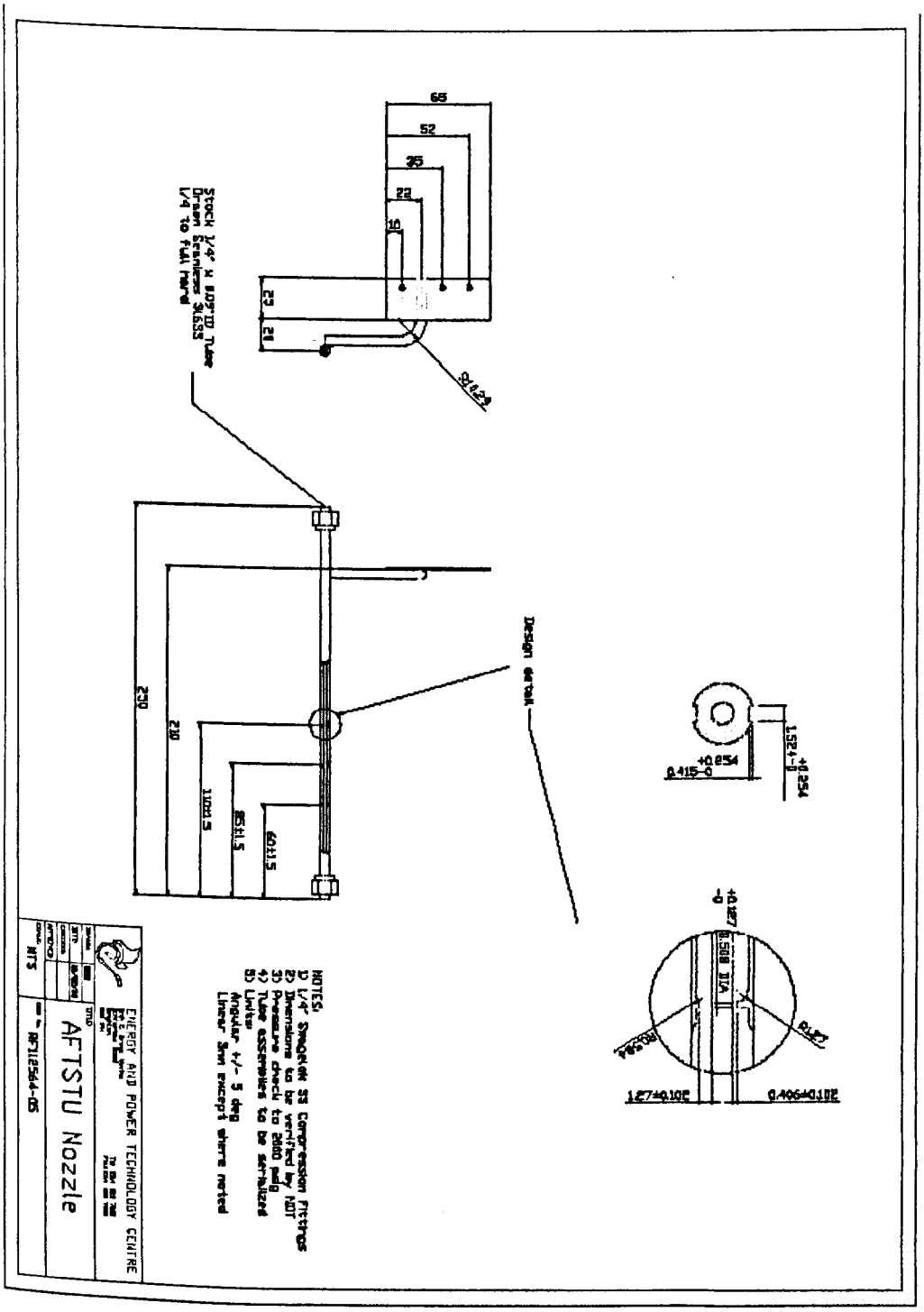

Combinatorial CFD/Reactor Modelling

```
%Import your data file from Fluent as 'data'

%Element Organiser
ElementList = [0 0 0 0];
%Number of elements in the z and r direction
iMax = 248;
jMax = 10;

%n= counter
n = 1;

%StartX is the x indentation due to missing the first column
StartX = 0.001;
dx = 0.001;

%data is the array imported from Fluent
data = sortrows(data,[2 3]);
data(:,2) = convergent(data(:,2)*1000)/1000;
%y position List is position of the rows of nodes
yPositionList = data(10:20,3)

for i = 1:iMax
   for j = 1:jMax
      %These are the Node Coordinates of the corners of the rectangular
      %elemeents
      xNode1 = convergent(i *dx*1000)/1000;
      xNode2 = convergent((StartX + i *dx)*1000)/1000;
      yNode1 = yPositionList(j);
      yNode2 = yPositionList(j+1);

      %finding the values at each node point
      %searches for x values that coincinde with x values above
      xTemp1 = data(find(data(:,2)==xNode1),:);
      xTemp2 = data(find(data(:,2)==xNode2),:);

      %finding the data values at each of the corners of the elements
      TemperatureNode11 = xTemp1(find(xTemp1(:,3)==yNode1),5);
      TemperatureNode12 = xTemp1(find(xTemp1(:,3)==yNode2),5);
      TemperatureNode21 = xTemp2(find(xTemp2(:,3)==yNode1),5);
      TemperatureNode22 = xTemp2(find(xTemp2(:,3)==yNode2),5);

      VelocityNode11 = xTemp1(find(xTemp1(:,3)==yNode1),4);
      VelocityNode12 = xTemp1(find(xTemp1(:,3)==yNode2),4);
      VelocityNode21 = xTemp2(find(xTemp2(:,3)==yNode1),4);
```

```
    VelocityNode22 = xTemp2(find(xTemp2(:,3)==yNode2),4);

    %Averaging all the values at the corners to give an element average
    ElementVelocity = (VelocityNode11 +VelocityNode12 + VelocityNode21
+VelocityNode22)/4;
    ElementTemperature = (TemperatureNode11 +TemperatureNode12 +
TemperatureNode21 +TemperatureNode22)/4;

    %Putting the values into a list
    ElementList(n,1)=i;
    ElementList(n,2)=j;

    ElementList(n,3)=dx/ElementVelocity;
    ElementList(n,4)=ElementTemperature;
    n = n+1;
  end
end
ElementList = sortrows(ElementList, [2 1]);

%runs the element organiser to collate the element details
ElementOrganiser;
ElementListSize = size(ElementList)
%Setting up the initial conditions
C0=zeros(26,1);
C0(1)=1e-8;
C0(3)=0.00168;
C0(5)=4.4;
C0(17)=1E-3;
%Data Reading from File
[no a b c H S  spec]=textread('AFTS.txt','%f %f %f %f %f %f %s',-1);
[ar br cr dr er fr A_a E_a]=textread('mechanism.txt','%f %f %f %f %f %f %f %f',-1);
%construction of Stoichiometric matrix based on reaction mechanism
n=length(ar);                    % no of reactions
m=26;
alpha=zeros(n,m);
for ii=1:n

    if br(ii)~=0
      alpha(ii,abs(br(ii)))=alpha(ii,abs(br(ii)))+abs(br(ii))/br(ii);
    end
    if cr(ii)~=0
      alpha(ii,abs(cr(ii)))=alpha(ii,abs(cr(ii)))+abs(cr(ii))/cr(ii);
    end
    if dr(ii)~=0
      alpha(ii,abs(dr(ii)))=alpha(ii,abs(dr(ii)))+abs(dr(ii))/dr(ii);
    end
```

```
        if er(ii)~=0
          alpha(ii,abs(er(ii)))=alpha(ii,abs(er(ii)))+abs(er(ii))/er(ii);
        end
        if fr(ii)~=0
          alpha(ii,abs(fr(ii)))=alpha(ii,abs(fr(ii)))+abs(fr(ii))/fr(ii);
        end

end


ConcentrationArray = [];
ConcIn = C0;
%RowNumber is the number of the row wishto investigate
RowIndex =10
NumberOfRows = 10
for i = (RowIndex-1)*ElementListSize(1)/NumberOfRows +
1:RowIndex*ElementListSize(1)/NumberOfRows
   Conc =
AFTSElements(ElementList(i,4),ElementList(i,3),ConcIn,alpha,A_a,E_a,ar,br,cr);
   ConcIn = Conc;
   ConcentrationArray = [ConcentrationArray Conc'];
end
hold all
plot(ConcentrationArray(3,:))

function ConcentrationArray = ElementPSRFunction(RowIndex,ElementList)
%runs the element organiser to collate the element details
%ElementOrganiser;
ElementListSize = size(ElementList)
%Setting up the initial conditions
C0=zeros(26,1);
C0(1)=1e-8;
C0(3)=0.00168;
C0(5)=4.4;
C0(17)=1E-3;
%Data Reading from File
[no a b c H S  spec]=textread('AFTS.txt','%f %f %f %f %f %f %s',-1);
[ar br cr dr er fr A_a E_a]=textread('mechanism.txt','%f %f %f %f %f %f %f %f,-1);
%construction of Stoichiometric matrix based on reaction mechanism
n=length(ar);                    % no of reactions
m=26;
alpha=zeros(n,m);
for ii=1:n

    if br(ii)~=0
```

```
        alpha(ii,abs(br(ii)))=alpha(ii,abs(br(ii)))+abs(br(ii))/br(ii);
    end
    if cr(ii)~=0
        alpha(ii,abs(cr(ii)))=alpha(ii,abs(cr(ii)))+abs(cr(ii))/cr(ii);
    end
    if dr(ii)~=0
        alpha(ii,abs(dr(ii)))=alpha(ii,abs(dr(ii)))+abs(dr(ii))/dr(ii);
    end
    if er(ii)~=0
        alpha(ii,abs(er(ii)))=alpha(ii,abs(er(ii)))+abs(er(ii))/er(ii);
    end
    if fr(ii)~=0
        alpha(ii,abs(fr(ii)))=alpha(ii,abs(fr(ii)))+abs(fr(ii))/fr(ii);
    end

end


ConcentrationArray = [];
ConcIn = C0;
%RowNumber is the number of the row wish to investigate
%RowIndex =1
NumberOfRows = 10
for i = (RowIndex-1)*ElementListSize(1)/NumberOfRows +
1:RowIndex*ElementListSize(1)/NumberOfRows
   Conc =
AFTSElements(ElementList(i,4),ElementList(i,3),ConcIn,alpha,A_a,E_a,ar,br,cr);
   ConcIn = Conc;
   ConcentrationArray = [ConcentrationArray Conc'];
end
hold all
%plot(ConcentrationArray(26,:))

ConcRows  = [];
ElementOrganiser
for j = 1:1
   Conc = ElementPSRFunction(j,ElementList);
   ConcRows = [ConcRows; Conc(3,:)]
end
grid on
plot(sum(ConcRows))
SpeciesSummation = sum(ConcRows);
```

APPENDIX D

Dynamic Mesh User Define Functions

/*This UDF must be implemented to the shadow which is subjected to move*/

```
DEFINE_GEOM(AFTS,domain,dt,position)
{
        # define rho_deposition 1000
        # define mw_precursor  402
        # define pre_exp 3000
        # define Active_energy  16.3
        # define rou_precursor 780
        # define Gas_Constant 1.9858775e-3
        # define inlet_velocity 1.557
      # define n                /*varies between 0.1-0.7*/



        real flow_time_step = RP_Get_Real("physical-time-step");

        int No_of_Faces;        /* the number of faces in this thread */
   int j;

        real deposition;        /*this is the deposit rate for the given wall position*/
        int array_Position;     /* this is the position in the spec array that corresponds to
the wall point we are moving*/
        real x[ND_ND]; /* this is required for the face positions*/
        real deltaX;
        real tau;
        real temp;

        face_t f;
        Thread *t;
        t = DT_THREAD(dt);
FILE *fp;


     tau=;                      /* use the proper value*/


        /* This is a counter of the number of faces in the dynamic thread*/
        j=0;
        begin_f_loop(f, t)
```

```
        {
                j=j+1;
        }
        end_f_loop(f, t);

        No_of_Faces = j;

        real spec[No_of_Faces];       /*this is an array that contains the deposition rate at
the positions along the wall*/
        real xPosition[No_of_Faces];/*this is an array that contains the xPosition of the
face cells*/


        /* this loop calcs the deposition rate at each of teh points along the wall*/
        j = 0;

        begin_f_loop(f, t)
        {

                        spec[j] = F_YI(f,t,7);
                        spec[j]=(1/tau) * ((spec[j])*(rou_precursor)/(mw_precursor*1e-3))
* (pre_exp)*exp(-Active_energy/(Gas_Constant*F_T(f,t)));
                        /* This bit above calculates the species concentration*/
                        F_CENTROID(x,f,t);
                        xPosition[j] = x[0];


                        j=j+1;
        }
        end_f_loop(f, t);
        /*points are added into the array from the rightmost end of the model so the first
element in the array corresponds
        to the maximum x coordinate */

        deltaX = xPosition[1]-xPosition[0];

        array_Position = 1+ No_of_Faces + (xPosition[0]-deltaX/2 - position[0])/deltaX;
        deposition = spec[No_of_Faces - array_Position];
                temp = sqrt(1 - 2 * deposition * flow_time_step / (rho_deposition *
position[1])) ;

        position[1] = position[1] * (temp);

        /* Write data file*/
        fp=fopen("data.txt","a");
```

```
        fprintf(fp,"x Position: %f, yPosition: %f\n",position[0], position[1]);

        fclose(fp);

        }
```

```
#include "udf.h"
#include "unsteady.h"
#include "mem.h"
#include "prop.h"
#include "math.h"


DEFINE_GEOM(WallMover1,domain,dt,position)
{

        # define rho_deposition 1000
        # define mw_precursor  402
        # define pre_exp 3000
        # define Active_energy  16.3
        # define rou_precursor 780
        # define Gas_Constant 1.985877e-3
        # define inlet_velocity 1.557
      # define n 0.1



        real flow_time_step = RP_Get_Real("physical-time-step");

        int No_of_Faces;        /* the number of faces in this thread */
   int j;

        real deposition;        /*this is the deposit rate for the given wall position*/
        int array_Position;     /* this is the position in the spec array that corresponds to
the wall point we are moving*/
        real x[ND_ND]; /* this is required for the face positions*/
        real deltaX;
   real tau;
        real temp;
        real temp2;
        face_t f;
```

```
        Thread *t;
        Thread *tShadow;
        t = DT_THREAD(dt);

      tau=1;

        tShadow = Lookup_Thread(domain,19);
        /* This is a counter of the number of faces in the dynamic thread*/
        j=0;
        begin_f_loop(f, t)
        {
                j=j+1;
        }
        end_f_loop(f, t);
        /*printf("The Value of j in this wall, %i ",j);*/
        No_of_Faces = j;

        real spec[No_of_Faces];       /*this is an array that contains the deposition rate at
the positions along the wall*/
        real xPosition[No_of_Faces]; /*this is an array that contains the xPosition of the
face cells*/

        /*tShadow = Thread_Shadow(t);*/

        /* this loop calcs the deposition rate at each of the points along the wall*/
        temp2 = position[1];
        j = 0;

        begin_f_loop(f, tShadow)
        {

                        spec[j] = F_YI(f,tShadow,7);

                        spec[j]=(1/tau) * ((spec[j])*(rou_precursor)/(mw_precursor*1e-3))
* (pre_exp)*exp(-Active_energy/(Gas_Constant*F_T(f,tShadow)));

                        F_CENTROID(x,f,tShadow);
                        xPosition[j] = x[0];


                        j=j+1;
      }
      end_f_loop(f, tShadow);

  /*printf("The Value of j, %i \n",j);*/
  /*printf("The value of the precurser %f \n",temp);*/
```

```
        /*points are added into the array from the rightmost end of the model so the first
element in teh array corresponds
        to the maximum x coodinate */

        deltaX = xPosition[1]-xPosition[0];

        array_Position = 1+ No_of_Faces + (xPosition[0]-deltaX/2 - position[0])/deltaX;
        deposition = spec[No_of_Faces - array_Position];


        temp = sqrt(1 - 2 * deposition * flow_time_step / (rho_deposition * position[1])) ;


        position[1] = position[1] * (temp);

        /*printf("The old Y position %f \n",temp2);*/
        /*printf("The new Y position %f \n", position[1]);*/
}
```